PNAS

Main Manuscript for

The fate of South America's endemic mammalian fauna in response to the most dramatic Cenozoic climate disruption

Lucas Buffan[1,*], Fabien L. Condamine[1], Narla S. Stutz[1], François Pujos[2], Pierre-Olivier Antoine[1], Laurent Marivaux[1]

[1] *Institut des Sciences de l'Evolution de Montpellier, Université de Montpellier, CNRS, IRD, Place Eugène Bataillon, 34095 Montpellier cedex 5, France*

[2] *IANIGLA, CCT–CONICET–Mendoza, Avenida Ruiz Leal s/n, Parque General San Martín, 5500 Mendoza, Argentina*

* Lucas Buffan

Email: Lucas.Buffan@umontpellier.fr

ORCID: Lucas Buffan (0000-0002-2353-1432), Fabien L. Condamine (0000-0003-1673-9910), Narla S. Stutz (0000-0002-1937-3902), François Pujos (0000-0002-6267-3927) Pierre-Olivier Antoine (0000-0001-9122-1818), Laurent Marivaux (0000-0002-2882-0874)

Author contributions: L.M., P.O.A. and F.L.C. designed the project; L.B. compiled the fossil occurrences data with clade-specific checking and cleaning of P.O.A., L.M., N.S.S. and F.P.; L.B. performed the analyses with advice from F.L.C. and wrote the paper with input from all co-authors throughout.

Competing Interests Statement: The authors declare having no competing interest.

Classification: Biological Sciences, Evolution

Keywords: Biological crisis; Eocene−Oligocene transition; Diversification dynamics; Multivariate analyses; Bayesian inference

This PDF file includes:

Main text

Figures 1 to 4

Abstract (<250 words)

Around 34 million years ago (Ma), the Eocene−Oligocene transition (EOT) marked the most dramatic global climatic cooling of the Cenozoic. On a planetary scale, paleontological evidence suggests that this transition was associated with major faunal turnovers, now regarded as a mass extinction crisis. In South America, there is no consensus on the response of the endemic mammals to this transition. Here, using a vetted fossil dataset and cutting-edge Bayesian methods, we analyzed the dynamics of South American mammal (SAM) diversification and their possible drivers across latitude (tropical vs. extratropical), taxonomic groups, and trophic guilds throughout the Eocene−Oligocene (*ca.* 56−23 Ma). Our results did not evidence any mass extinction among SAM at the EOT. Instead, they experienced a gradual and long-term diversity decline from the middle Eocene to the early Oligocene, followed by a sudden waxing-and-waning diversity associated with a large taxonomic – but not ecological – turnover. Tropical and extratropical lineages have had very distinct macroevolutionary histories. No effective change in the pace at which tropical lineages diversify was found, thus favoring the tropical stability hypothesis proposed by Wallace. Diversity-dependent effects, temperature, and Andean uplift were recovered as probable drivers of SAM diversification across the period but not the abundance of open landscapes, thereby rejecting the common hypothesis linking Oligocene faunal changes to grassland expansion. Our findings illustrate the uniqueness of the deep-time interplay between endemic SAM and their physical environment in a context of climatic hinge, highlighting the need to consider regional idiosyncrasies for understanding the co-evolution of life and climate.

Significance statement (<120 words)

Understanding what drove the emergence and demise of lineages during biodiversity crises may provide key insights at the time of the sixth mass extinction. Here, using an unprecedented fossil database, we explored how South American mammals (SAM) responded to the most dramatic Cenozoic climate cooling episode, the Eocene−Oligocene transition (*ca.* 34 Ma). We find that SAM experienced a gradual and long-standing diversity decline strongly related to late Eocene climate cooling, followed by a major taxonomic turnover in the Oligocene, driven by diversity-dependent factors and Andean uplift, but not grassland expansion. SAM were therefore more subject to long-term diversity changes rather than abrupt ones, contrary to what would be expected in a mass extinction scenario.

Introduction

Today, South America is home to a unique mammalian fauna, hosting one of the most species-rich regions of the world, Amazonia (1). Although the extant mammalian taxonomic diversity in the continent is highly diverse, it is a poor reflection of what can be drawn from the fossil record. In fact, throughout most of the Cenozoic (*i.e.,* the last 66 million years), South America was isolated from other landmasses (2). In this insular context, terrestrial mammal lineages that inhabited this huge landmass experienced unique radiations (3–7). According to Simpson (8), South American mammal (SAM) communities through the Cenozoic are well summarized by three successive 'faunal strata'. The first one, stretching from the early Paleocene (66 million years ago, Ma) to the late Eocene (*ca.* 37 Ma), is characterized by the early establishment and radiation of endemic lineages, mostly xenarthrans, metatherians and native ungulates. Then, from the early Oligocene (*ca.* 33 Ma) until the Late Miocene-Early Pliocene (*ca.* 5 Ma), key morphological innovations appeared among native lineages, leading to a so-called 'faunal modernization' (9). In the meantime, rodents and primates, African lineages that most likely reached South America in the middle-late Eocene (10–12), diversified locally (4, 6). At the latest Miocene/Pliocene, this endemic fauna was massively disrupted. The closure of the Panama isthmus (13) paved the way for major faunal exchanges between North and South America, described as the 'Great American Biotic Interchange' (14), and immigrant taxa from North America (*e.g.,* carnivores, perissodactyls, artiodactyls, or proboscideans) appeared in the South American fossil record. In the few subsequent millions of years, many endemic South American lineages declined, yet went totally extinct (*e.g.,* litopterns, notoungulates, sparassodonts, glyptodonts, ground sloths).

Close to the limit between Simpson's first and second faunal strata, *ca.* 33.9 Ma, the Eocene−Oligocene transition (EOT) marked the most dramatic Cenozoic climatic change episode worldwide (15). At that time, simultaneously, global climate massively cooled down (16), ocean level dropped (17), and the whole Antarctic continent turned into a giant ice sheet (18). The prevailing mechanism proposed to explain these major environmental changes is the onset of the Antarctic circumpolar current (19). Concomitantly, a major biotic turnover among mammals, known as the 'Grande Coupure', occurred in Europe (20). This event, punctuated by the arrival of immigrant taxa from Asia, saw the demise of many endemic European lineages (21–23). Although European-oriented case studies dominate the literature about the topic, similar disruptions among mammalian faunas occurred at the same time in other regions of the world, such as Asia (24–26), North America (27, 28), Africa (29) or to some extent Madagascar (30). Recently, Hoyal Cuthill et al. (31) even came to rank this geological boundary as the second most important extinction event throughout the history of life.

In central and southern South America, substantial changes have been documented in metatherians (32, 33) and native ungulates (9, 34) near the EOT. As an echo to the 'Grande Coupure', Goin et al. (33) even introduced the term 'Bisagra Patagónica' (*Patagonian Hinge*) to characterize the changes among metatherian communities in Patagonia possibly related to the EOT. General morphological trends have been highlighted in 'modernized' notoungulate faunas, with a net increase in body mass and cheek teeth's crown height (35). The latter changes, by analogy with the evolutionary fate

of extant groups, suggested the emergence of the grazing feeding mode, and was postulated to result from the expansion of grasslands, promoted by post-EOT climate cooling and aridification (34, 36, 37). In northern South America, changes in marsupial and rodent communities around the EOT have also been suggested despite the paucity of known Paleogene low-latitude fossil localities to date (38).

Despite general agreement that a faunal remodeling occurred in SAM communities near the EOT, the evolutionary tempo and mode remain unknown. At macroevolutionary scales, as we would expect in a mass extinction scenario, it is unclear whether this faunal renewal was characterized by extinction of Eocene lineages followed by diversification of the surviving ones (e.g., 38), or whether lineages gradually transitioned until they became 'modernized'. A crucial question underlying these conflicting macroevolutionary hypotheses is whether or not extinction occurred in the tropics, and at what level. Indeed, it has long been postulated that the climatic stability of tropics would make tropical lineages less vulnerable to extinction than extratropical lineages (40). Also, the ecological selectivity and the likely drivers of this apparent faunal transition have remained underexplored. For instance, there is so far no consensus regarding the role of temperature (41, 42) or grassland expansion (43) in shaping the macroevolutionary fate of SAMs. Finally, there is a lack of integrative frameworks at the continental scale, with most case studies at the local scale, mostly in southern South America. Nevertheless, the Paleogene mammal fossil record in South America is spatially and temporally uneven. Spatial gaps cover large areas, such as most of Amazonia, and important time intervals remain unsampled (*SI Appendix,* **Fig. S1** and **S3**). Accordingly, it has been historically challenging to address questions regarding the history of SAMs at the continental scale.

Here, we aim to fill these gaps by examining the available fossil record of SAMs. We assembled a genus-level fossil dataset consisting of 3,378 occurrences (distributed in 1,115 species, 536 genera, 96 families, and 18 orders) spanning from the late Paleocene to the Early Miocene. Relying on a fossil-based Bayesian birth-death framework accounting for variable preservation rates through time and across taxa (44), we estimated the tempo and modes of the mammalian diversification dynamics in South America throughout the Eocene–Oligocene interval (*ca.* 56–23 Ma). We then disentangled the underlying taxonomic, functional, and geographic (tropical vs. extratropical) bases of the inferred continent-scale patterns of diversity and diversification among SAM faunas. We finally quantified the most likely biotic and abiotic drivers explaining their diversification dynamics.

Results and Discussion

No mass extinction: South American mammal diversity gradually declined well before the EOT

We analyzed the fossil database (**Tab S1**) both at the genus and species levels using the process-based Bayesian framework of diversification accounting for varying preservation implemented in PyRate (45). Our results highlight that the overall mammal diversity gradually declined from the end of the early Eocene–shortly after the Early Eocene Climate Optimum (EECO, 45)–to the end of the early Oligocene (decline by respectively 34% and 52% in the number of genera and species between 48 and 32 Ma), and then further increased in the late Oligocene (**Fig. 1D** and *SI Appendix*, **Fig. S8-11**). No massive loss of lineages appears to us at the EOT. This diversity trajectory results from a significant decrease in origination rate during the early Eocene (**Fig. 1B** and *SI Appendix*, **Fig. S8-11**). Additionally, we recover a joint significant increase in the pace of origination and extinction (i.e., increased turnover) during the late Eocene, with the extinction rate always being higher than the origination rate (slightly negative net diversification rate; **Fig. 1B-C** and *SI Appendix*, **S8-11**). Similar diversification patterns are recovered when analyzing the dataset at the genus or species level (*SI Appendix,* **Fig. S8-11**), after removing singletons (*SI Appendix*, **Fig. S12-13**) or disabling several occurrences of the same lineage that co-occur temporally and geographically (*SI Appendix,* **Fig. S14-15**). Moreover, general trends in diversity and diversification dynamics are conserved when working with occurrences assigned to South American Land Mammal Ages (SALMAs; *SI Appendix,* **Fig. S9** and **S11**) instead of sub-epochs (see ***Methods***; *SI Appendix*, **Fig. S1-2** and *Extended Material and Methods*), or when considering attempts to derive early Oligocene ages to east Amazonian occurrences originally assigned to an Eocene age (*SI Appendix*, **Fig. S32**).

Recently, an analysis of the global Phanerozoic fossil record classified the EOT as the second most intense mass extinction episode (31). Although this ranking was unexpectedly high, drastic extinctions at the EOT are supported by analyses of the European (20) and Asian (24) mammal fossil record. Applying a methodological framework similar to ours, Weppe et al. (23) recovered a strong extinction signal among endemic Western European artiodactyls at the EOT, with the loss of 62% of genera and 75% of species in only 1 My. Other studies working on mass extinctions illustrated similarly high levels of lineage loss for various study models, for instance in insects at the Permian/Triassic boundary (82% genus loss) (47) or in elasmobranchs – sharks, skates and rays – at the Cretaceous/Paleogene boundary (44.94% genus and 62.6% species loss) (39). Here, given the relatively small amount of lineages lost at the Eocene−Oligocene boundary (19% genera, 25% species), our results are not consistent with a mass extinction event among SAMs at the EOT. Instead, we highlight a long-term decline in SAM diversity, from the middle Eocene onward, contrasting with the expected short temporality of a mass extinction crisis. To our knowledge, our work is the first to provide quantitative support for such a pattern. These differences between South America and other continents could come from the tropical nature of a significant part of the landmass. Stemming from the cornerstone hypothesis of Wallace linking the striking similarities between tropical biomes from all-over the world to the uniformity of tropical climate across space and (shallow) time (40), tropical climate stability would act as a buffer for

tropical lineages against extinction. Also, the isolated condition of the landmass has been proposed as a probable cause explaining the singularity of SAM near-EOT macroevolutionary fate, as it greatly limited the possibilities for immigration events. Yet, immigrations were hypothesized to have played a key role in EOT-related extinctions in other parts of the world (3, but see 22).

Ubiquitous taxonomic – but not ecological – turnover among the main mammalian groups across the study period

Our analyses of the overall SAM diversification dynamics failed at characterizing any mass extinction event at the time of the EOT, but recovered a late-Eocene increase in mammal turnover (joint increase in origination and extinction rates), followed by an Oligocene waxing-and-waning diversity (**Fig. 1B** and **D**). As a result, Eocene and Oligocene SAMs appear taxonomically dissimilar. Indeed, the proportion of shared genera between each fauna, represented by the Jaccard's similarity index, is below 20% for four out of the five main groups we studied (**Fig. 1A** and *SI Appendix*, **Fig. S38**). The corrected genus longevity estimates corroborate results already established in the literature about mammal taxonomic replacement near the EOT, but also highlight previously undescribed patterns (**Fig. 1A** and *SI Appendix*, **Fig. S18-21**).

For notoungulates, the most taxon-rich order of our dataset (encompassing a third of our total occurrences; *SI Appendix*, **Tab. S1**), our inferences corroborate a long-recognized turnover at the order scale between the late Eocene and the early Oligocene (9). This goes in line with a recent species-level analysis of southern South American notoungulate diversification dynamics, pointing toward an enhanced turnover in the early Oligocene, mostly among smaller-sized taxa (34). According to our findings, this turnover is particularly striking at the family level, with the synchronous extinction and origination of three (Archaeopithecidae, Notostylopidae, and Oldfieldthomasiidae) and four families (Homalodontheriidae, Hegetotheriidae, Mesotheriidae, and Toxodontidae), respectively (*SI Appendix*, **Fig. S19-20**). Most of these newly-arising families, in addition to two surviving ones (Archaeohyracidae and Interatheriidae), convergently evolved larger body sizes and higher teeth crown height (hypsodonty) than their basal counterparts, mostly during the Oligocene (though the first records of a hypsodont notoungulate lineage dates back to the middle Eocene, 20 Million years before its first record outside South America) (35, 36). As notoungulates likely represented a huge proportion of herbivorous lineages, these innovations likely implied changes in the architecture of the primary feeder mammalian guild between the Eocene and the Oligocene ecosystems at continent scale.

Considering the other native ungulate orders (i.e., Litopterna, Astrapotheria and Pyrotheria), apart from the late Eocene extinction of Trigonostylopidae (Astrapotheria), evidence for higher-level taxonomic changes near the EOT is less obvious (*SI Appendix*, **Fig. S23**). However, there seems to be a strong intra-family taxonomic renewal among most litopterns (i.e., Proterotheriidae, Macraucheniidae, and Adianthidae) and astrapotheriids (Astrapotheria) between the Eocene and Oligocene. These groups have been affected by a diversity decline from the late Eocene to the early Oligocene (*SI Appendix*, **Fig. S16D-F and S17D-F**). Given that, just like notoungulates, these groups likely had herbivorous diets, the

highlighted changes also surely affected the architecture of the ecosystems between the Eocene and the Oligocene.

In the case of metatherians (*SI Appendix*, **Fig. S18**), our results are in line with previous findings about their taxonomic renewal near the EOT (3). On one hand, entire superfamilies or sub-orders like Bonapartherioidea or Polydolopiformes (both subclades of the order Polydolopimorphia according to Goin et al. (3)) went extinct during the early Oligocene, meanwhile others, like Argyrolagoidea (also a subclade of Polydolopimorphia according to Goin et al. (3)), Paleothentoidea (order Paucituberculata) and Hathliacynidae (order Sparassodonta) originated and/or diversified. We may precise that the superfamily Palaeothentoidea appeared in the middle-late Eocene with the two stem genera *Sasawatu* and *Perulestes*, but the Palaeotenthidae and Abderitidae families diversified from the early Oligocene onward. On the other hand, intra-clade taxonomic replacement occured among Borhyaenoidea (Sparassodonta) and Microbiotheria. As mentioned before, Goin et al. (33) established that the most dramatic turnover among metatherian faunas occurred near the EOT (the 'Bisagra Patagónica'). Our corrected genus age reconstructions clearly bring qualitative support to such a macroevolutionary fate. However, when estimating metatherian diversification dynamics, no significant rate shift was found, and the overall number of genera through time remained stable (*SI Appendix*, **Fig. S17M-O)**. Quantitatively, our diversification analyses supported a constant turnover rate across the Eocene−Oligocene interval, which is likely a consequence of the low representation of metatherian in our dataset (219 occurrences, 54 genera).

As for cingulates, representing the majority of our xenarthran occurrences, we highlight a slowdown in Dasypodinae diversity, and the origin of Euphractinae in the middle-late Eocene (*SI Appendix*, **Fig. S21**), in agreement with Ciancio et al. (48). Just like for metatherians, our diversification reconstructions provided support for a constant-rate diversification throughout the period of interest, with a stable number of genera (*SI Appendix*, **Fig. S16I-L** and **17I-L**).

Regarding caviomorph rodents, the oldest representatives of the clade are found to originate in the end of the Eocene (**Fig. 1A** and *SI Appendix*, **Fig. S22**). Then, the group diversified at a constant rate until it reached a mid-Oligocene peak in extinction rate (*SI Appendix*, **Fig. S16G-I** and **S17G-I**), and no main taxonomic replacement near the EOT is to be noticed.

To track the evolution of ecological composition between the Eocene and Oligocene SAM, we summarized trophic paleocommunities by four dental ecomorphotype-derived categories: herbivorous, carnivorous, insectivorous and omnivorous. We used the origination and extinction ages estimated by PyRate to assess the number of genera through time within each ecological category and further computed the relative proportion of each trophic category at the geological sub-epoch level (*SI Appendix*, **Fig. S1** and *Extended Materials and Methods*). Our findings illustrate that the structure of trophic paleocommunities remained stable throughout the entire time interval (**Fig. 2**). We report a slight trend toward an increase in the relative proportion of herbivorous lineages in assemblages of decreasing age, at the expanse of omnivorous and insectivorous. In addition, ecological dissimilarity increases with the

age difference between two assemblages, but remains low (below 25%), especially between the late Eocene and early Oligocene assemblages, when it equals 6.1% (**Fig. 2**).

Our results provide support for a taxonomic renewal between Eocene and Oligocene SAM faunas, with few changes in the architecture of ecosystems, thereby suggesting intra-guild renewal. Interestingly, the onset of this faunal turnover temporally matches the timing of 'the most fundamental biotic division in the Cenozoic' in the marine realm, that is, between the middle and the late Eocene (49).

Latitudinal heterogeneity in diversification histories

Since the late break-up of the Gondwana supercontinent ~130 Ma, the South American landmass has offered a duality between tropical and non-tropical habitats (2). This duality is particularly interesting as it allows for testing a long-standing question in macroevolution as to whether diversification processes occurred the same way inside and outside the tropics (40). Based on a time series of paleoclimate zone maps (50, 51), we assigned each of our occurrences a tropical or extratropical affinity (*SI Appendix*, **Fig. S3**), and analyzed genus-level diversification dynamics within each biome separately. Our findings revealed that extratropical genera exhibited diversity and diversification patterns extremely similar to those obtained from the complete dataset across the Eocene–Oligocene interval (**Fig. 3D-F** and *SI Appendix*, **Fig. S8-11**). Their diversity gradually declined from the middle Eocene to early Oligocene, with a late Eocene turnover increase (**Fig. 3D-F**). This proximity between extratropical and continent-wide patterns was expected, given that extratropical taxa constitute the majority of genera present in our dataset (85.8%, S*I Appendix,* **Tab. S10**). Nevertheless, results are different when constraining our analyses to tropical genera (**Fig. 3A-C**). No significant change was found in the tropical origination rate, and one significant negative shift was found for the tropical extinction rate in the late Oligocene (but see later for an interpretation of this extinction peak) (**Fig. 3A** and **S24**). Their inferred diversity curve exhibits an opposite trend to the one obtained from extratropical genera. Tropical genera diversity increased exponentially during the Eocene and reached a plateau in the early Oligocene (**Fig. 3C**). In the late Oligocene, our reconstructions tend to suggest that tropical mammals experienced a diversity decline associated to the aforementioned increase in extinction rate. We propose this apparent decline to result from the scarcity of low-latitude formations of Oligocene age, given that there are almost no tropical Deseadan (~29.4-24.2 Ma) mammal remains unearthed to date (though see 51), therefore more reflecting a sampling artifact rather than a true tropical SAM extinction in the late Oligocene. Consequently, after discarding this likely artefactual extinction peak, our results suggest that tropical lineages experienced no change in diversification rates, providing support for Wallace's theory of tropical stability (40). Also, when considering attempts to derive early Oligocene ages to east-Amazonian occurrences originally assigned to an Eocene age (53), the overall tropical diversity pattern remains unchanged. Indeed, the previously highlighted Eocene increase in diversity lasts a few more million years within the Early Oligocene, until the onset of the 'decline' – that we propose to be artefactual (*SI Appendix*, **Fig. S33**).

Our results suggest that highly distinct evolutionary regimes shaped tropical and extratropical mammal assemblages in South America. However, there is no clear evidence supporting commonly-

assumed macroevolutionary hypotheses regarding how tropics shaped diversification processes (**Fig. 3** and *SI Appendix*, **Fig. S25-S29**). Two macroevolutionary scenarios are usually invoked to explain the differences in diversity between tropical and extratropical biomes (54). On one side, tropical lineages would have higher origination rates due to the higher diversity of habitats offered by the tropics ('cradle' hypothesis). On the other, tropical climate stability would make tropical lineages less prone to extinction ('museum' hypothesis) (53, but see 54). Here, tropical lineages appear to have a higher origination and a lower extinction rate than their extratropical counterparts in the middle Eocene. This would typically be in line with Rolland et al. (56), who estimated temporal trends of speciation and extinction rates across latitudes using the mammal tree of life, and found that tropical mammals had a higher speciation and a lower extinction rate than their extratropical counterparts throughout the Cenozoic. More recently, an emphasis was put on higher-latitude tropical extinctions to explain the build-up of present-day tetrapod diversity (51, 57). In alternative scenarios, varying dispersal rates can explain differences between tropical and extratropical diversity (58). There is a consensus that tropical-to-extratropical transitions are prevalent, supporting the so-called 'out-of-the-tropics' hypothesis (51), although extratropical-to-tropical transitions have been suggested (57).

Drivers behind the Eocene−Oligocene macroevolutionary dynamics of SAM

After exploring the dynamics of SAM diversity and diversification, we investigated their underlying drivers, addressing: what drove SAM diversity to decline in the 52-33.9 Ma interval? What caused their late Eocene increase in turnover? How do we explain such levels of taxonomic dissimilarity between Eocene and Oligocene SAM?

Our Multivariate Birth-Death (MBD) analyses indicate that the dissimilar Eocene and Oligocene faunas were ruled by different drivers (**Fig. 4**). Overall, diversity-dependent effects largely impacted SAM diversification history throughout our study period, but these processes shaped both faunas differently. We recovered strong negative correlations of Eocene (post-EECO, 52-33.9 Ma) origination rate (correlation parameter G_λ = -3.24, shrinkage weight [w_λ] = 0.89) and Oligocene extinction rate (G_μ = -2.43, w_μ = 0.83) with self-diversity (**Fig. 4,** *SI Appendix,* **Tab. S3-6**). This suggests that Eocene mammal origination decreased when their diversity increased, which can be interpreted as a carrying capacity effect, that can occur at macroevolutionary scales (59). The other diversity-dependent correlation indicates that the Oligocene mammal extinction rate decreased when their diversity increased. In the framework of the marked taxonomic turnover highlighted by our analyses, this effect might have arisen from facilitating interactions between recently-originated taxa (see forthcoming paragraph), but it could also be indirectly related to enhanced ecosystems productivity or niche partitioning events, which cannot be captured by the MBD analyses.

We further investigated the effect of genus age on its extinction probability. No effect of taxon age could be retrieved from the analysis of the 'early' dataset (56-39 Ma, *i.e.,* before the increase in extinction rate at 39 Ma, *SI Appendix,* **Fig. S10** and **S41**), but we found evidence for a significant Age-Dependent Extinction (ADE) in the 'late' dataset (39-23.03 Ma), with an increasing probability of extinction with decreasing genus age (*SI Appendix,* **Fig. S41** and **Tab. S9**). In the framework of a faunal renewal, we could have expected the opposite relationship, where older lineages would be more likely to go extinct than recently-originated ones. One possible explanation could come from the concomitant increase in origination rate that we discussed previously (**Fig. 1B** and *SI Appendix,* **Fig. S10A**). The latter would counterbalance the higher prevalence of these newly-originated genera to become extinct, in turn leading to a progressive faunal turnover, as older lineages naturally go extinct. A similar negative relationship between taxon age and extinction probability has been frequently illustrated, for several study models and taxonomic scales (60–64). Factors proposed to explain this ADE pattern at the genus level often include genus range size, species richness and sampling bias (61). Here, fossil sampling bias is less likely to affect our results as PyRate already accounts for it. The current spatial (*SI Appendix,* **Fig. S3**) and taxonomic (*SI Appendix,* **Fig. S30**) incompleteness of our data does not allow us to reliably test either of the two remaining factors.

The MBD analyses also provided support for a positive correlation between global temperature and Eocene mammal origination rate (G_λ = 0.24, w_λ = 0.82). This explains the previously-described gradual decline in SAM diversity in the mid-late Eocene, qualitatively matching with the post-EECO overall decline in temperature (**Fig. 1D** and **4B**). It is now clearly established that temperature change directly impacts biodiversity, at every timescales (65–67), and temperature was already identified as a key driver influencing the diversification of an endemic European artiodactyl family at the EOT (68). This said, based on isotope analyses of Patagonian ungulate enamel or on paleobotanical data, it has been proposed that the South American climate, at least in the Southern part of the continent, remained merely stable across the Eocene−Oligocene interval (41, 42, 69). However, as illustrated by Antoine et al. (38), we assume that the spatial scale (i.e., continental vs. global) does not affect the trends and directionality of temperature changes through time, but rather their amplitude. Hence, in the framework of our MBD analyses, the use of a global estimate of paleotemperature is still relevant, as we are more interested in trends than having actual paleotemperature values. Also, to date, no regional paleotemperature reconstruction for the South American continent has been produced with the same resolution as the global estimate used in this study (16).

We obtained a weak but significant positive correlation between the Oligocene mammal extinction rate and the Andean uplift (G_μ = 0.02, w_μ = 0.87) (**Fig. 4,** *SI Appendix,* **Tab. S3-6**). Mountain-building processes are known to greatly influence species diversity (70), and previous studies illustrated the key importance of the Andes in shaping diversity patterns of a wide range of South-American organisms, even in the early stages of the build-up of the chain (71–73). In a context of active margin, the Andean orogeny has been associated with volcanic activity, which, in conjunction to subsequent forest fires, resulted in a massive dust emission. This dust emission has been postulated to promote grazer-like herbivore

origination and diversification, in particular at the EOT and thereafter (42, 74). Due to the high proportion of herbivores in our dataset (S*I Appendix,* **Tab. S10** and **Fig. 2**), we could have expected Andean uplift to be either positively related to SAM origination, negatively related to SAM extinction, or both. Here, our results suggest that Andean uplift promoted extinction among SAM faunas, thus not providing support for any of the previously-stated hypotheses. Instead, they lead us to hypothesize that the building of the Andes, possibly by reshaping the landscapes locally, re-organizing climate advections, triggering volcanism or any other factor, was an obstacle, rather than a facilitator, for Oligocene mammal diversification.

Interestingly, none of our proxies for land opening, *i.e.,* phytolith-derived floral composition – proxy for grassland spreading, or habitat openness (43) – and relative Leaf Area Index (rLAI) – proxy for forest density (75) – was found to be correlated with any diversification rate, even when constraining our analyses to notoungulates, our most taxon-rich herbivorous clade (S*I Appendix,* **Fig. S35**). The convergent evolution of high-crowned cheek teeth and larger body sizes among several notoungulate families near the EOT, suggesting the emergence of the grazing feeding mode, has long been regarded as evidence for the expansion of grasslands in response to climate cooling and aridification (36). However, subsequent studies highlighted that grasslands did not spread that much during the mid-Eocene to Oligocene of Patagonia, meanwhile hypsodont taxa evolved and diversified (43), and more generally, that South American paleobiome composition remained stable throughout that period (69). In addition, trait-based correlation analyses failed at recovering any temporal relation between the evolution of hypsodonty and the abundance of open habitats (35). Here, our results for the entire dataset are pointing in the same direction, thereby suggesting that mammal diversification was not influenced by the proportion of open habitats in South America. As mentioned earlier, this could be a direct consequence of the apparent biome stability of the continent at that time, and could probably represent one additional feature making the macroevolutionary behavior of SAMs near the EOT so unique compared to other regions of the world.

When carrying out the MBD analyses without partitioning Eocene and Oligocene faunas, we still found strong negative correlations of origination (G_λ = -2.16, w_λ = 0.90) and extinction (G_μ = -2.18, w_μ = 0.81) rates with self-diversity, and a weak positive correlation of extinction rate with the Andean uplift (G_μ = 0.003, w_μ = 0.70) (*SI Appendix,* **Fig. S34, Tab. S3-6**). However, we no longer retrieved any correlation of origination rate with temperature, highlighting the prominent and exclusive role of temperature in shaping Eocene mammal diversity.

Limits and perspectives

One of the main limitations of our work comes from the fact that many of the taxa we are dealing with (e.g., notoungulates, sparassodonts, glyptodons, ground sloths, etc.) have no modern representatives. This raises a major issue for the inferences about their ecology as we do not have any proper reference to lean on. For instance, many studies – including the present work – failed at relating

grassland spreading with the apparition of high-crowned and/or ever-growing cheek teeth, whereas it is known to be the case in the history of iconic extant groups, such as horses (36).

Next, as previously mentioned, our data was particularly subject to spatial heterogeneity (34). There is a sampling gap in Amazonia (*SI Appendix,* **Fig. S3**), yet known to be the cradle for most Neotropical groups, ranging from angiosperms to vertebrates (76). The still poorly-known record of fossil mammals from this region surely hides part of the picture of the continent-scale mammal diversification, and even more considering the spatial heterogeneity of diversity dynamics (77, 78). We tested the robustness of our interpretations regarding this spatial heterogeneity by carrying out sensitivity analyses to evaluate the extent to which it affected our results, by subsampling our occurrence data to unique taxa-locality combinations, leading to no major difference with the trends we derived from our complete dataset (*SI Appendix,* **Fig. S14** and **S33**).

Temporal and taxonomic completeness were also sources of limitations. As for temporal biases, we saw that gaps remain in the South American Land Mammal Age scale, illustrating the temporal sparsity of the SAM fossil record (*SI Appendix,* **Fig. S1**). This adds some degree of uncertainty to our taxon age estimations, and further diversity and diversification inference (34). To intend to cope with this issue, we assigned each of our occurrences with the boundaries of the sub-epoch they most overlapped with (*SI Appendix,* **Fig. S2**). In fact, such an age smoothing did not lead to any major difference in our diversification analyses, further illustrating PyRate's ability to deal with data incompleteness. Furthermore, our work also led us to appreciate the unequal representation of some lineages compared to others, with around 36% of our genera and 54% of our species only represented by a single occurrence in our dataset (*i.e.,* singletons) (*SI Appendix,* **Tab. S1**). As a result, our average preservation rates per lineages were low (*SI Appendix,* **Fig. S30-31**), below the values that are usually observed in recent studies (23, 79). This said, removing singletons did not seem to have any major effect on the inferred diversification patterns (*SI Appendix,* **Fig. S12-13** and **S32**). Overall, despite our sensitivity tests, our dataset undersamples South America's past mammalian diversity, and no statistical framework may fully recover the entire picture of its underlying macroevolutionary processes.

Here, we provide the first integrative study of the macroevolutionary fate of the extinct mammals from South America across the Eocene−Oligocene interval using the fossil record. Interestingly, our results challenge the occurrence of a landmass-scale mass extinction of mammals at the EOT (31), contrary to what has been suggested for other regions of the world (e.g. 23). Rather, we showed that SAM underwent a temperature- and diversity-dependent gradual diversity decline during the Eocene, followed by an Oligocene waxing-and-waning likely associated with the build-up of the Andes and other diversity-dependent effects. Remarkably, we found that lineages inhabiting tropical and extratropical areas had very different macroevolutionary histories, supporting Wallace's theory of tropical stability (40). Enhanced knowledge of the past of SAM will provide key insights into the origin and dynamics of one of the world's most species-rich regions, a central and historic topic in the field of macroevolution.

Material and Methods

Additional methodological details are provided in the *SI Appendix*.

Fossil data compilation and analytical framework. We downloaded and cleaned all genus-level South American terrestrial mammal occurrences from *The Paleobiology Database* (https://paleobiodb.org/) spanning the late Paleocene to the early Miocene (60-16 Ma) (3,384 occurrences; *SI Appendix, Extended Materials and Methods* and **Tab. S1**). Cleaning consisted of a manual revision of the taxonomic name (e.g., synonymies, missing open nomenclature elements, typos) and time range of each occurrence (*SI Appendix,* **Fig. S4** and *Manual Cleaning Details*). Using paleocoordinate reconstructions (80, 81) and paleobiome maps (50), we assigned each occurrence a tropical or extratropical affinity, and collapsed their associated dental ecomorphotype-derived trophic classes into four categories: carnivorous, herbivorous, omnivorous and insectivorous (S*I Appendix,* **Tab. S10**).

We analyzed our database using PyRate v.3 (82), and approximated the posterior distribution of the origination and extinction times (T_s and T_e, respectively) of each genus and the rate of the preservation process using the RJMCMC algorithm. We then used these T_s and T_e to estimate the underlying diversification process (origination and extinction rates) with the Birth-Death model with Constrained Shifts (BDCS) (83) (*SI Appendix, Extended Materials and Methods*).

We ran the RJMCMC model for 50 million generations and sampled every 50,000, with a time-dependent preservation process allowing for rate shift between geological stages (*SI Appendix,* **Fig. S5-6** and *Extended Materials and Methods*). We allowed for a gamma-distributed preservation heterogeneity across lineages. We ran the BDCS model for 10 million generations, sampled every 10,000, and allowed diversification (i.e., origination and extinction) rates to vary between each geological sub-Epochs (*SI Appendix,* **Fig. S1**). Diversification analyses were replicated 20 times after randomly drawing fossil ages between their upper and lower age boundaries, and posterior estimates across all replicates that achieved convergence (n=11, *SI Appendix* **Fig. S40**) were combined. To test the robustness of our macroevolutionary inference, we conducted sensitivity analyses by either removing singletons or subsampling our fossil database to unique locality-lineage combinations *(SI Appendix, Extended Materials and Methods*). We assessed the convergence of each parameter with the pymc 5.9.2 python library (84). We considered parameters achieved convergence if their Effective Sample Size (ESS) was above 200.

Age-dependent Extinction (ADE) model. We assessed the effect of taxon age on its extinction probability by fitting the ADE model to our genus-level occurrence data (60). We ran the model for 100 million generations and sampled every 50,000, with preservation rates varying between geological stages and across lineages according to a *Gamma* model. We focused on the shape (ϕ) of the Weibull distribution, knowing that $\phi < 1$ indicates a decreasing extinction probability with increasing taxon age and $\phi > 1$ indicates an increasing extinction probability with increasing taxon age (no effect if $\phi = 1$). ϕ was considered as significantly different from one if one was excluded from a significant proportion of its

posterior distribution. We performed 20 independent ADE analyses of randomized datasets before and after the increase in turnover to assess the age selectivity of this taxonomic renewal (*SI Appendix,* **Fig. S8-11**, **S41** and *Extended Materials and Methods*). We monitored parameter convergence with the pymc 5.9.2 python library, and parameters were considered convergent if their ESS was above 200.

***Selection of environmental variables*.** To investigate possible environmental correlates for the changes in SAM diversification dynamics over the Eocene−Oligocene interval, we selected two global (i.e., atmospheric temperature and sea level) and four continental-scale (i.e., Andean uplift, Neotropical plant diversity, forest density and habitat openness) variables (*SI Appendix,* **Fig. S39** and **Tab. S2**). Temperature is known for influencing macroevolutionary processes across several groups, including mammals (67, 85), and sea level can impact the connectivity of habitats. Even in its early phase, the Andean uplift was evidenced as a major diversification driver for many South American groups (72). Diversity of SAM, in particular herbivorous taxa, can be controlled by plant diversity. Finally, relative Leaf Area Index (proxy for forest density, 72) and patterns of relative abundance of open habitats (35, 43, 86) are both indicators of the relative abundance of grasslands, which has long been regarded as shaping herbivore diversity (36). As highlighted by Weppe et al. (23), it is important to consider regional-scale variables because environmental changes across the Eocene−Oligocene interval were shown to be regionally heterogeneous (69, 87).

Multivariate Birth-Death (MBD) model. We carried out environment-dependent diversification analyses involving the aforementioned variables by running the MBD model included in PyRate (88). This model carries out two independent correlations involving a set of environmental covariates and diversification rates (λ and μ) newly-estimated from empirical T_s and T_e. Each variable is assigned to two correlation coefficients, one for the correlation with λ ($G_{i,\lambda}$, where i is the index of the variable in the set of covariates) and the other for the correlation with μ ($G_{i,\mu}$). An MCMC algorithm jointly estimates baseline origination and extinction rates and all the G_λ and G_μ, while controlling for over-parameterization. Each G_λ and G_μ is assigned a shrinkage weight ($w(G_\lambda)$ or $w(G_\mu)$), ranging between 0 and 1, testing the significance of the correlation. A correlation of coefficient $G_{\lambda,i}$ is considered significant if $w(G_{\lambda,i}) > 0.5$ and if a sufficiently high proportion of its posterior density does not overlap with 0. Each set of MBD analyses was run across 10 million iterations, sampling every 10,000. We carried out exponential correlations. Parameter convergence (i.e., ESS > 200) was assessed using the *pymc* 5.9.2 Python library (84).

Data, Materials, and Software Availability

All the occurrence data used in this study are available on a Figshare repository (https://doi.org/10.6084/m9.figshare.26495989) and all the data analysis and visualization codes have been deposited in GitHub (https://github.com/Buffan3369/Neotropical_mammals.git and https://github.com/Alexis-Marion/CorsaiR.git).

Acknowledgments

We are grateful to all the people who collected and entered the data we used in The Paleobiology Database. Moreover, we thank Chris Scotese (Northwestern Univ., Evanston, USA), Ignacio Quintero (IBENS, France) and Miranta Kouvari for their data sharing; Gilles Escarguel (LEHNA, Lyon, France), Myriam Boivin (CONICET, San Salvador de Jujuy, Argentine) and Ana Rodrigues (CEFE, Montpellier, France) for their useful feedbacks on the present study. Also, we thank Alexis F.P. Marion (ISEM, France) for coding collaborations and thoughtful remarks; and all members of the *Phylogénie et Évolution Moléculaire* and *Paléontologie* teams at ISEM for their useful inputs and feedback on the present work. This research was supported by the French *Agence Nationale de la Recherche* (ANR) in the framework of the LabEx CEBA (ANR-10-LABX-25-01; strategic project EMERGENCE). L.B. was funded by a grant offered by the *École Normale Supérieure de Lyon*. N.S. was funded by the Brazil Conselho Nacional de Desenvolvimento Científico e Tecnológico (CNPq) grant nº 443571/2023-6. This is Paleobiology Database publication no. **XXX** and ISEM-Sud article no. **202X-XXX**.

References

1. M. R. Willig, D. M. Kaufman, R. D. Stevens, Latitudinal Gradients of Biodiversity: Pattern, Process, Scale, and Synthesis. *Annu. Rev. Ecol. Evol. Syst.* **34**, 273–309 (2003).

2. C. R. Scotese, An Atlas of Phanerozoic Paleogeographic Maps: The Seas Come In and the Seas Go Out. *Annu. Rev. Earth Planet. Sci.* **49**, 679–728 (2021).

3. F. J. Goin, M. O. Woodburne, A. N. Zimicz, G. M. Martin, L. Chornogubsky, *A brief history of South American Metatherians: evolutionary contexts and intercontinental dispersals*, Springer Dordrecht (2016).

4. M. Boivin, L. Marivaux, P.-O. Antoine, L'apport du registre paléogène d'Amazonie sur la diversification initiale des Caviomorpha (Hystricognathi, Rodentia): implications phylogénétiques, macroévolutives et paléobiogéographiques. *Geodiversitas* **41**, 143–245 (2019).

5. D. A. Croft, J. N. Gelfo, G. M. López, Splendid Innovation: The Extinct South American Native Ungulates. *Annu. Rev. Earth Planet. Sci.* **48**, 259–290 (2020).

6. R. M. D. Beck, D. de Vries, M. C. Janiak, I. B. Goodhead, J. P. Boubli, Total evidence phylogeny of platyrrhine primates and a comparison of undated and tip-dating approaches. *J. Hum. Evol.* **174**, 103293 (2023).

7. J. V. Tejada, *et al.*, Bayesian Total-Evidence Dating Revisits Sloth Phylogeny and Biogeography: A Cautionary Tale on Morphological Clock Analyses. *Syst. Biol.* **73**, 125–139 (2024).

8. G. G. Simpson, *Splendid isolation : the Curious History of South American Mammals*, Yale University Press, New Haven (1980).

9. D. A. Croft, J. J. Flynn, A. R. Wyss, The Tinguiririca Fauna of Chile and the early stages of "modernization" of South American mammal faunas. *Arq. Mus. Nac. Rio Jan.* **66**, 191–211 (2008).

10. P.-O. Antoine, *et al.*, Middle Eocene rodents from Peruvian Amazonia reveal the pattern and timing of caviomorph origins and biogeography. *Proc. R. Soc. B Biol. Sci.* **279**, 1319–1326 (2011).

11. M. Bond, *et al.*, Eocene primates of South America and the African origins of New World monkeys. *Nature* **520**, 538–541 (2015).

12. L. Marivaux, *et al.*, An eosimiid primate of South Asian affinities in the Paleogene of Western Amazonia and the origin of New World monkeys. *Proc. Natl. Acad. Sci.* **120**, e2301338120 (2023).

13. C. Montes, *et al.*, Middle Miocene closure of the Central American Seaway. *Science* **348**, 226–229 (2015).

14. L. G. Marshall, Land Mammals and the Great American Interchange. *Am. Sci.* **76**, 380–388 (1988).

15. H. K. Coxall, P. N. Pearson, "The Eocene–Oligocene Transition" in *Deep-Time Perspectives on Climate Change: Marrying the Signal from Computer Models and Biological Proxies*, M. Williams, A. M. Haywood, F. J. Gregory, D. N. Schmidt, Eds. (Geological Society of London, 2007), pp. 351–387.

16. T. Westerhold, *et al.*, An astronomically dated record of Earth's climate and its predictability over the last 66 million years. *Science* **369**, 1383–1387 (2020).

17. K. G. Miller, *et al.*, Cenozoic sea-level and cryospheric evolution from deep-sea geochemical and continental margin records. *Sci. Adv.* **6**, eaaz1346 (2020).

18. Z. Liu, *et al.*, Global Cooling During the Eocene-Oligocene Climate Transition. *Science* **323**, 1187–1190 (2009).

19. A. Toumoulin, *et al.*, Quantifying the Effect of the Drake Passage Opening on the Eocene Ocean. *Paleoceanogr. Paleoclimatology* **35**, e2020PA003889 (2020).

20. H. G. Stehlin, Remarques sur les faunules de mammifères des couches éocènes et oligocènes du Bassin de Paris. *Bull. Société Géologique Fr.* 488–520 (1909).

21. S. Legendre, *et al.*, Évolution de la diversité des faunes de Mammifères d'Europe occidentale au Paléogène (MP 11 à MP 30). *Bull. Société Géologique Fr.* **162**, 867–874 (1991).

22. G. Escarguel, S. Legendre, B. Sigé, Unearthing deep-time biodiversity changes: The Palaeogene mammalian metacommunity of the Quercy and Limagne area (Massif Central, France). *Comptes Rendus Geosci.* **340**, 602–614 (2008).

23. R. Weppe, F. L. Condamine, G. Guinot, J. Maugoust, M. J. Orliac, Drivers of the artiodactyl turnover in insular western Europe at the Eocene–Oligocene Transition. *Proc. Natl. Acad. Sci.* **120**, e2309945120 (2023).

24. J. Meng, M. C. McKenna, Faunal turnovers of Palaeogene mammals from the Mongolian Plateau. *Nature* **394**, 364–367 (1998).

25. B. P. Kraatz, J. H. Geisler, Eocene–Oligocene transition in Central Asia and its effects on mammalian evolution. *Geology* **38**, 111–114 (2010).

26. J. Sun, *et al.*, Synchronous turnover of flora, fauna and climate at the Eocene–Oligocene Boundary in Asia. *Sci. Rep.* **4**, 7463 (2014).

27. B. Figueirido, C. M. Janis, J. A. Pérez-Claros, M. De Renzi, P. Palmqvist, Cenozoic climate change influences mammalian evolutionary dynamics. *Proc. Natl. Acad. Sci.* **109**, 722–727 (2012).

28. R. K. Stucky, "24. Mammalian Faunas in North America of Bridgerian to Early Arikareean 'Ages' (Eocene and Oligocene)" in *Eocene-Oligocene Climatic and Biotic Evolution*, (Princeton University Press, 2014), pp. 464–493.

29. D. de Vries, S. Heritage, M. R. Borths, H. M. Sallam, E. R. Seiffert, Widespread loss of mammalian lineage and dietary diversity in the early Oligocene of Afro-Arabia. *Commun. Biol.* **4**, 11–72 (2021).

30. L. R. Godfrey, *et al.*, Mid-Cenozoic climate change, extinction, and faunal turnover in Madagascar, and their bearing on the evolution of lemurs. *BMC Evol. Biol.* **20**, 97 (2020).

31. J. F. Hoyal Cuthill, N. Guttenberg, G. E. Budd, Impacts of speciation and extinction measured by an evolutionary decay clock. *Nature* **588**, 636–641 (2020).

32. M. A. Abello, N. Toledo, E. Ortiz-Jaureguizar, Evolution of South American Paucituberculata (Metatheria: Marsupialia): adaptive radiation and climate changes at the Eocene-Oligocene boundary. *Hist. Biol.* **32**, 476–493 (2020).

33. F. J. Goin, M. A. Abello, L. Chornogubsky, Middle Tertiary marsupials from central Patagonia (early Oligocene of Gran Barranca): understanding South America's Grande Coupure. *Paleontol. Gran Barranca Camb. Univ Press N. Y. 448* 71–107 (2010).

34. A. Solórzano, M. Núñez-Flores, E. Rodríguez-Serrano, The rise and fall of notoungulates: How Andean uplift, available land area, competition, and depredation driven its diversification dynamics. *Gondwana Res.* (2024). https://doi.org/10.1016/j.gr.2024.08.002.

35. A. Solórzano, M. Núñez-Flores, Evolutionary trends of body size and hypsodonty in notoungulates and their probable drivers. *Palaeogeogr. Palaeoclimatol. Palaeoecol.* **568**, 110306 (2021).

36. G. L. Stebbins, Coevolution of Grasses and Herbivores. *Ann. Mo. Bot. Gard.* **68**, 75–86 (1981).

37. M. A. Reguero, A. M. Candela, G. H. Cassini, "Hypsodonty and body size in rodent-like notoungulates" in *The Paleontology of Gran Barranca. Evolution and Environmental Change through the Middle Cenozoic of Patagonia.*, (Cambridge University Press, 2010), pp. 358–367.

38. P.-O. Antoine, *et al.*, Biotic community and landscape changes around the Eocene–Oligocene transition at Shapaja, Peruvian Amazonia: Regional or global drivers? *Glob. Planet. Change* **202**, 103512 (2021).

39. G. Guinot, F. L. Condamine, Global impact and selectivity of the Cretaceous-Paleogene mass extinction among sharks, skates, and rays. *Science* **379**, 802–806 (2023).

40. A. R. Wallace, *Tropical Nature, and Other Essays* (Macmillan and Company, 1878).

41. M. J. Kohn, *et al.*, Climate stability across the Eocene-Oligocene transition, southern Argentina. *Geology* **32**, 621–624 (2004).

42. M. J. Kohn, *et al.*, Quasi-static Eocene–Oligocene climate in Patagonia promotes slow faunal evolution and mid-Cenozoic global cooling. *Palaeogeogr. Palaeoclimatol. Palaeoecol.* **435**, 24–37 (2015).

43. C. A. E. Strömberg, R. E. Dunn, R. H. Madden, M. J. Kohn, A. A. Carlini, Decoupling the spread of grasslands from the evolution of grazer-type herbivores in South America. *Nat. Commun.* **4**, 1478 (2013).

44. D. Silvestro, J. Schnitzler, L. H. Liow, A. Antonelli, N. Salamin, Bayesian Estimation of Speciation and Extinction from Incomplete Fossil Occurrence Data. *Syst. Biol.* **63**, 349–367 (2014).

45. D. Silvestro, N. Salamin, J. Schnitzler, PyRate: a new program to estimate speciation and extinction rates from incomplete fossil data. *Methods Ecol. Evol.* **5**, 1126–1131 (2014).

46. J. C. Zachos, G. R. Dickens, R. E. Zeebe, An early Cenozoic perspective on greenhouse warming and carbon-cycle dynamics. *Nature* **451**, 279–283 (2008).

47. C. Jouault, A. Nel, V. Perrichot, F. Legendre, F. L. Condamine, Multiple drivers and lineage-specific insect extinctions during the Permo–Triassic. *Nat. Commun.* **13**, 7512 (2022).

48. M. R. Ciancio, A. A. Carlini, K. E. Campbell, G. J. Scillato-Yané, New Palaeogene cingulates (Mammalia, Xenarthra) from Santa Rosa, Perú and their importance in the context of South American faunas. *J. Syst. Palaeontol.* **11**, 727–741 (2013).

49. D. R. Prothero, The Late Eocene-Oligocene Extinctions. *Annu. Rev. Earth Planet. Sci.* **22**, 145–165 (1994).

50. C. R. Scotese, H. Song, B. J. W. Mills, D. G. van der Meer, Phanerozoic paleotemperatures: The earth's changing climate during the last 540 million years. *Earth-Sci. Rev.* **215**, 103503 (2021).

51. I. Quintero, M. J. Landis, W. Jetz, H. Morlon, The build-up of the present-day tropical diversity of tetrapods. *Proc. Natl. Acad. Sci.* **120**, e2220672120 (2023).

52. P.-O. Antoine, R. Salas-Gismondi, F. Pujos, M. Ganerød, L. Marivaux, Western Amazonia as a Hotspot of Mammalian Biodiversity Throughout the Cenozoic. *J. Mamm. Evol.* **24**, 5–17 (2017).

53. K. E. Campbell, P. B. O'Sullivan, J. G. Fleagle, D. de Vries, E. R. Seiffert, An Early Oligocene age for the oldest known monkeys and rodents of South America. *Proc. Natl. Acad. Sci.* **118**, e2105956118 (2021).

54. G. L. Stebbins, "Trends of Angiosperm Phylogeny - The Ecological Basis of Diversity" in *Flowering Plants: Evolution above the Species Level*, The Belknap Press of Harvard University Press, (1974), pp. 156–170.

55. T. Vasconcelos, B. C. O'Meara, J. M. Beaulieu, Retiring "Cradles" and "Museums" of Biodiversity. *Am. Nat.* **199**, 194–205 (2022).

56. J. Rolland, F. L. Condamine, F. Jiguet, H. Morlon, Faster Speciation and Reduced Extinction in the Tropics Contribute to the Mammalian Latitudinal Diversity Gradient. *PLOS Biol.* **12**, e1001775 (2014).

57. A. S. Meseguer, F. L. Condamine, Ancient tropical extinctions at high latitudes contributed to the latitudinal diversity gradient. *Evolution* **74**, 1966–1987 (2020).

58. D. Jablonski, K. Roy, J. W. Valentine, Out of the Tropics: Evolutionary Dynamics of the Latitudinal Diversity Gradient. *Science* **314**, 102–106 (2006).

59. D. Storch, J. G. Okie, The carrying capacity for species richness. *Glob. Ecol. Biogeogr.* **28**, 1519–1532 (2019).

60. O. Hagen, T. Andermann, T. B. Quental, A. Antonelli, D. Silvestro, Estimating Age-Dependent Extinction: Contrasting Evidence from Fossils and Phylogenies. *Syst. Biol.* **67**, 458–474 (2018).

61. S. Finnegan, J. L. Payne, S. C. Wang, The Red Queen Revisited: Reevaluating the Age Selectivity of Phanerozoic Marine Genus Extinctions. *Paleobiology* **34**, 318–341 (2008).

62. F. L. Condamine, J. Romieu, G. Guinot, Climate cooling and clade competition likely drove the decline of lamniform sharks. *Proc. Natl. Acad. Sci.* **116**, 20584–20590 (2019).

63. D. Silvestro, *et al.*, A 450 million years long latitudinal gradient in age-dependent extinction. *Ecol. Lett.* **23**, 439–446 (2020).

64. J. G. Saulsbury, C. T. Parins-Fukuchi, C. J. Wilson, T. Reitan, L. H. Liow, Age-dependent extinction and the neutral theory of biodiversity. *Proc. Natl. Acad. Sci.* **121**, e2307629121 (2024).

65. IPCC, "Climate Change 2023: Synthesis Report. Contribution of Working Groups I, II and III to the Sixth Assessment Report of the Intergovernmental Panel on Climate Change [Core Writing Team, H. Lee and J. Romero (eds.)]" (IPCC, 2023).

66. F. L. Condamine, J. Rolland, H. Morlon, Macroevolutionary perspectives to environmental change. *Ecol. Lett.* **16**, 72–85 (2013).

67. F. L. Condamine, J. Rolland, H. Morlon, Assessing the causes of diversification slowdowns: temperature-dependent and diversity-dependent models receive equivalent support. *Ecol. Lett.* **22**, 1900–1912 (2019).

68. R. Weppe, M. J. Orliac, G. Guinot, F. L. Condamine, Evolutionary drivers, morphological evolution and diversity dynamics of a surviving mammal clade: cainotherioids at the Eocene–Oligocene transition. *Proc. R. Soc. B Biol. Sci.* **288**, 20210173 (2021).

69. M. J. Pound, U. Salzmann, Heterogeneity in global vegetation and terrestrial climate change during the late Eocene to early Oligocene transition. *Sci. Rep.* **7**, 43386 (2017).

70. A. Antonelli, *et al.*, Geological and climatic influences on mountain biodiversity. *Nat. Geosci.* **11**, 718–725 (2018).

71. A. Antonelli, J. A. A. Nylander, C. Persson, I. Sanmartín, Tracing the impact of the Andean uplift on Neotropical plant evolution. *Proc. Natl. Acad. Sci.* **106**, 9749–9754 (2009).

72. L. M. Boschman, F. L. Condamine, Mountain radiations are not only rapid and recent: Ancient diversification of South American frog and lizard families related to Paleogene Andean orogeny and Cenozoic climate variations. *Glob. Planet. Change* **208**, 103704 (2022).

73. P. Vallejos-Garrido, *et al.*, The importance of the Andes in the evolutionary radiation of Sigmodontinae (Rodentia, Cricetidae), the most diverse group of mammals in the Neotropics. *Sci. Rep.* **13**, 2207 (2023).

74. P. A. Selkin, *et al.*, Climate, dust, and fire across the Eocene-Oligocene transition, Patagonia. *Geology* **43**, 567–570 (2015).

75. R. E. Dunn, C. A. E. Strömberg, R. H. Madden, M. J. Kohn, A. A. Carlini, Linked canopy, climate, and faunal change in the Cenozoic of Patagonia. *Science* **347**, 258–261 (2015).

76. A. Antonelli, *et al.*, Amazonia is the primary source of Neotropical biodiversity. *Proc. Natl. Acad. Sci.* **115**, 6034–6039 (2018).

77. J. T. Flannery-Sutherland, D. Silvestro, M. J. Benton, Global diversity dynamics in the fossil record are regionally heterogeneous. *Nat. Commun.* **13**, 2751 (2022).

78. J. T. Flannery-Sutherland, *et al.*, Late Cretaceous ammonoids show that drivers of diversification are regionally heterogeneous. *Nat. Commun.* **15**, 5382 (2024).

79. C. Jouault, F. L. Condamine, F. Legendre, V. Perrichot, The Angiosperm Terrestrial Revolution buffered ants against extinction. *Proc. Natl. Acad. Sci.* **121**, e2317795121 (2024).

80. C. Scotese, N. M. Wright, PALEOMAP Paleodigital Elevation Models (PaleoDEMs) for the Phanerozoic PALEOMAP Project. (2018).

81. L. A. Jones, *et al.*, palaeoverse: A community-driven R package to support palaeobiological analysis. *Methods Ecol. Evol.* **14**, 2205–2215 (2023).

82. D. Silvestro, N. Salamin, A. Antonelli, X. Meyer, Improved estimation of macroevolutionary rates from fossil data using a Bayesian framework. *Paleobiology* **45**, 546–570 (2019).

83. D. Silvestro, B. Cascales-Miñana, C. D. Bacon, A. Antonelli, Revisiting the origin and diversification of vascular plants through a comprehensive Bayesian analysis of the fossil record. *New Phytol.* **207**, 425–436 (2015).

84. T. Wiecki, *et al.*, pymc-devs/pymc: v5.9.2. (2023). https://doi.org/10.5281/zenodo.4603970.

85. A. D. Barnosky, Distinguishing the effects of the Red Queen and Court Jester on Miocene mammal evolution in the northern Rocky mountains. *J. Vertebr. Paleontol.* **21**, 172–185 (2001).

86. L. Palazzesi, V. Barreda, Fossil pollen records reveal a late rise of open-habitat ecosystems in Patagonia. *Nat. Commun.* **3**, 1294 (2012).

87. A. Toumoulin, *et al.*, Evolution of continental temperature seasonality from the Eocene greenhouse to the Oligocene icehouse –a model–data comparison. *Clim. Past* **18**, 341–362 (2022).

88. S. Lehtonen, *et al.*, Environmentally driven extinction and opportunistic origination explain fern diversification patterns. *Sci. Rep.* **7**, 4831 (2017).

89. W. Gearty, L. A. Jones, rphylopic: An R package for fetching, transforming, and visualising PhyloPic silhouettes. *Methods Ecol. Evol.* **14**, 2700–2708 (2023).

90. W. Gearty, deeptime: Plotting Tools for Anyone Working in Deep Time. R package version 1.0.1. (2023). Deposited 2023.

Figure Captions

Figure 1. Bayesian inferences of taxon longevities (**A**), diversification (**B-C**) and diversity (**D**) dynamics of South American Mammals from the early Eocene to the late Oligocene (genus level).
The plot on the left (**A**) shows the longevity – i.e., interval between origination and extinction times – of each Eocene−Oligocene (373 out of 529 genera) South American mammal genus estimated with PyRate. J-values are Jaccard's similarity indices between the Eocene and Oligocene assemblages for each of the five groups. The right part of the panel shows the origination (blue) and extinction (red) rates through time (**B**), the net diversification rate (origination minus extinction) (**C**), and diversity (**D**) of all South American mammals throughout the study period. Full lines represent median estimates and ribbons their associated 95% higher posterior density. Light brown vertical bands indicate two key climate events, the Early Eocene Climate Optimum (EECO, ~53-51 Ma) and the Middle Eocene Climate Optimum (MECO, ~41.5-41 Ma). Stars on the (**B**) plot indicate significant rate shifts. Organisms' silhouettes are from PhyloPic (https://www.phylopic.org) and were added thanks to the R package rphylopic (89)**.** Silhouettes were contributed by Julián Bayona, 2016 (CC BY-SA 3.0), Kai R. Kaspar (CC BY-SA 3.0), Milena Cavalcanti, Patricia Pilatti & Diego Astúa (CC BY 4.0). Geological and South American Land Mammal Ages (SALMA) timescales were depicted thanks to the deeptime R package (90)**.**
Abbreviations for SALMA. Des: Deseadan, Ting: Tinguirirican, Must: Mustersan, Bar: Barrancan, Sap: "Sapoan Fauna", R: Riochican, It: Itaboraian. The small band between Tinguirirican and Deseadan is the "La Cantera fauna".

Figure 2. Evolution of genus-level functional assemblages between the Eocene and the Oligocene. The plot on the left shows the median (full line) and 95% HPD (ribbon) of estimated genus richness among the four trophic classes we defined based on dental ecomorphotypes: carnivorous (red), herbivorous (green), insectivorous (purple) and omnivorous (blue). Pie charts indicate the relative abundance of each trophic group for each sub-epoch. The matrix on the right shows pairwise Bray-Curtis dissimilarities between sub-epoch-level trophic communities, with darker color indicating higher dissimilarities. Geological and SALMA timescales were added thanks to the deeptime R package (90)**.**
Abbreviations for SALMA. Des: Deseadan, Ting: Tinguirirican, Must: Mustersan, Bar: Barrancan, Sap: "Sapoan Fauna", Rio: Riochican. The small band between Tinguirirican and Deseadan is "La Cantera fauna".

Figure 3. Diversification (**A-B** and **D-E**) and diversity (**C** and **F**) dynamics of South American mammal genera between the Eocene and Oligocene arranged by paleotropical affinity. Trends are assessed for the tropical (**A-C**) and extratropical (**D-F**) biomes. Origination and extinction rates are respectively depicted in blue and red. Stars indicate significant rate shifts. The timing and significance of rate shifts was assessed by the RJMCMC model (**Fig. S36-37**). Their difference, being the net diversification rate, is represented in black. Diversity through time is plotted in green. Light brown vertical bands indicate two

key climate events, the Early Eocene Climate Optimum (EECO, ~53-51 Ma) and the Middle Eocene Climate Optimum (MECO, ~41.5-41 Ma). The question mark on the tropical diversity-through-time plot (**C**) indicates that the late-Oligocene tropical diversity decline that is observed is likely due to the quasi-absence of fossil material of late Oligocene age (Deseadan SALMA) so far unearthed. The maps on the right show the localities of our extratropical (top) and tropical (bottom) occurrences. Geological and SALMA timescales were added thanks to the deeptime R package (90)**.**

Figure 4. Bayesian estimation of correlation parameters on origination (blue) and extinction (red) rates with paleoenvironmental variables. (**A**) We analyzed separately the post-Early Eocene Climate Optimum (52-33.9 Ma, top row) and Oligocene (33.9-23.03 Ma, bottom row) mammal faunas, therefore not treating our dataset as a whole throughout our study period. The 2.5%, 50% and 97.5% quantiles are indicated in the distribution of each parameter by vertical lines, respectively from left to right. The interval between the leftmost and the rightmost vertical line of each parameter is therefore its 95% Highest Posterior Density (HPD). Significant correlations, i.e., having shrinkage weights higher than 0.5 and the correlation parameter not including 0 in their 95% HPD, are highlighted by stars and darker shades. Details of the environmental variables can be found in **Fig. S39** and **Tab. S2** ('forest density' refers to the relative Leaf Area Index, abbreviated rLAI). A graphical interpretation of the highlighted effects of environment covariates on South American mammal diversity is proposed in (**B**). Arrows with a sharp head indicate positive correlations, whereas flat heads indicate negative ones. Following color legend in (**A**), the arrow indicates the rate on which the correlation was found, with red being the extinction rate and blue the origination rate. Temperature during the Eocene (displayed in pink) was taken from Westerhold et al. (16).

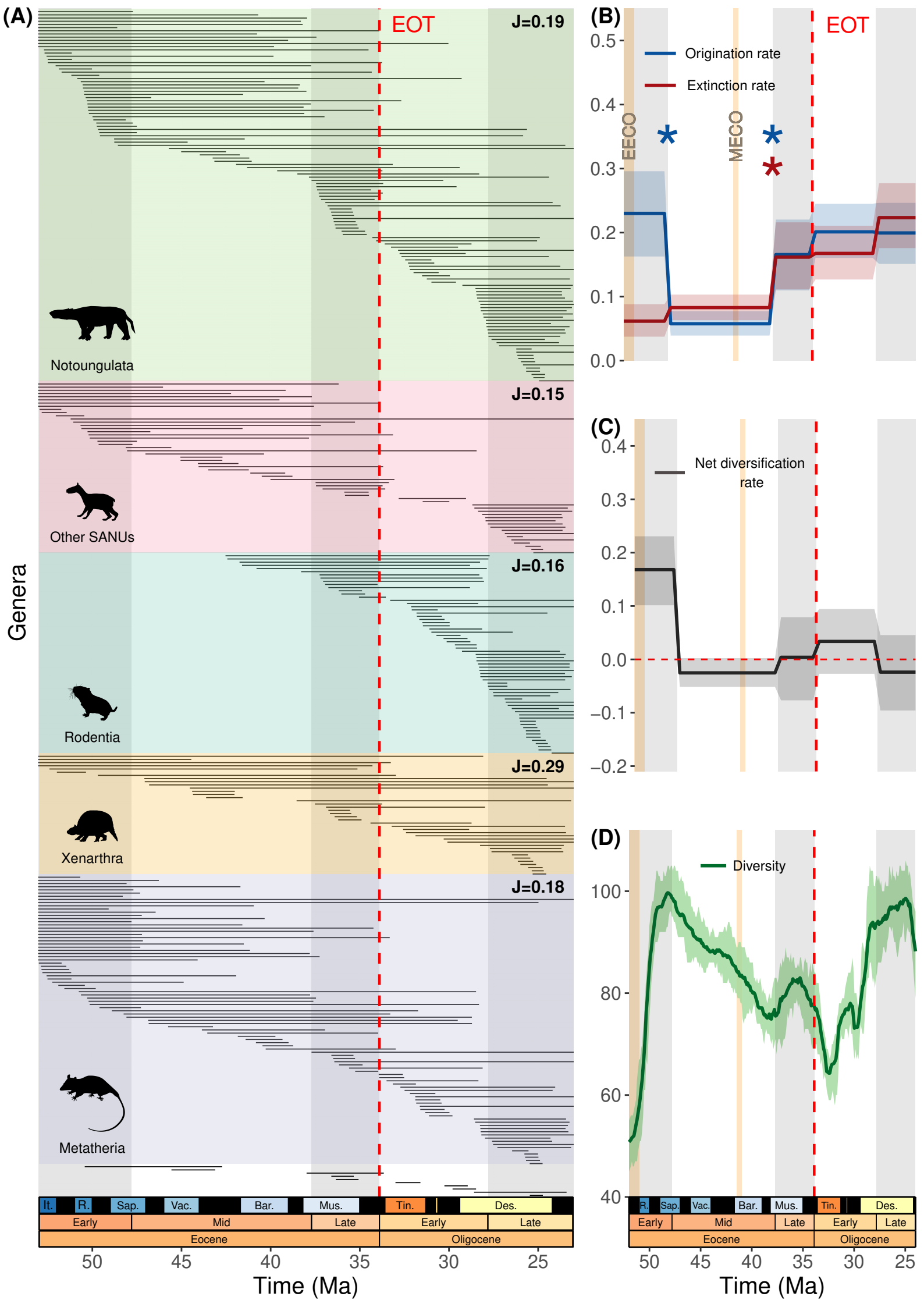
(A)
EOT
J=0.19
Notoungulata
J=0.15
Other SANUs
J=0.16
Rodentia
J=0.29
Xenarthra
J=0.18
Metatheria
Genera
It.
R.
Sap.
Vac.
Bar.
Mus.
Tin.
Des.
Early
Mid
Late
Early
Late
Eocene
Oligocene
50
45
40
35
30
25
Time (Ma)
(B)
EOT
Origination rate
Extinction rate
EECO
MECO
0.5
0.4
0.3
0.2
0.1
0.0
(C)
Net diversification rate
0.4
0.3
0.2
0.1
0.0
−0.1
−0.2
(D)
Diversity
100
80
60
40
R.
Sap.
Vac.
Bar.
Mus.
Tin.
Des.
Early
Mid
Late
Early
Late
Eocene
Oligocene
50
45
40
35
30
25
Time (Ma)

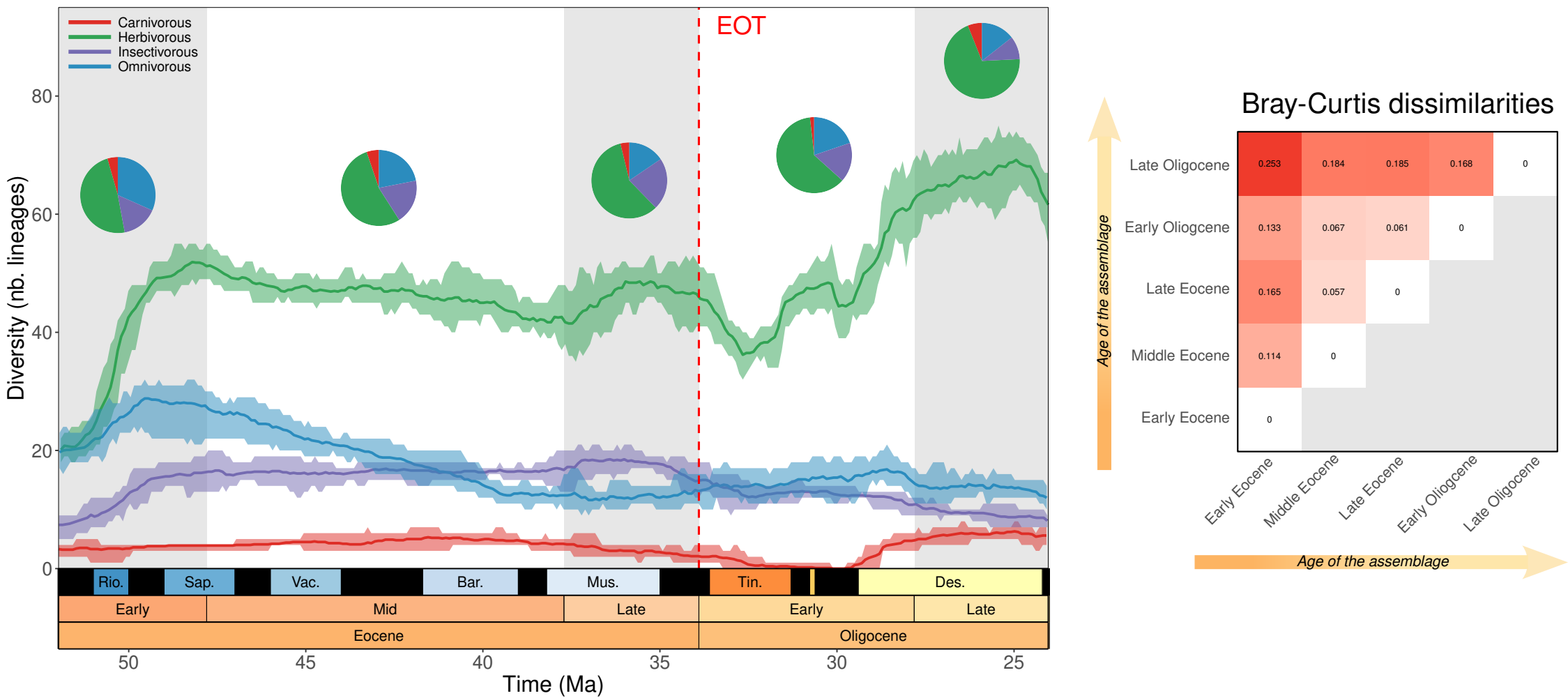
Carnivorous
Herbivorous
Insectivorous
Omnivorous
EOT
Diversity (nb. lineages)
0
20
40
60
80
Rio.
Sap.
Vac.
Bar.
Mus.
Tin.
Des.
Early
Mid
Late
Early
Late
Eocene
Oligocene
50
45
40
35
30
25
Time (Ma)
Bray-Curtis dissimilarities
Late Oligocene
Early Oliogcene
Late Eocene
Middle Eocene
Early Eocene
0.253
0.184
0.185
0.168
0
0.133
0.067
0.061
0
0.165
0.057
0
0.114
0
0
Age of the assemblage
Early Eocene
Middle Eocene
Late Eocene
Early Oliogcene
Late Oligocene
Age of the assemblage

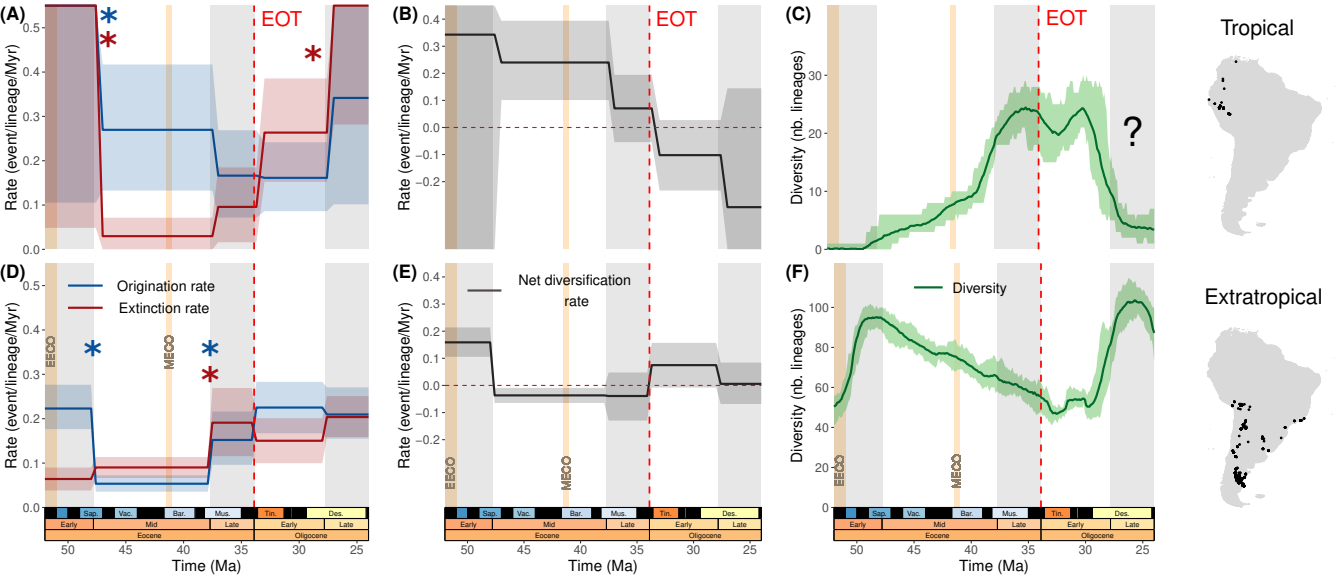
(A)
(B)
(C)
(D)
(E)
(F)
EOT
Rate (event/lineage/Myr)
Diversity (nb. lineages)
Origination rate
Extinction rate
Net diversification rate
Diversity
EECO
MECO
?
Tropical
Extratropical
Sap.
Vac.
Bar.
Mus.
Tin.
Des.
Early
Mid
Late
Eocene
Oligocene
Time (Ma)

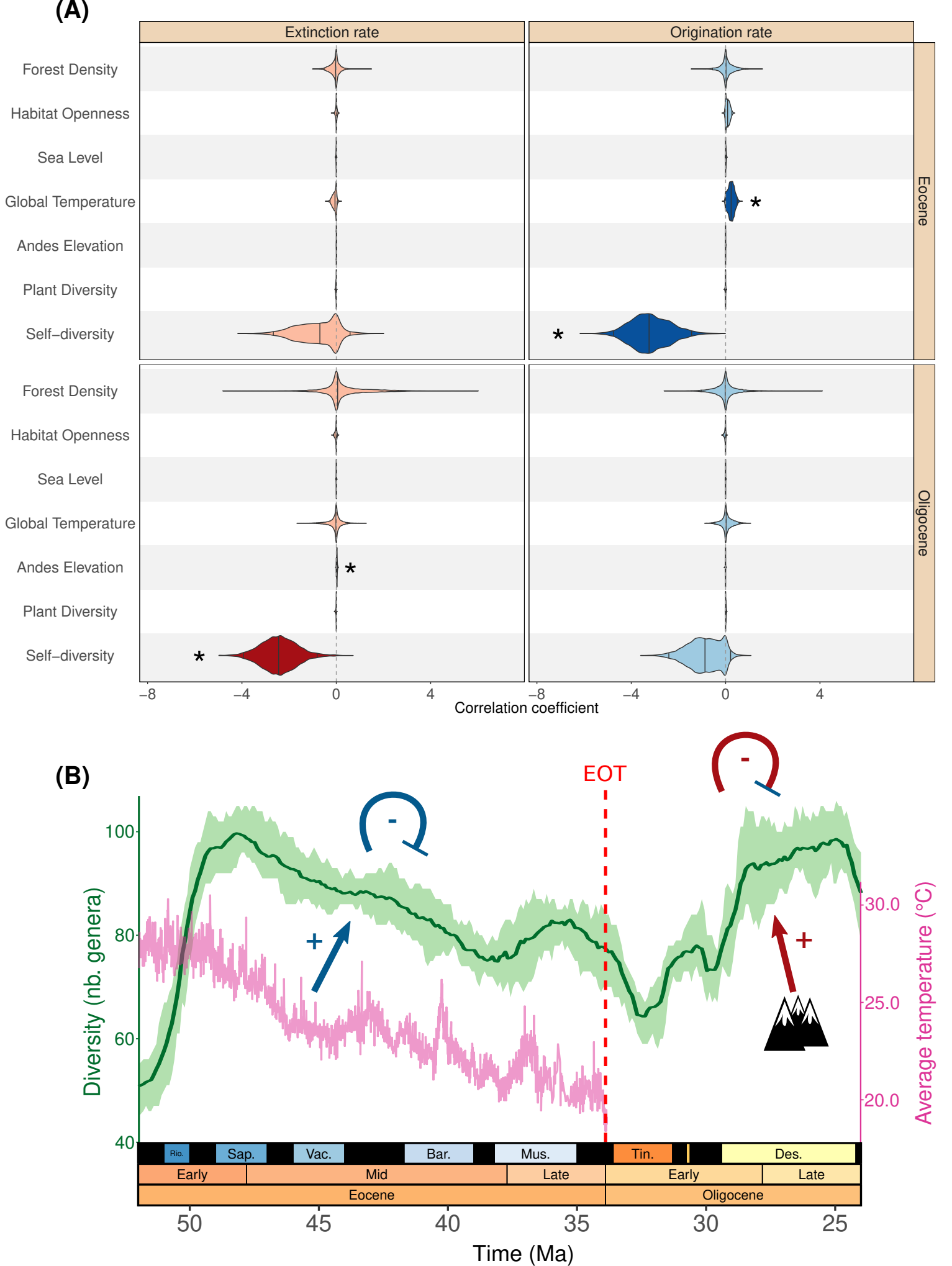
(A)
Extinction rate
Origination rate
Forest Density
Habitat Openness
Sea Level
Global Temperature
Andes Elevation
Plant Diversity
Self−diversity
Eocene
Oligocene
*
−8
−4
0
4
Correlation coefficient
(B)
EOT
-
+
Diversity (nb. genera)
Average temperature (°C)
100
80
60
40
30.0
25.0
20.0
Rio.
Sap.
Vac.
Bar.
Mus.
Tin.
Des.
Early
Mid
Late
Early
Late
Eocene
Oligocene
50
45
40
35
30
25
Time (Ma)

PNAS

Supporting information for

The fate of South America's endemic mammal fauna in response to the most dramatic Cenozoic climate disruption

Lucas Buffan[1,*], Fabien L. Condamine[1], Narla S. Stutz[1], François Pujos[2], Pierre-Olivier Antoine[1]
Laurent Marivaux[1]

[1] Institut des Sciences de l'Evolution de Montpellier, Université de Montpellier, CNRS, IRD, Place Eugène Bataillon, 34095 Montpellier cedex 5, France
[2] IANIGLA, CCT–CONICET–Mendoza, Avenida Ruiz Leal s/n, Parque General San Martín, 5500 Mendoza, Argentina

* **Corresponding author**: Lucas.Buffan@umontpellier.fr

This PDF file includes:

- Extended Materials and Methods
- Manual cleaning details
- Supp. Figures 1 to 41
- Supp. Tables 1 to 9
- SI references

Other supporting materials for this manuscript include the following:

- Raw and cleaned occurrence data (https://doi.org/10.6084/m9.figshare.26495989)

Supplementary text

1. Extended Materials and methods

Fossil data compilation

We first downloaded all Cenozoic mammal occurrences at least with a genus-level resolution from South America from The Paleobiology Database (`?base_name=Mammalia&taxo_reso=genus&cc=SOA`) on 2023-12-11 (n=10,440 occurrences). Because diversification regimes do not occur in the same way on land and in the sea (1), and because the scope of this paper is terrestrial, we removed taxa with marine affinities, *i.e.*, occurrences assigned to the orders "Cetacea" and "Sirenia" or the families "Otariidae" and "Phocidae" (n=354 occurrences). Subsequently, as ref. (2) performed an intensive cleaning of a significant proportion of South American mammalian fossil occurrences (especially Sparassodonts and Native Ungulates), we matched the time ranges of the occurrences we shared with them to those that they proposed (n=2,998 occurrences). For the remaining occurrences, we ensured that their time ranges matched the boundaries of their associated interval. For instance, the Mustersan occurrences were all found to be associated with the 48–42 Ma interval. However, radiochronological evidence has shown that this age is younger, constraining its boundaries to 38.2–35 Ma (conservative estimates have even constrained it to 38.2–38 Ma, based on the only clear datations from well-defined levels) (3) (**Fig. S1**). It is quite concerning to see that such major changes remain uncorrected, especially in public encyclopedies, often used as primary sources of information for non-specialists (*e.g.*, https://en.wikipedia.org/wiki/Mustersan). Age boundaries were expressed as either an International Chronostratigraphic Chart (ICC) stage/epoch or a South American Land Mammal Age (SALMA). In the latter case, we used a SALMA scale built de-novo based on a literature review (*e.g.*, 4). Then, based on the literature and the expertise of the co-authors, we manually revised the entire dataset, occurrence by occurrence. This "manual cleaning" aimed at correcting errors in the database, mostly regarding the age range and the taxonomic assignment (*e.g.*, synonymized genus names, typos, missing elements of open nomenclature) of each occurrence (**Fig. S2**). We intended to make this step as clear as possible by documenting most of the changes we made, and why (*see Manual Occurrence Cleaning part*). Finally, in order to decrease the number of parameters to estimate, we restricted our dataset to the late Paleocene-Early Miocene (60–16 Ma). The final dataset comprised 3,384 occurrences, including 529 genera and 1,108 identified species (see **Tab. S1** for a more detailed description of the data). Occurrence data can be found at https://doi.org/10.6084/m9.figshare.26495989.

Further input treatments

Subsequent data manipulation and visualization were carried out using the Tidyverse (5) suite of R packages, the paleoverse (6) and the deeptime (7) R packages. Out of 3,384 occurrences, 2,108 occurrences (representing *approx.* 62% of the total) were assigned to a SALMA. Due to temporal gaps in the South American Mammal fossil record this timescale is not continuous (**Fig. S1**). Yet, gaps can highly bias fossil-based diversification inferences, as, for instance, shown in insects (8). Therefore, we decided to assign sub-epoch ages to the SALMA-associated occurrences (**Fig. S1-2**), ensuring ourselves to sample the whole study period more evenly. As illustrated by many studies (2, 9), the taxonomic scale impacts fossil-derived diversification patterns. Defining species in the fossil record is difficult and prone to debate, and working at the species scale is particularly sensitive to biases such as synonymy or missing open literature elements (*e.g.*, 'cf.', 'aff.', etc.). Therefore, we analyzed our mammalian fossil database both at the genus and species levels (**Fig. S2**), but privileged the genus scale for our macroevolutionary conclusions. We further applied several treatments to our data. First, we tested the effect of removing singletons because our

genus-level and species-level occurrence datasets comprise 36% and 54% of singletons, respectively (*i.e.*, taxa only represented by a single occurrence in the entire dataset; **Tab. S1**). It is worth noting that including singletons in diversification inferences is still under debate (10–12). Also, PyRate was validated using simulated data with a proportion of singletons that, to our knowledge, never exceeded 34% (13). Hence, we possibly ignore how the model might behave with such high proportions of singletons as those we have, though it was found to be robust against data incompleteness. Second, we did not allow a given genus (or species) to have geographically and temporally-identical occurrences (as done by ref. (10)). Next, in order to have a better view on the different tempos of diversification between tropical and extratropical biomes, we assigned each occurrence a tropical or extratropical affinity. Traditionally – both when dealing with extant or fossil lineages – such a geographic splitting is made by defining a latitudinal threshold above (or under, depending on the hemisphere) which occurrences are considered tropical. The latter is commonly set as -23.4° in latitude, but sometimes also -23°, -23.5° or even -30°. However, such a threshold is unsatisfactory, mainly because it does not consider tropics' expansions and contractions through geological times (see refs. (14, 15) for a discussion on the topic). Therefore, based on their middle age, we binned our occurrences into 5-Myr time bins and reconstructed their paleocoordinates (using the mid age of the bin as reconstruction age) with the PALEOMAP Global Plate Model (16). Paleorotations were produced via an access to the GPlates Web Service (https://gwsdoc.gplates.org/) API implemented in the `paleorotate` function of the paleoverse R package (6). Then, to assign them a tropical/extratropical affinity, we overlaid these point data with Köppen-Geiger paleoclimate zones produced every 5 My (14, 17). Finally, our fossil occurrence data came with "diet" assignments, derived from dental ecomorphotypes, which we further revised and collapsed to only keep four different classes: carnivorous, herbivorous, insectivorous, and omnivorous.

Bayesian inference of diversification accounting for preservation

We used the Bayesian framework of fossil-based diversity and diversification inference accounting for preservation implemented in PyRate v.3 (18, 19). Relying on birth-death and preservation processes, PyRate jointly estimates the times of origination and extinction and the preservation rate of each taxon, as well as the origination and extinction rates of the underlying birth-death process. We approximated the posterior distribution of each parameter through Reversible-Jump Markov Chain Monte Carlo (RJMCMC) (13). The RJMCMC algorithm provides an objective estimate of the number of diversification rate shifts, but empirical case studies found that it could also be sensitive to gaps in the fossil record (8). Hence, we also analyzed our fossil dataset under a Birth-Death model with Constrained rate Shifts (BDCS) (20). In the BDCS model, origination and extinction rates can only vary in a piecewise-constant way between a predefined set of time bins. Given the temporal heterogeneity of our data (**Fig. S1** and **S4**), this framework was particularly relevant to us because the BDCS model can smooth rates through time when rates are very different within a bin due to preservation issues. We both tested geological stages and 5 My-long intervals as input bins. To achieve convergence, when working with full datasets, we ran 50,000,000 iterations at the genus level and 100,000,000 iterations at the species level, and sampled every 50,000. When working with taxonomically- or diet-specific datasets, we ran 20,000,000 iterations, sampling every 20,000. For each tested condition, we ran PyRate on 10 or 20 datasets of independently-sampled ages and retained those of which the majority of the parameters (posterior above all) converged. Parameters were considered convergent when their Effective Sample Size (ESS) was above 200. Convergence checks were assessed thanks to the PyMC 5.9.2 python library (21). For each set of runs, burn-in value was specified in an automatized pipeline as the value maximizing the ESS of the parameters (choosing between 1%, 5%, 10%, 25% and 50% of the posterior distribution), rather than using the same fixed value every time. Parallel computing

was made possible thanks to the parallel software (22). In the RJMCMC analyses, we allowed for a minimal time window between two origination/extinction rate shifts of 1 My (`-mindt 1`). We also allowed for preservation rate heterogeneity across taxa (`-mG`) as it is more realistic to consider uneven preservations across lineages (some lineages undergo better preservation than others). We set Gamma priors of shapes 1.1 (default value) and model-estimated rates for both origination and extinction rates (`-pL 1.1 0` and `-pM 1.1 0` options). The preservation rate prior was also sampled in a Gamma distribution of model-estimated rate, but we put a slightly larger shape (`-pP 2 0`), offering more flexibility (10). We assessed the most suitable preservation model for our data using the maximum-likelihood based model selection test included in PyRate (`-PPmodeltest` option), which resulted in favor of the Time-dependent Preservation Process (TPP) model allowing rate shifts between every geological stage (**Fig. S5-S6**). Last, we tested for the sensitivity of our analyses to singleton removal (`-singleton 1` option) (**Fig. S12-S13**). As the BDCS model takes longer to run than the RJMCMC model, we ran the former directly based on the origination and extinction times (respectively Ts and Te) table estimated with the latter (`-d` option). In fact, the joint estimation of Ts, Te and the preservation process is the same between both models. What changes is the diversification (birth-death) model they fit to the reconstructed diversity to assess the origination and extinction rates through time (λ and μ, respectively). BDCS models were run across 10,000,000 iterations, sampling every 10,000. All subsequent analyses were performed in R v4.4.0 (23).

Age-Dependent Extinction

To assess the effect of taxon age on its extinction probability, we fitted the Age-Dependent Extinction (ADE) model to our data (`-ADE 1` option in PyRate) (24). This model assumes that taxon extinction probability is only a function of its age, and fits a Weibull probability density to the extinction rate de-novo estimated from occurrence data. The presence (or not) of an ADE in our data is given by the value of the shape (ϕ) parameter of the Weibull function: if $\phi > 1$, extinction probability increases with taxon age; if $\phi < 1$ extinction probability decreases with taxon age; and if $\phi = 1$, no ADE can be characterized. In practice, we consider that the shape parameter significantly differs from one when one is not included in its 95% HPD. We ensured to fit this model within time windows with a relatively constant extinction rate. As we only retrieved one significant shift in extinction rate around 39 Ma (**Fig 1** and **S8-11**), we therefore investigated the effect of the ADE between 56 and 39 Ma, and between 39 and 23.03 Ma (`-filter` option) (**Fig S41**). Just like in the previous section, we set a time-variable preservation process (`-qShift` option) and allowed for preservation rate heterogeneity across taxa (`-mG` option). We ran the model for 40 million MCMC generations and sampled every 40,000 iterations. Parameters were considered convergent when their ESS was above 200. Convergence checks were achieved using the PyMC3 python library (21).

Dissimilarity across time among faunal assemblages

To quantify the extent to which our successive faunal assemblages differed from one another, both in terms of taxonomic and trophic composition, we computed two commonly-used dissimilarity indices to compare ecological communities. We used Jaccard's similarity index to compare the taxonomic composition of the five main mammal subdivisions we defined (notoungulates, other native ungulates, rodents, xenarthrans, and metatherians). Considering $n(E)$ and $n(O)$ the total number of taxa within Eocene and Oligocene faunas, respectively, and $n(E \cap O)$ the number of shared taxa between both assemblages, this index is simply expressed as:

$$J = \frac{n(E \cap O)}{n(E)n(O)}$$

This index is very intuitive and does not require any knowledge about the abundance of each taxon within both communities. It ranges from zero to one, and the closer it gets to one, the more similar the two assemblages compared are. Conversely, we compared sub-epoch-level functional compositions of the mammal assemblages by using the Bray-Curtis dissimilarity index, accounting for variations in relative abundance among the four trophic classes we defined based on dental ecomorphotypes (carnivorous, herbivorous, omnivorous, and insectivorous). Considering two assemblages A and B, p classes (here, $p = 4$), and $n(A, i)$ and $n(B, i)$ the respective numbers of taxa belonging to the class i within the assemblages A and B, this index is expressed as:

$$BC = 1 - \frac{2\sum_{i=1}^{p} min(n(A,i), n(B,i))}{\sum_{i=1}^{p}(n(A,i) + n(B,i))}$$

It also ranges from zero to one, but in that case, values closer to one indicate increasingly dissimilar assemblages.

Multivariate Birth Death (MBD) model and Selection of environmental variables

To assess the impact of environmental factors on the diversification patterns of SAMs during the EOT, we ran a Multivariate Birth-Death (MBD) model in PyRate (25). This model carries out two independent correlations involving a set of environmental covariates (that can be biotic and/or abiotic) and diversification rates newly-estimated from empirical T_s and T_e: one with the origination rate (λ), and the other with the extinction rate (μ). Each variable is therefore assigned to two correlation coefficients, one for the correlation with λ ($G_{\lambda,i}$, where i is the index of the variable in the set of covariates) and the other for the correlation with μ ($G_{\mu,i}$). An MCMC algorithm jointly estimates baseline origination and extinction rates and all the G_λ and G_μ, while controlling for over-parameterization. Each $G_{\lambda,i}$ and $G_{\mu,i}$ is assigned a shrinkage weight ($w(G_{\lambda,i})$ or $w(G_{\mu,i})$), ranging between 0 and 1, testing its significance – hence, the significance of the correlation itself. A correlation of coefficient $G_{\lambda,1}$ is considered significant if $w(G_{\lambda,1}) > 0.5$ and if a sufficiently high proportion of its posterior density does not overlap with 0. We selected seven abiotic and one biotic variable that appeared relevant to our case study (**Tab. S2**). The abiotic variables included two global and four local-scale ones. Temperature is known for being a major actor in the diversification of a wide range of clades (*e.g.*, 26). Hence, we included in our model the average Cenozoic temperature dataset assembled by ref. (27), using atmospheric $\delta^{18}O$ and $\delta^{13}C$ records from ref. (28). In addition, as they are expected to play a key role in habitat fragmentation on macroevolutionary scales, we added global sea level trends (29) and the average Andean uplift (30). We also added the Neotropical plant diversity dataset assembled (31). Last, there is a debate regarding the role of land opening in shaping the evolution of SAM faunas, notably among herbivores. We therefore included two regional proxies for land opening: Patagonian patterns of relative abundance of open habitats (32–34) and Patagonian relative leaf area index (35). Each abiotic correlate was subsampled or interpolated to a 500 ky time step. In addition, we tested for diversity-dependence effects that could either come from the diversity of the tested clade itself (self-diversity, `-rmDD 0` option) or other clades (allowing to hypothesize possible inter-clade interactions). As we expected environmental dissimilarities between the Eocene and the Oligocene at the continent scale, especially in high latitudes (where most of our occurrences come from), we did not expect Eocene and Oligocene faunas to have the same environmental constraints. That is why, in addition to searching for environment signature in the diversification pattern across all our study period, we also decoupled trends among post-early Eocene Climate Optimum Eocene faunas (51–33.9 Ma), and Oligocene faunas (33.9–

23.03 Ma). Each MBD model was run across 10,000,000 iterations, sampling every 10,000. We only carried out exponential correlations (`-m 0` option). Convergence of the parameters was assessed using the pymc 5.9.2 Python library (21), and parameters were considered convergent if their ESS were greater than 200. A summary of our entire methodological pipeline is provided in **Fig.S2**.

Considering the reliability of crowdsourced data

Over the past few decades, massive efforts have been devoted toward centralizing all published fossil data into large databases (*e.g.*, https://nowdatabase.org/, https://paleobiodb.org/, https://www.neotomadb.org/). Such an amount of easily-accessible data provided the invaluable opportunity for scientists to investigate large-scale patterns and processes of biodiversity using fossils, the only direct evidence of life in the past. In our case, our primary source of data came from The Paleobiology Database (https://paleobiodb.org/). However, we spotted many errors in the raw data, mostly regarding occurrences' age or taxonomic name (typos, unaccounted synonymies, missing open nomenclature elements, etc.). Most of these errors could not have been detected, and further corrected, without the authors' prior knowledge on the group (see **Fig. S2** and **S4**). The need for occurrence data revision was already illustrated by ref. (36), who pointed out significant differences when carrying out diversification analyses from uncleaned and cleaned occurrence data. Therefore, we argue that although powerful statistical tools exist, tackling macroevolutionary issues cannot be done without preliminary biological knowledge on the focal group.

2. Manual cleaning details

In this part, we provide some details on the Paleogene fossil occurrence cleaning effort we carried out. All co-authors were involved in this part, and some changes have not been documented. Our raw and final datasets can be found attached with this manuscript. Computer-supervised cleaning steps are documented in our GitHub repository (https://github.com/Buffan3369/Neotropical_mammals.git).

The age ranges of the occurrences belonging to the Paso del Sapo fauna (Western Patagonia, *"Sapoan fauna"* SALMA) were set close to the Ypresian–Lutetian boundary. More precisely, occurrences from the *La Barda* or the *Laguna fría* localities were respectively set to 45-47 Ma and 48-49 Ma (37).
Occurrences assigned to the former *Casamayoran* SALMA were re-assigned to a Middle Eocene age (37.71-47.8 Ma), except when more precision was provided in subsequent studies (*i.e.,* radiochronological dating)

Astrapotheria

Grypolophodon imperfectus (coll. nb. 176290, (38)) was removed as nomen dubium.
Parastrapotherium holmbergi (coll. nb. 176290, (39)) formation was set to Sarmiento, stage to Deseadan–Colehuehuappian, and age range to 20–29 Ma.
Xenastrapotherium sp. (coll. nb. 55602, (40)) and *Xenastrapotherium amazonense* (coll. nb. 55602, (41)) were reassigned to Laventan stage (11.8–13.8 Ma) according (42).
Notorhinus denticulatus (coll. nb. 176290, (39)) removed as nomen dubium. *Astrapotherium* (coll. nb. 50074, (43)) re-assigned to Santacrucian.

Stem Metatheria

Wirunodon chanku (coll. nb. 149523, (44)) age range was set to early Oligocene (28.7–33.9 Ma). The three occurrences of the *Rumiodon* genus were attributed to early Oligocene (28.7–33.9 Ma) All occurrences of the *Protodidelphis* genus were attributed to late Paleocene-early Eocene (47.8–59.2 Ma), just like all occurrences from the *Carolopaulacoutoia* and *Didelphopsis* genera.
Marmosopsis sp. (coll. nb. 133039, (37)) age range was set to Late Paleocene-early Eocene (47.8–59.2 Ma).

Cingulata

Added one occurrence of *Eosclerocalyptus* (6.4–6.6 Ma), *Doellotatus chapadmalensis* (5.9–6 Ma) and *Macrochorobates scalabrinii* (6.4–6.6 Ma) from the Maimará formation, Maimará locality, Jujuy, Argentina (45).

Didelphimorphia

Added one occurrence of the extant genus *Chacodelphys* (46).
All occurrences assigned to the *Micoureus* genus were re-assigned to the *Marmosa* genus, the former being a sub-genus of the latter (47).
Based on (48), we added a new occurrence of *Marmosa* in the TAR-31 locality of Shapaja, Peru, late Middle Miocene (11.67–15.63 Ma).
Paradidelphys sp. (coll. nb. 157795, (49)) was synonimized with *Thylophorops* (50).
Added one occurrence of *Thylamys* cf. *colombianus* from the TAR-31 locality of Shapaja, Peru (47).
Added one occurrence of *Sparassocynus maimarai* from the Maimará formation, Maimará locality, Jujuy, Argentina (45).

Didolontidae (SANU family with uncertain affinity)

Archaeohyracotherium mediale (Didolodontidae, coll. nb. 176164, (38)) was synonimized with *Asmithwoodwardia subtrigona* (Protolipternidae) by ref. (51).
Argyrolambda conidens was synonimized with *Didolodus multicuspis* (51).
Didolodus sp. (coll. nb. 199563, (52)) was removed as associated to “unidentified Didolontidae” in the paper.

Litopterna

Enneoconus parvidens (coll. nb. 176164, (53)) was synonimized with *Ernestokokenia nitida* by ref. (51).

Microbiotheria

Clenia brevis was excluded from the *Clenia* genus by ref. (54). Hence, we rename the genus aff. *Clenia*.

Notoungulata

All occurrences referred to as *Bryanpattersonia nesodontoides* were synonimised with *Archaeotypotherium propheticus* according to (55).
All occurrences referred to as *Bryanpattersonia sulcidens* were renamed *Protarchaeohyrax gracilis* according to (55). All occurrences of *Anisotemnus distentus* were assigned to Middle Eocene (37.71-47.8 Ma) according to (56). Removed two occurrences of *Archaeotypotherium propheticus* (coll. nb. 176286), absent from the original publication (38). Age range of *Coelostylodon florentinoameghinoi* and *C. caroloameghinoi* (coll. nb. 13779) was set to Barrancan (39-41.7 Ma), in line with the original reference. Assign all *Eomorphippus obscurus* occurrences described in Simpson (38) (coll. nb. 38653) a Mustersan age (35-38.2 Ma).

Paucituberculata

Acdestodon genus was synonimised with *Acdestis* (57). Added one occurrence aff. *Palaeothentes* from the TAR-31 locality of Shapaja, Peru (47). *Propalaeothentes* was synonimised with *Palaeothentes* (57). Added *Palaeopanorthus primus* from the Colhuehuappian of Chubut, Argentina (57).

Pilosa

Added one occurrence of *Proscelidodon* (Upper Miocene-Lower Pliocene) and one cf. *Pleurolestodon* (5.8–5.9 Ma) from the Maimará formation, Maimará locality, Jujuy, Argentina (45).

Polydolopimorphia

Chulpasia sp. (coll. nb. 132938, (58)) was removed as only one record of *Chulpasia* (species *mattaueri*) has been found in Peru.
Groeberia minoprioi (coll. nb. 92669, (59)) age range was set to late Eocene-early Oligocene (27.82–37.71 Ma). *Patagonia peregrina* (coll. nb. 27311, (54)) age range was set to Chattian (23.03–27.82 Ma). All occurrences of *Polydolops clavulus* were renamed *Archaeodolops clavulus*, according to (60). Added one occurence of *Archaeodolops clavulus*, according to the same paper.
All occurrences of *Proargyrolagus bolivianus* were attributed to the Salla formation, Bolivia. Hence, their age boundaries were restricted to 24.5–26 Ma.
Amphidolops serrula (coll. nb. 13779, (61)) was re-assigned to Late Paleocene (oldest recorded Polydolopid).
Polydolops sp. (coll. nb. 14208, (62)) was removed as age boundaries (Early Miocene) were way outside known boundaries for records of this genus (Middle Eocene).
Added occurrence from a newly described genus of the Prepidolopidae family from the TAR-74 locality of San Martín, named Prepidolopidae *gen_A* (52).

Primates

Ages of Deseadian soriacebines *Branisella* and *Canaanimico* were restricted to the 24.5–26 Ma interval according to (63).

Pyrotheria

Re-assigned the four occurrences of *Griphodon* described in refs. (64) as cf. *Griphodon* sp1 to sp4.

Rodentia

We should mention that all the rodents considered in this study belong to the order Caviomorpha, and arrived in the South American landmass in the middle Eocene (65). ***Added Occurrences***
Ricardomys longidens, Laventan age, San Martín department, Peru (66).
Microscleromys sp. (two occurrences), *Microscleromys cribriphilus*, *Microscleromys paradoxalis*, *Microsteiromys jacobsi*, *Nuyuyomys chinqaska*, *Scleromys*, Laventan age, San Martín department, Peru (66).
Balsayacuy sp., Rupelian age (restricted to the 27.82–31.1 Ma interval), Departamento de Ucayali, Santa Rosa locality, Peru (67). Described as an occurrence of *Balsayacuy huallagaensis*, but species attribution doubtful. Hence, restricted to genus level. From the same paper (same locality and same age), we also add one occurrence of *Shapajamys minor*, one of *Ucayalimys amahuacensis* and one of *Vucetichimys pterilophodonica*.
Erethizon sp., Vorohuean (Marplatan) age, Uquía formation, Quebrada de Humahuaca locality, Jujuy state, Argentina (68).
Eoincamys valverdei and *Tarapotomys subandinus*, early Oligocene of respectively TAR-72 and TAR-22, San Martín, Peru (69).
?Palaeocavia (5.8–5.9 Ma), *Pithanotomys? solisae* (5.8–5.9 Ma), *Pithanotomys* sp. (5.8–5.9 Ma) *Palaeocavia* sp. (5.9–6.0 Ma) and *Palaeocavia humahuaquense* (6.4–6.6 Ma) from the Maimará formation, Maimará locality, Jujuy, Argentina (45).

Corrections
Cachiyacuy contamanensis (coll. nb. 149523, (70)) was renamed *Cachiyacuy* sp. as taxonomic assignation is under debate. Two *Cachiyacuy contamanensis* occurrences from the same collection, same paper, were renamed cf. *Cachiyacuy contamanensis*, for the same reason.
Kichkasteiromys raimondii: age range set to 34–35 Ma.
Time boundaries of *Cachiyacuy* cf. *contamanensis* and *Cachiyacuy contamanensis* (coll. nbs. 207061 and 207062, (71)) were set to Priabonian (33.9–37.2 Ma). Same for *Cachiyacuy* cf. *kummeli*, *Eoespina* and cf. *Eoespina* (coll. nb. 207062, 207062 and 207065, (71)) Remaining occurrences of the genus *Cachiyacuy* (four in total) were set to late Eocene (33.9–41.2 Ma).
Canaanimys maquiensis (coll. nb. 149523, (70)) was renamed *Canaanimys* sp. as taxonomic assignation under debate.
Time boundaries of four *Cachiyacuy kummeli* occurrences (coll. nb. 144474, (65); 176136, (72), 207067 and 207062 (71)) were set to Bartonian-Priabonian (33.9–41.2 Ma). Same for *Eobranisamys* sp. (coll. nb. 176151, (72)) and for all occurrences from the 144474 collection, including one *Chachapoyamys* cf. *kathetos* (66), one *Eoespina* sp. (65), one *Canaanimys maquiensis* (65) and one *Eobranisamys javierpardoi* (72).
Ages of all occurrences from the collection 149523 were restricted to Rupelian. These included two cf. *Cachiyacuy kummeli* occurrences (70), one *Canaanimys* sp. (70), one *Eobranisamys riverai*, one *Eobranisamys romeropittmanae*, one *Eoespina woodi*, one *Eoincamys ameghinoi*, one *Eoincamys pascuali*, one *Eopicure kraglievichi*, one *Eosachacui lavocati*, one *Eosallamys paulacoutoi*, one *Eosallamys simpsoni* (73), one *Pozomys* sp., two *Pozomys ucayalensis* (70), one *Eodelphomys almeidacomposi*, one *Eopululo wigmorei* (73).

Ages of two *Sallamys pascuali* occurrences (coll. nb. 95688, (74); 133539, (75)), three *Branisamys luribayensis* (coll. nb. 95688 (74); 95688 (76); 133539 (75)) were sharpened to the 25–26 Ma interval.
Ages of one *Pozomys ucayalensis* (coll. nb. 176129, (72)) were set to Bartonian-Priabonian (33.9–41.2 Ma). Ages of two *Eoespina* sp. occurrences (coll. nb. 176140, (72)) was restricted to late Eocene.
Ages of one *Eoespina* and one cf. *Eoespina* occurrence (coll. nb. 207062 and 207065, (71)) were set to Rupelian.
Eoincamys pascuali (coll. nb. 207064, (71)) was renamed *Eonincamys* sp. Age range of all Late Oligocene occurrences from the Salla formation, La Paz, Bolivia, was set to 24.5–26 Ma. *Eopululo wigmorei* (coll. nb. 225588, (52)) species name was set to *Eopululo* sp. according to (66).
Names of all *Eumysops chapalmalensis* occurrences were set to *Eumysops chapadmalensis*.

Removed occurrences
Cachiyacuy kummeli (coll. nb. 207067, (71)), renamed *C.* cf. *kummeli* (doublon) according to (66).
Canaanimys sp. (coll. nb. 176136, (64)), taxonomic revision (66).
Canaanimys maquiensis (two occurrences, coll. nb. 207066 and 207067, (71)), taxonomic revision (66).
Chachapoyamys kathetos (coll. nb. 207067, (66)), re-assigned to *C.* cf. *kathetos* (doublon) (66).
Four Brazilian occurrences of the genera *Eobranisamys* (two) and *Eoincamys* (two) with ages for being rework (coll. nb. 57989, (77); coll. nb. 217834, (78)).
Tarapotomys sp. (2 occurrences) (coll. nb. 199560, (69); coll. nb. 199563, (52)), respectively re-described as aff. *Tarapotomys* sp. and *Tarapotomys subandinus* in (66).
Incamys bolivianus (coll. nb. 95688, (74)), doulon.
Asteromys bolivianus (coll. nb. 133591, (79)), doublon.
All *Rattus rattus* occurrences, as introduced by humans.

Sparassodonta

Cleaning was highly based on Tarquini et al. 2022 (2). In addition, we removed our single *Argyrolestes peralestinus* occurrence (coll. nb. 176285, (80)) as nomen dubium (81).

Supplementary figures

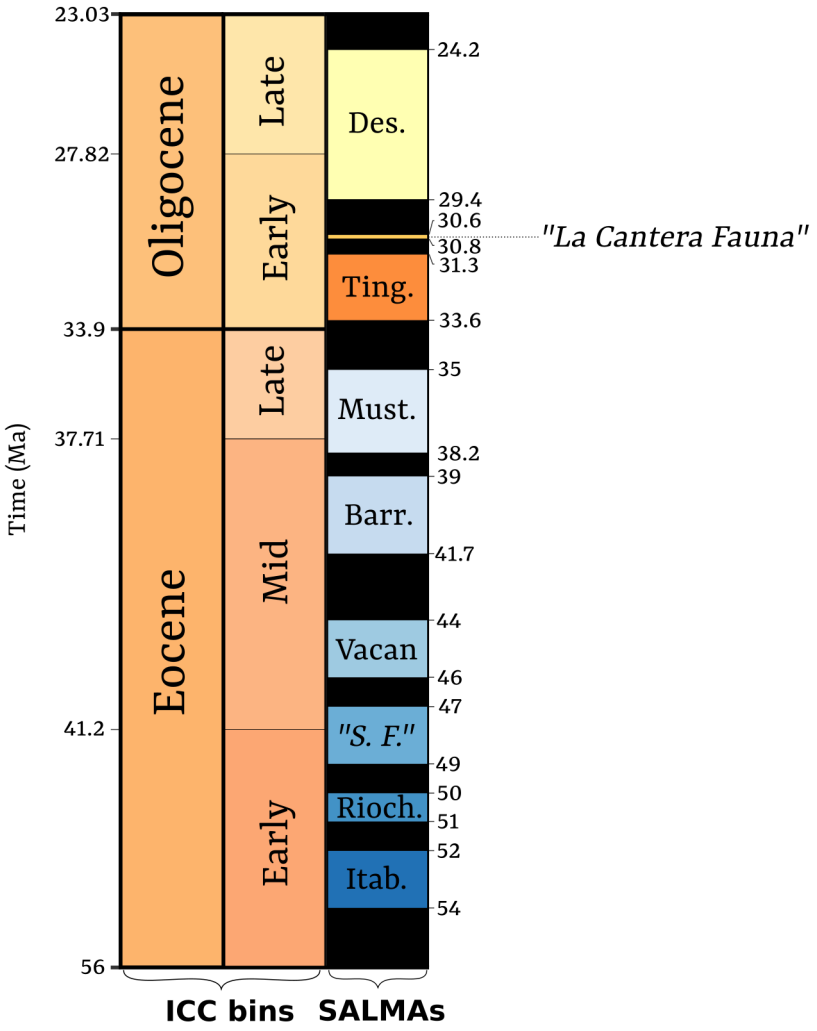

Supp. Figure 1: Time bins used in this study. Bins representing International Chronostratigraphic Chart 2022 (ICC bins) geological epochs (leftmost vertical band) and sub-epochs (middle vertical band), and representing South American Mammal Ages (SALMAs, rightmost vertical band) are depicted. SALMA boundaries were determined from Dunn et al. (2013), Woodburne et al. (2014) and Kouvari (2023). Note that an absolute estimate does not exist for the majority of them. Black rectangles stand for gaps in the South American mammalian fossil record. *Abbreviations for SALMAs. Des: Deseadan, Ting: Tinguirirican, Must: Mustersan, Barr: Barrancan, "S. F." : "Sapoan Fauna", Rioch: Riochican, Itab: Itaboraian.*

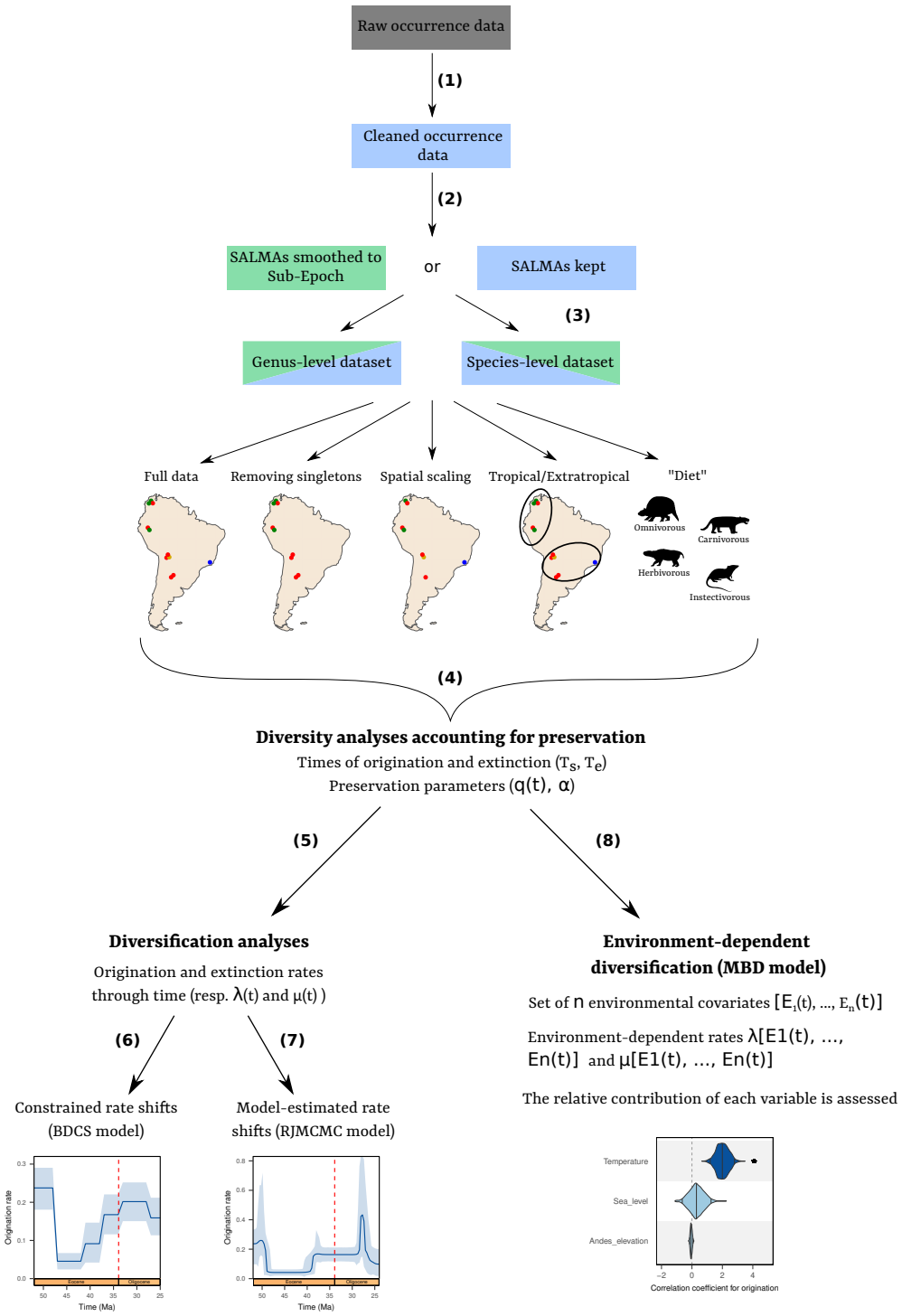

Supp. Figure 2: Schematic view of our data methodological pipeline.

We downloaded our data on The Paleobiology Database (https://paleobiodb.org/). We made sure to match each occurrences' time range with the boundaries of its corresponding interval, either being a geological stage/epoch (55% of our occurrences) or a South American Land Mammal Age (SALMA) (45% of our occurrences). Then, we cleaned the data, verifying for each occurrence its age range, taxonomic name (correcting synonyms), restoring missing elements of open nomenclature (*eg*., "?", "cf.", "aff."), removing duplicates and adding eventually newly-published data (1). Afterwards, occurrences associated to a SALMA were either binned to their corresponding sub-Epoch ('SALMA smoothed to Sub-Epoch') (**?**) or left as they were ('SALMA kept') (2). We also both analyzed diversification patterns at the species and the genus level (3). Several subsettings were tested, considering (i) full data, (ii) data without singletons, (iii) spatially scaled data, (iv) tropical partitioning and (v) "diet" (based on dental ecomorphotype). Once subsetted, each individual occurrence dataset was used as an input for our diversity inference accounting for preservation (4). Then, we proceeded to the diversification inference, either by (5) fitting birth-death models with constrained rate shifts (BDCS) (6) and model-estimated rate shifts (RJMCMC) (7) or by fitting environment-dependent multivariate birth-death models (MBD) (8). Last, we fitted an age-dependent extinction (ADE) model to our occurrence data within two time frames with constant extinction rate (9).

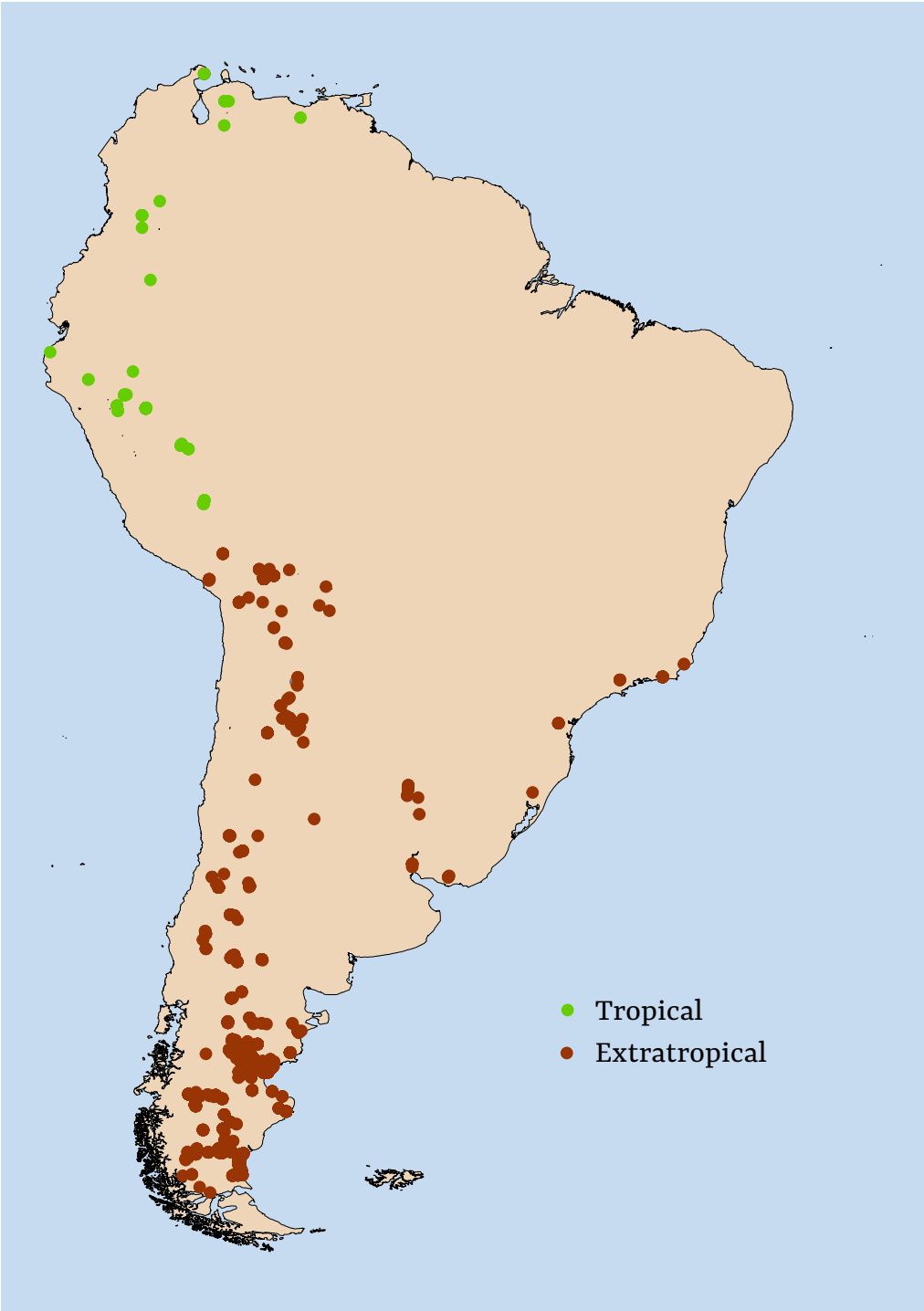

Supp. Figure 3: Map of the fossil-bearing localities considered in this study (435 collections).

These collections comprise a total of 3384 retained occurrences, including 156 of palaeotropical affinity (in green, 43 collections) and 3326 of extra-palaeotropical affinity (in brown, 391 collections).

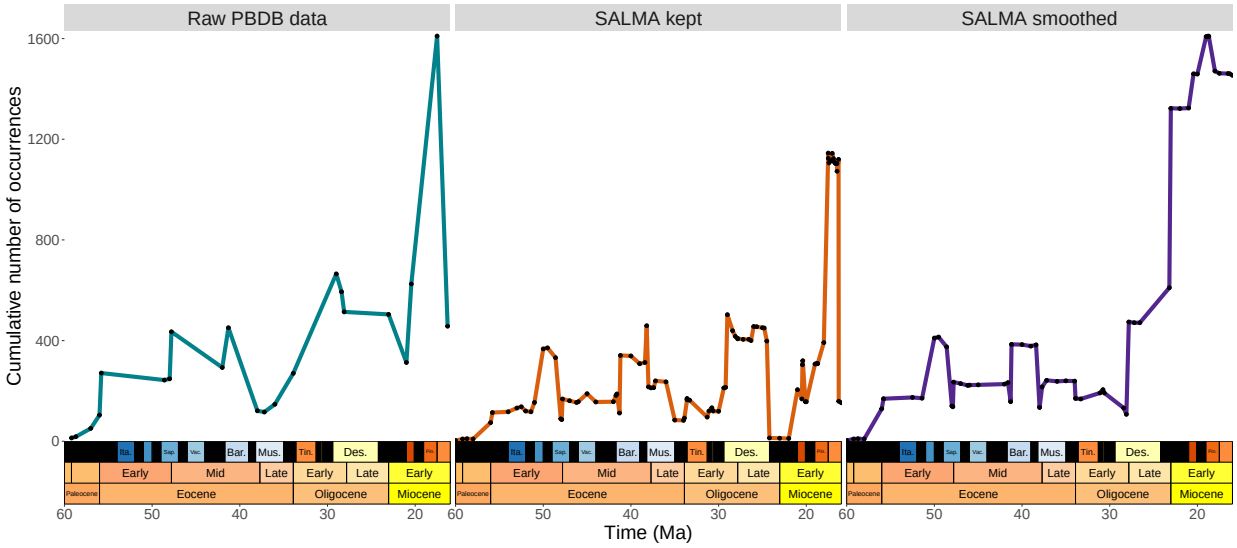

Supp. Figure 4: Cumulative number of occurrences through time within our study period. The cumulative number of occurrences is computed forward in time, starting from the lower age boundary of the oldest occurrence. Given a time t_1, this metric grows by the difference between the number of occurrences having t_1 as lower and upper boundaries. In practice, the times when this metric was computed are represented by the black dots. On the left, results from the raw data downloaded from PBDB are shown. In the middle, results from cleaned occurrences are shown. On the right, results from the same cleaned data but after smoothing occurrences associated to a South American Land Mammal Age (SALMA) to their corresponding sub-epoch (see **Fig. S1**) are shown.

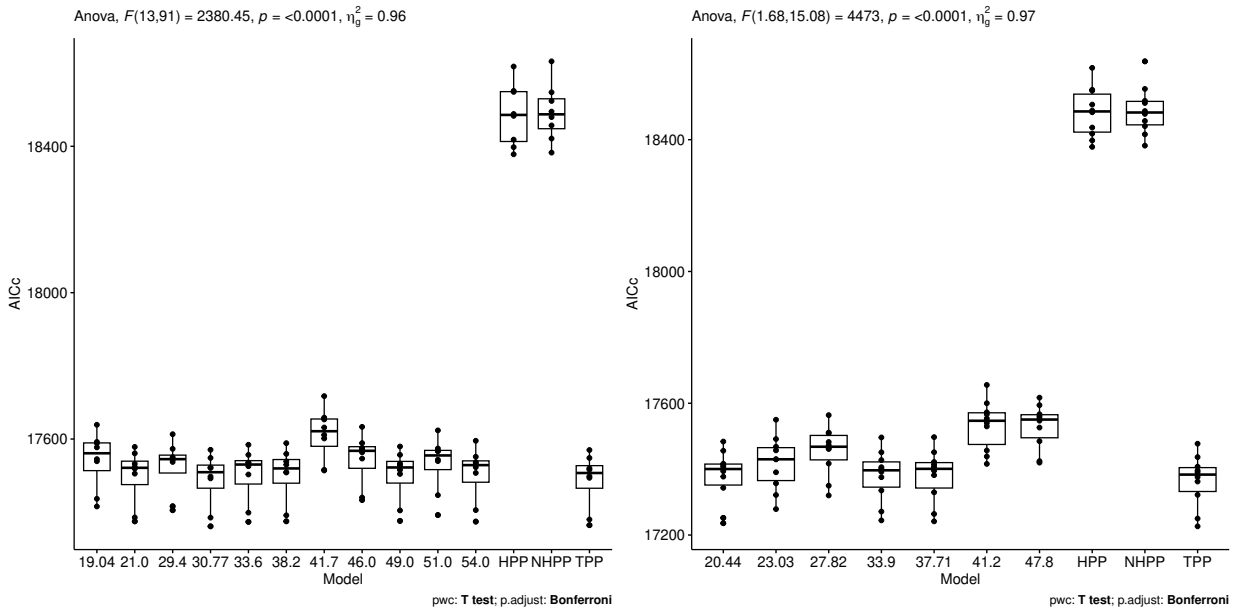

Supp. Figure 5: Preservation model selection under two TPP scenarios applied to the genus dataset with smoothed SALMAs. Models on the left of the x axis indexed by numbers are TPP with one removed bin, corresponding to the number. In the three cases, the lowest AICc is reached with the TPP model. Results were obtained on 10 replicates. (left) TPP with rate shift at every South American Land Mammal Age (SALMA) (mean AICc for TPP : 17486.42). (right) TPP with rate shift at every stage (mean AICc for TPP : 17364.53). Details for the AIC of all models can be found in Dataset S1.

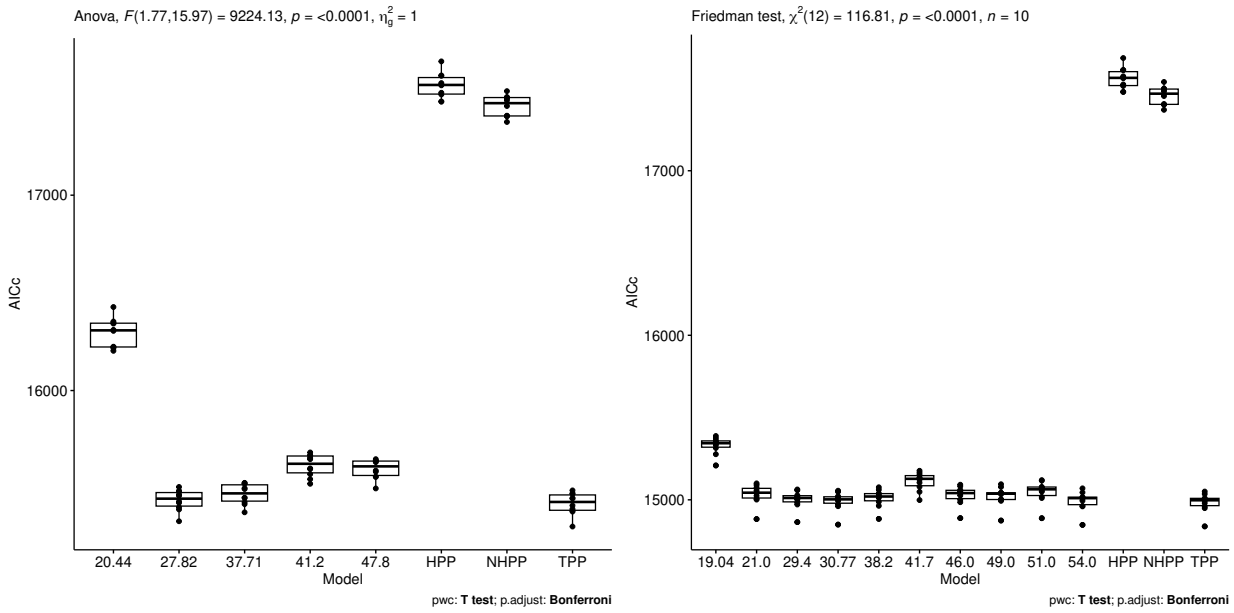

Supp. Figure 6: Preservation model selection under two TPP scenarios applied to the genus dataset without smoothing SALMAs. Models on the left of the x axis indexed by numbers are TPP with one removed bin, corresponding to the number. (left) TPP with rate shift at every stage (mean AICc for TPP : 15420.42). (right) TPP with rate shift at every SALMA (mean AICc for TPP : XXX). Details for the AIC of all models can be found in Dataset S1.

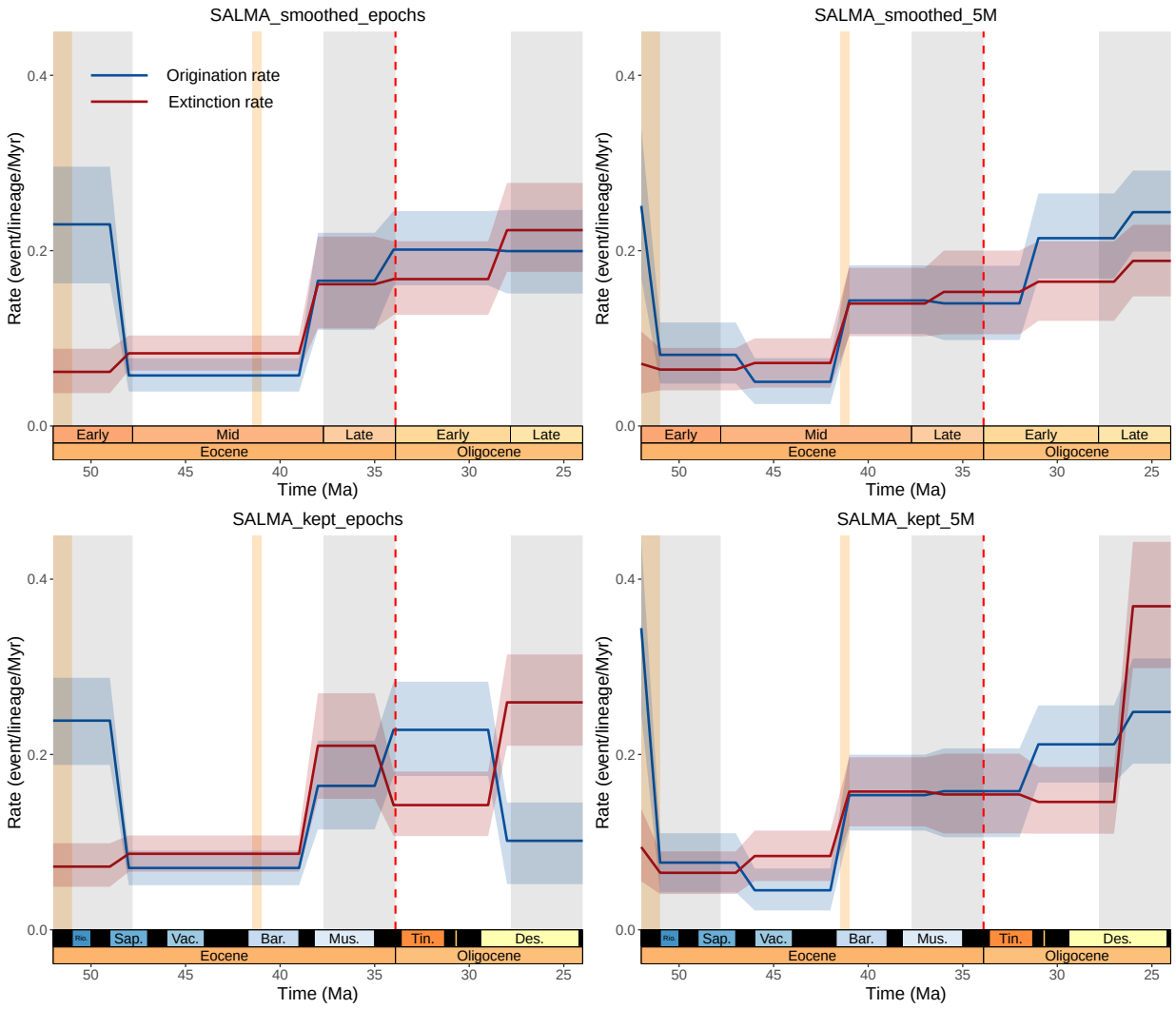

Supp. Figure 7: Diversification rates of our full dataset after (or not) smoothing SALMAs to their corresponding sub-Epochs, estimated under the BDCS model with two different time bins for rate shifts. Origination rates are displayed in blue and extinction rates in red. Solid lines show average rates, and shaded areas their corresponding 95% HPD. Light brown vertical bands respectively display the early Eocene Climate Optimum (EECO, 53-51 Ma) and the Mid-Eocene Climate Optimum (MECO, 42-41 Ma).

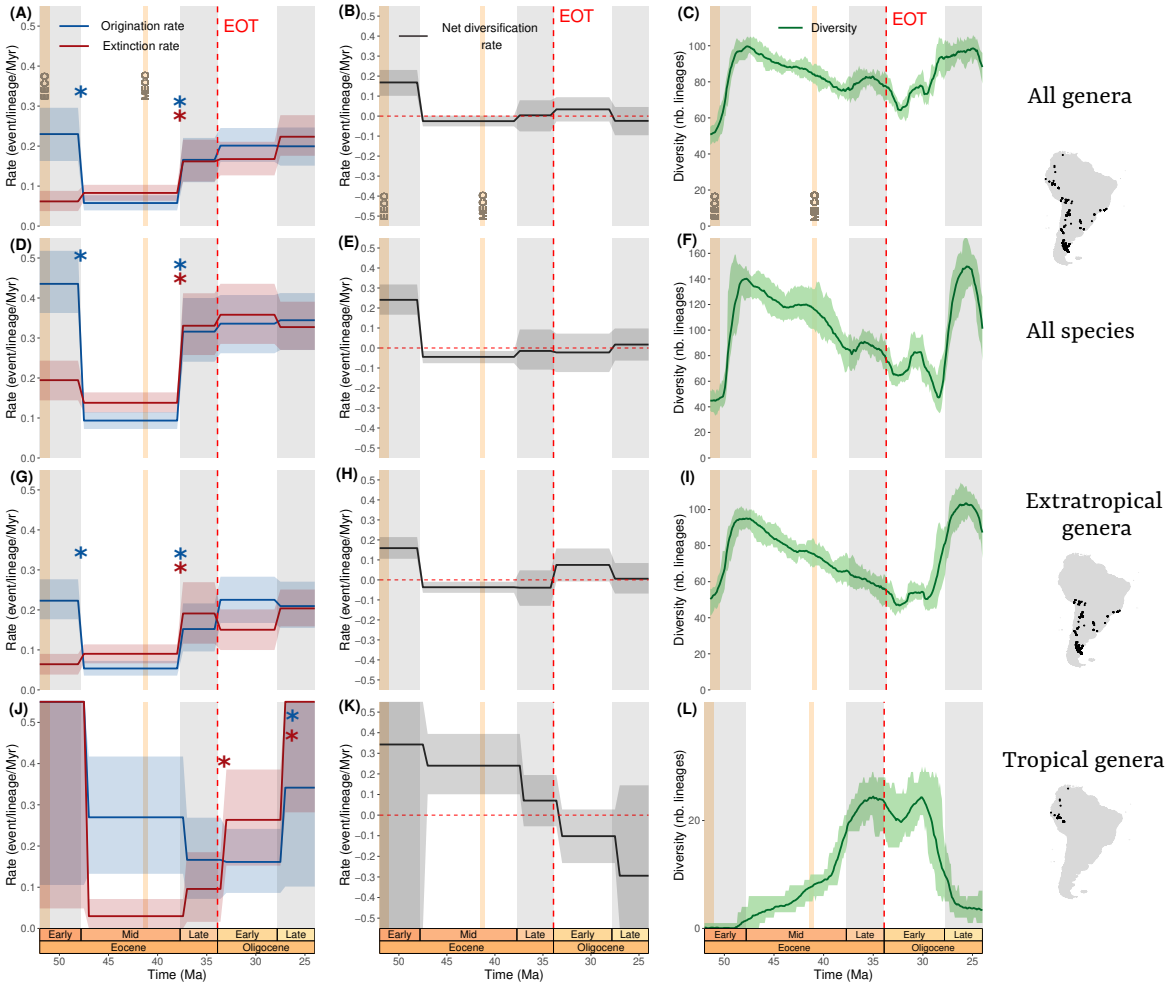

Supp. Figure 8: Diversification and diversity dynamics of South American Mammals from the early Eocene to the Late Oligocene. Trends are represented for all genera (A-C), all species (D-F), extratropical (G-I) and tropical genera (J-L). Light orange bands represent the early Eocene (53-51 Ma) and the Mid-Eocene (~41 Ma) Climate Optima, respectively abbreviated as EECO and MECO. Blue and red stars respectively represent significant shifts in origination and extinction rates.

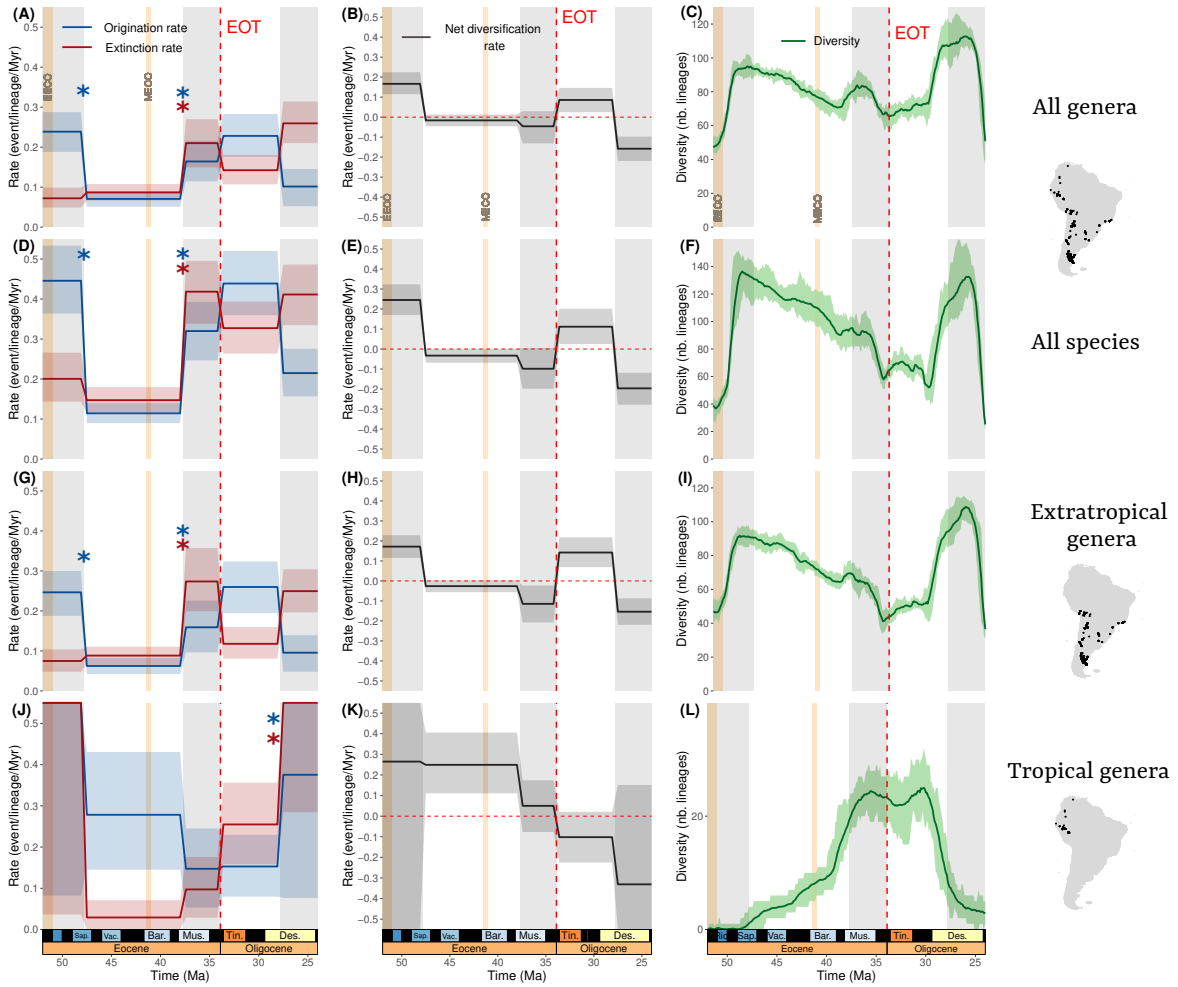

Supp. Figure 9: Diversification and diversity dynamics of South American Mammals from the early Eocene to the Late Oligocene without binning SALMAs to their corresponding sub-epochs. Trends are represented for all genera (A-C), all species (D-F), extratropical (G-I) and tropical genera (J-L). Light orange bands represent the early Eocene (53-51 Ma) and the Mid-Eocene (~41 Ma) Climate Optima, respectively abbreviated as EECO and MECO. Blue and red stars respectively represent significant shifts in origination and extinction rates.

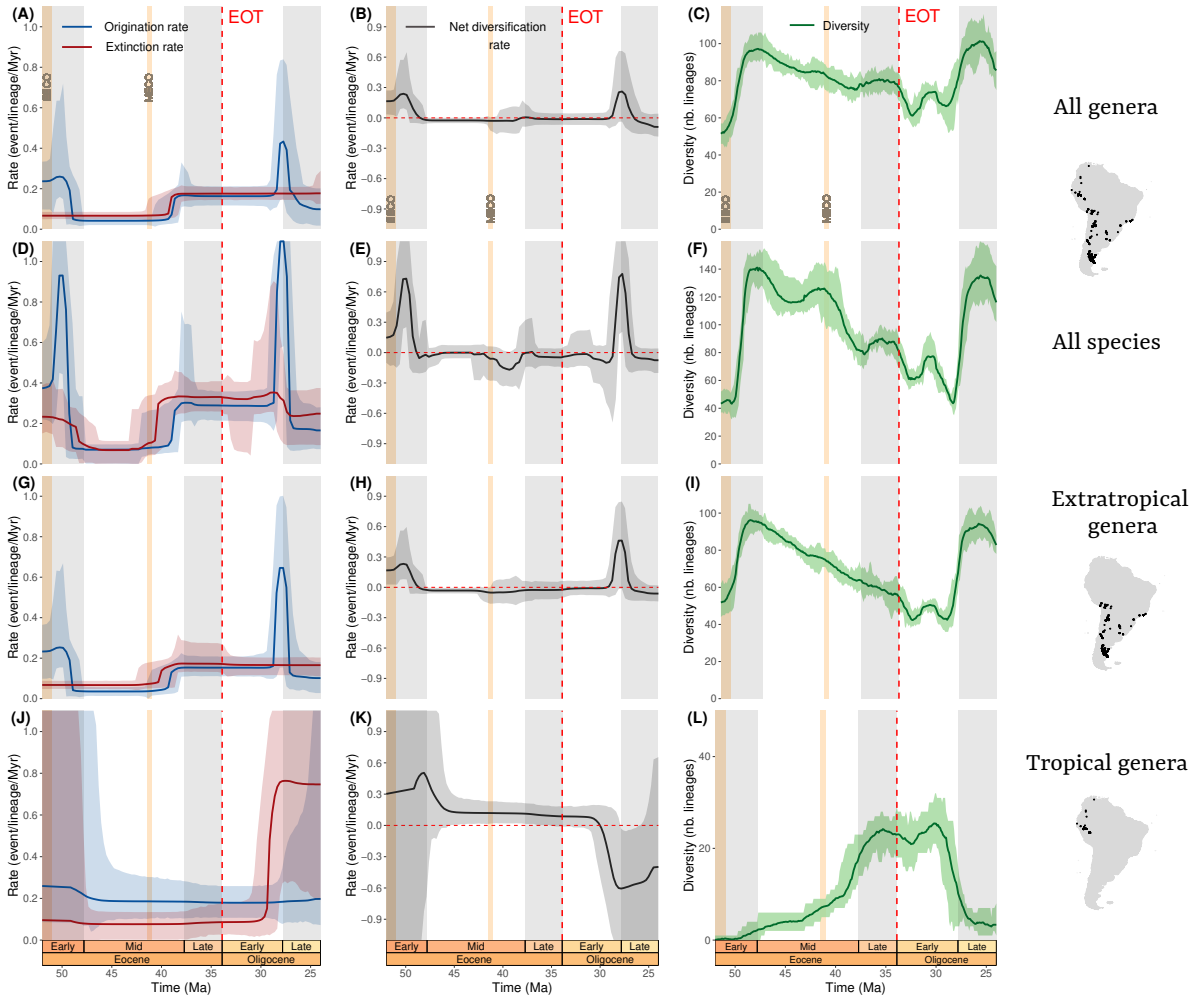

Supp. Figure 10: Diversification (estimated with RJMCMC) and diversity dynamics of South American Mammals from the early Eocene to the Late Oligocene (SALMAs binned to their corresponding Sub-Epochs). Trends are represented for all genera (A-C), all species (D-F), extratropical (G-I) and tropical genera (J-L). Light orange bands represent the early Eocene (53-51 Ma) and the Mid-Eocene (~41 Ma) Climate Optima, respectively abbreviated as EECO and MECO. Blue and red stars respectively represent significant shifts in origination and extinction rates.

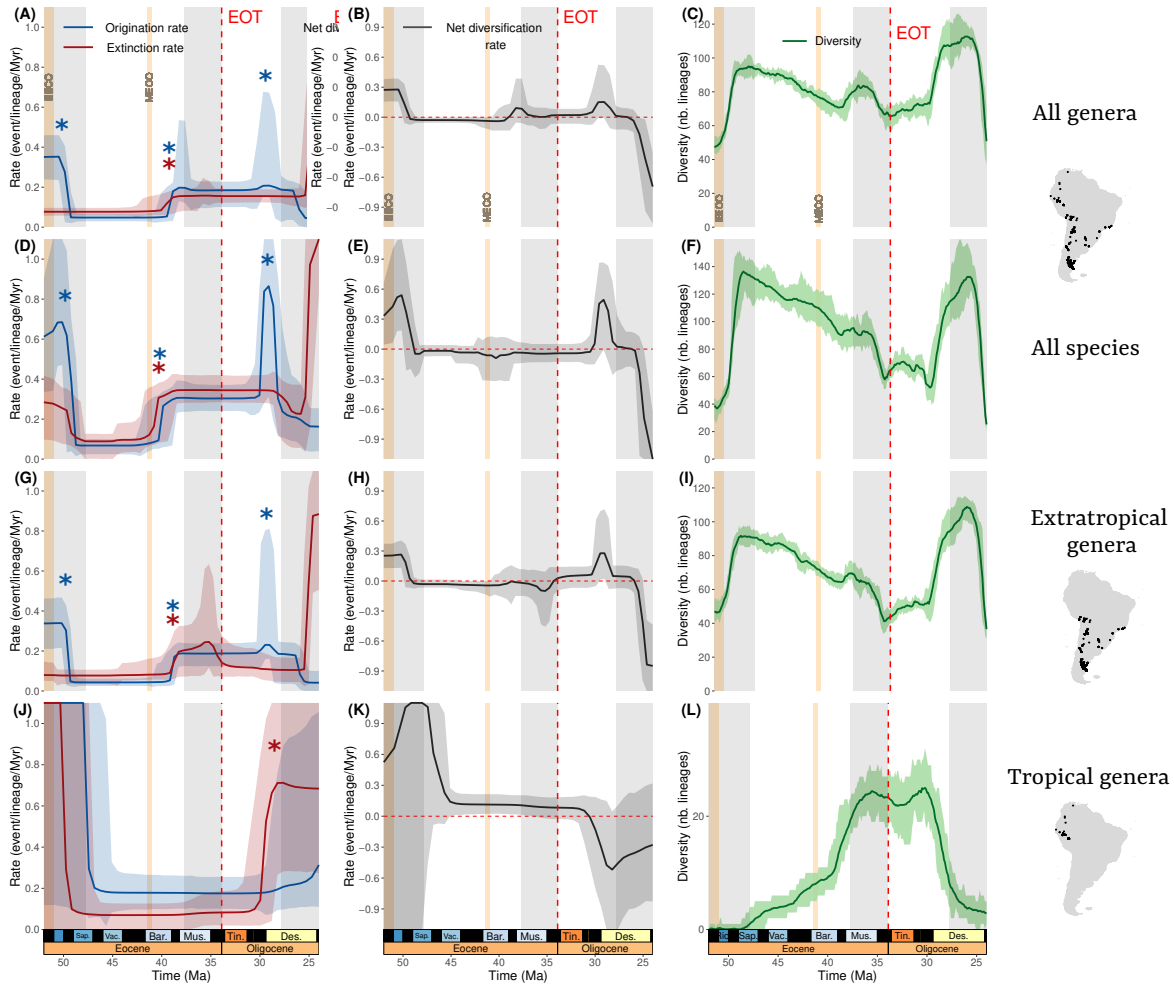

Supp. Figure 11: Diversification (estimated with RJMCMC) and diversity dynamics of South American Mammals from the early Eocene to the Late Oligocene (without binning SALMAs to their corresponding Sub-Epochs). Trends are represented for all genera (A-C), all species (D-F), extratropical (G-I) and tropical genera (J-L). Light orange bands represent the early Eocene (53-51 Ma) and the Mid-Eocene (~41 Ma) Climate Optima, respectively abbreviated as EECO and MECO. Blue and red stars respectively represent significant shifts in origination and extinction rates.

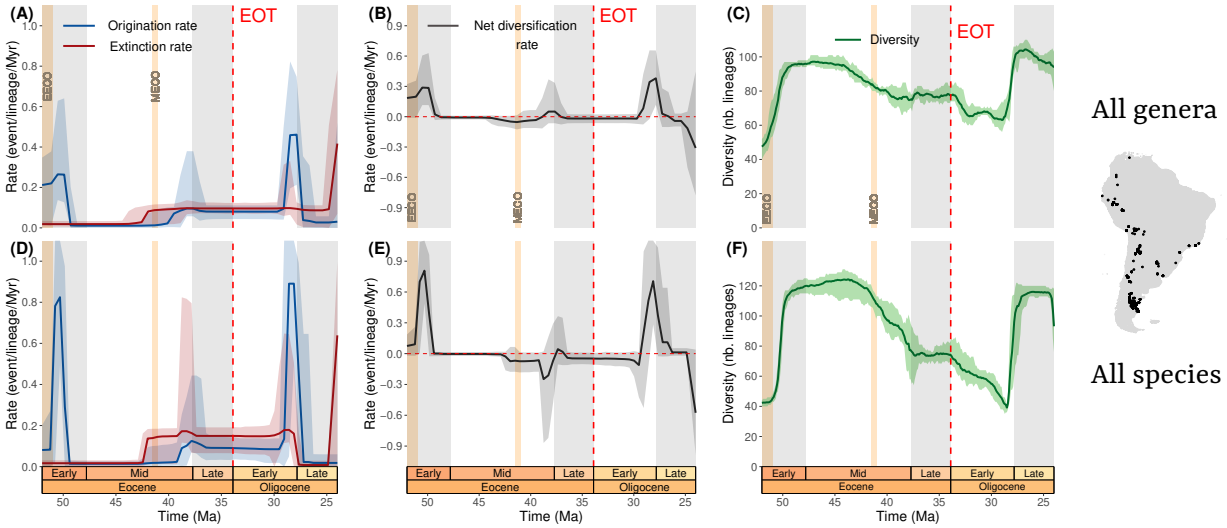

Supp. Figure 12: Diversification (estimated with RJMCMC) and diversity dynamics of South American Mammals from the early Eocene to the Late Oligocene after removing singletons (SALMA smoothed).

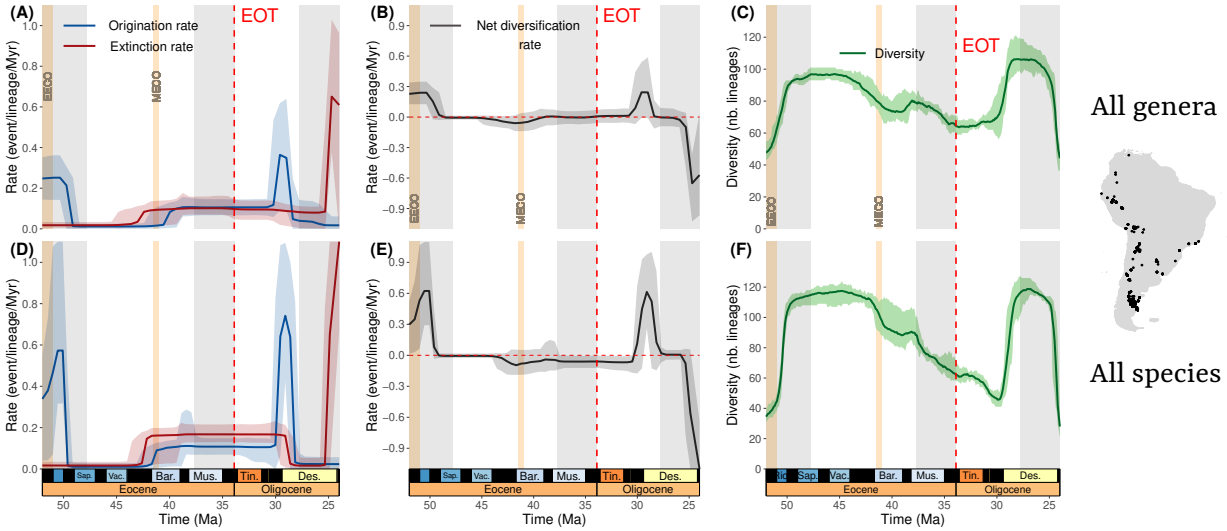

Supp. Figure 13: Diversification (estimated with RJMCMC) and diversity dynamics of South American Mammals from the early Eocene to the Late Oligocene after removing singletons (SALMA kept).

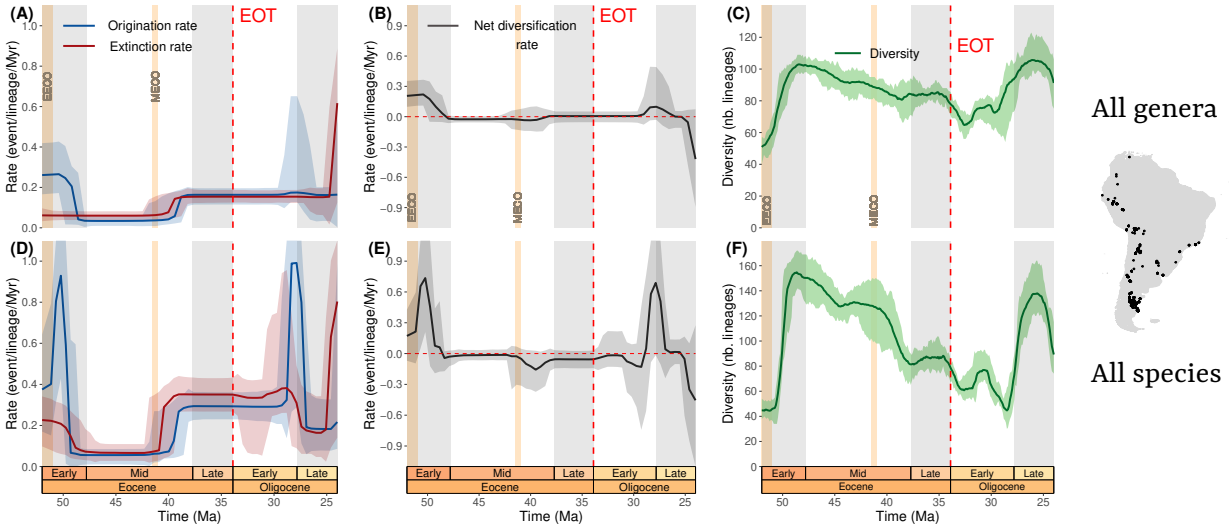

Supp. Figure 14: Diversification (estimated with RJMCMC) and diversity dynamics of South American Mammals from the early Eocene to the Late Oligocene after subsetting our dataset to unique locality-lineage combinations (SALMA smoothed).

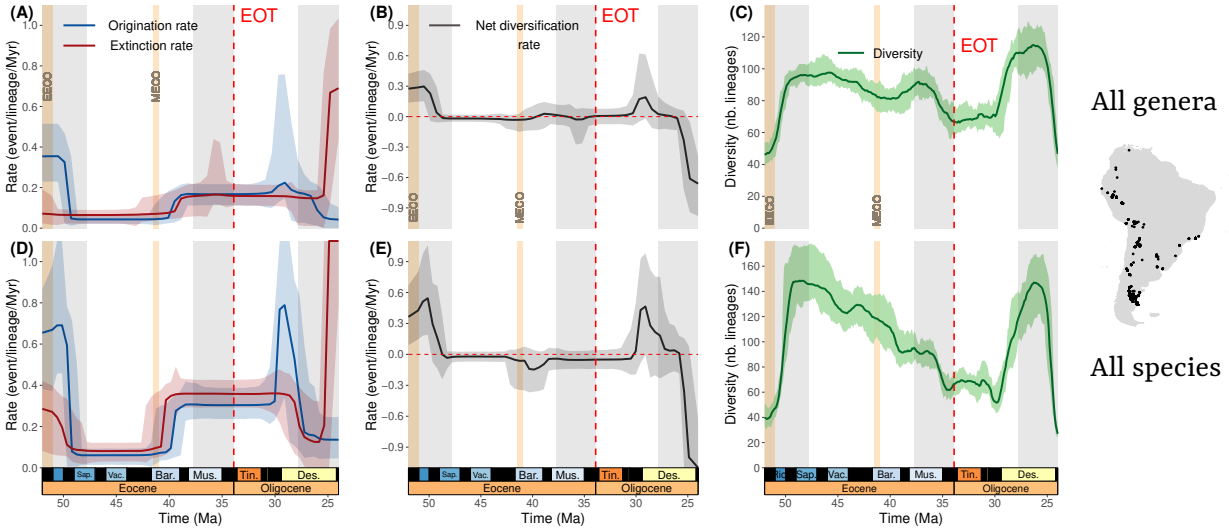

Supp. Figure 15: Diversification (estimated with RJMCMC) and diversity dynamics of South American Mammals from the early Eocene to the Late Oligocene after subsetting our dataset to unique locality-lineage combinations (SALMA kept).

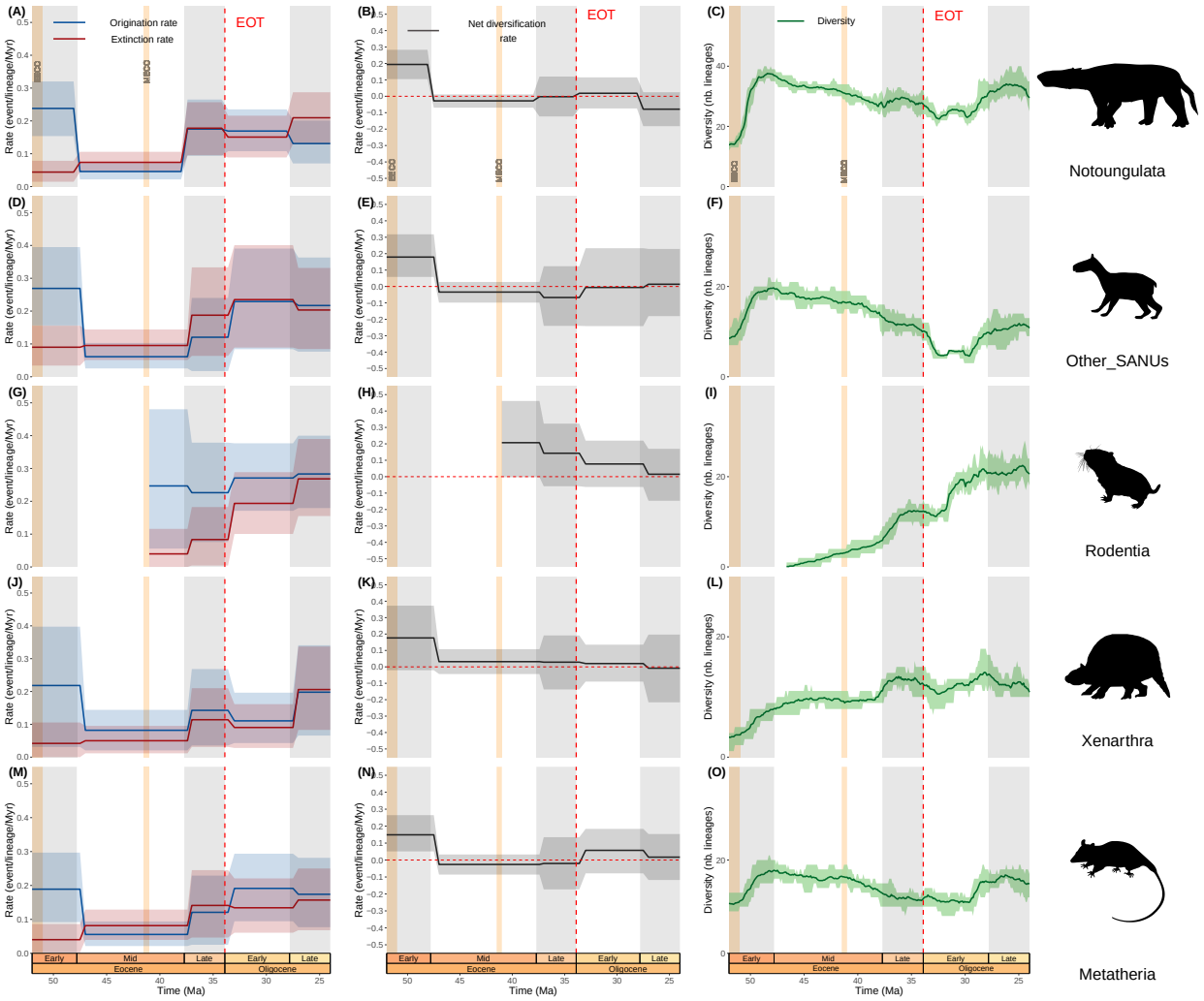

Supp. Figure 16: Genus-level diversity and diversification dynamics of five mammal groups from the early Eocene to the Late Oligocene. Diversification trends are analyzed under the BDCS algorithm using the origination and extinction times inferred by the analysis of the full dataset. Trends are represented for notoungulates (A-C), all the other native ungulates ("Other_SANUs", *i.e.*, Litopterna, Astrapotheria, Pyrotheria, Xenungulata) (D-F), rodents (G-I), xenarthrans (J-L) and metatherians (M-O). Light orange bands represent the early Eocene (53-51 Ma) and the Mid-Eocene (~41 Ma) Climate Optima, respectively abbreviated EECO and MECO.

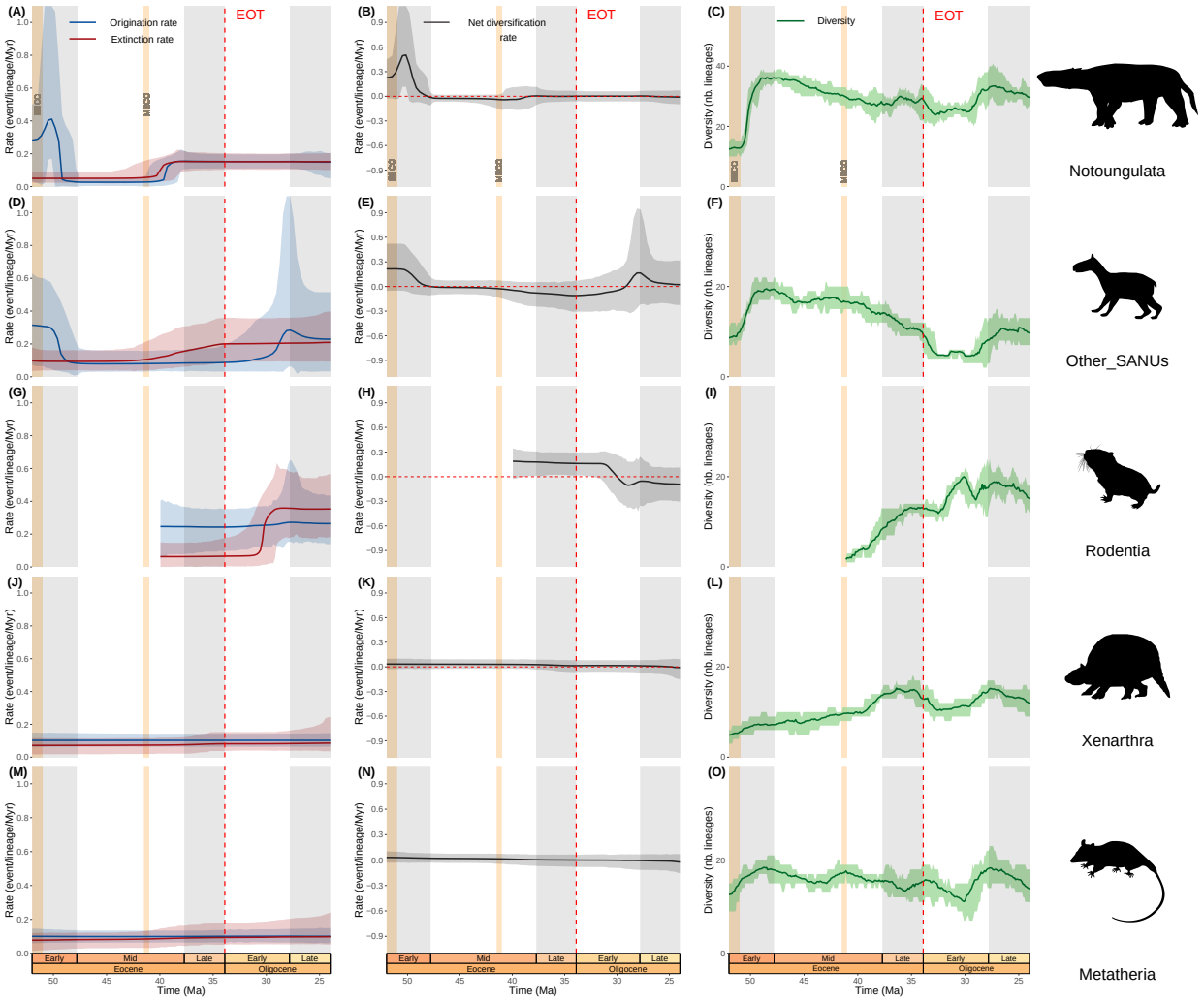

Supp. Figure 17: Genus-level diversity and diversification dynamics (inferred with RJMCMC) of five mammal groups from the early Eocene to the Late Oligocene. Diversification trends are analyzed under the RJMCMC algorithm (de-novo estimation of origination and extinction times). Trends are represented for notoungulates (A-C), all the other native ungulates ("Other_SANUs", *i.e.*, Litopterna, Astrapotheria, Pyrotheria, Xenungulata) (D-F), rodents (G-I), xenarthrans (J-L) and metatherians (M-O). Light orange bands represent the early Eocene (53-51 Ma) and the Mid-Eocene (~41 Ma) Climate Optima, respectively abbreviated EECO and MECO.

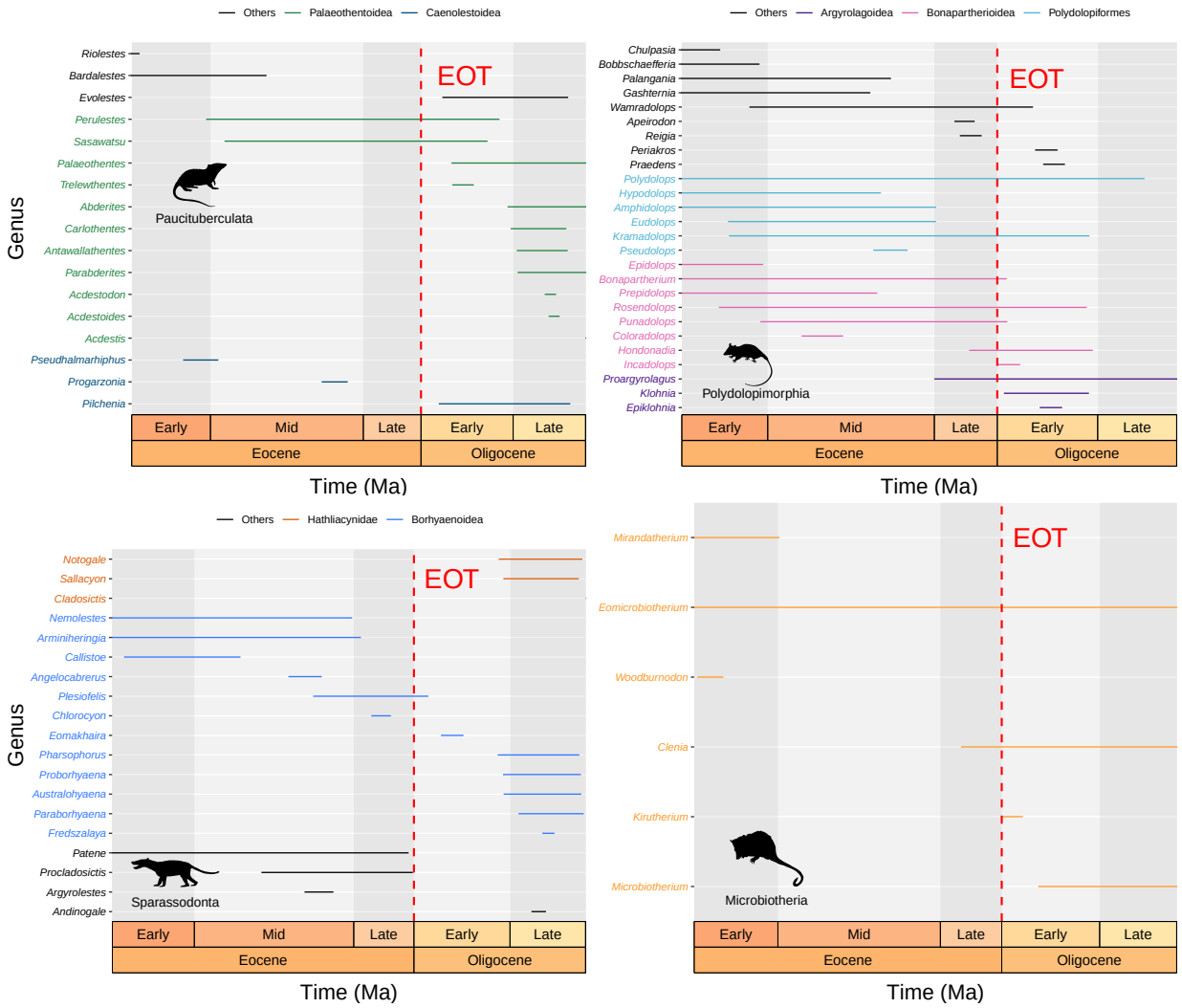

Supp. Figure 18: Metatherian genera longevity across the Eocene-Oligocene. Each panel represents a phylogenetic order, within which each genera are colored based on their superfamily. Following Antoine et al. (2021), we chose to nest the superfamily Argyrolagoidea inside Polydolopimorphia, but we know that this phylogenetic placement is under debate (see Beck (2017)).

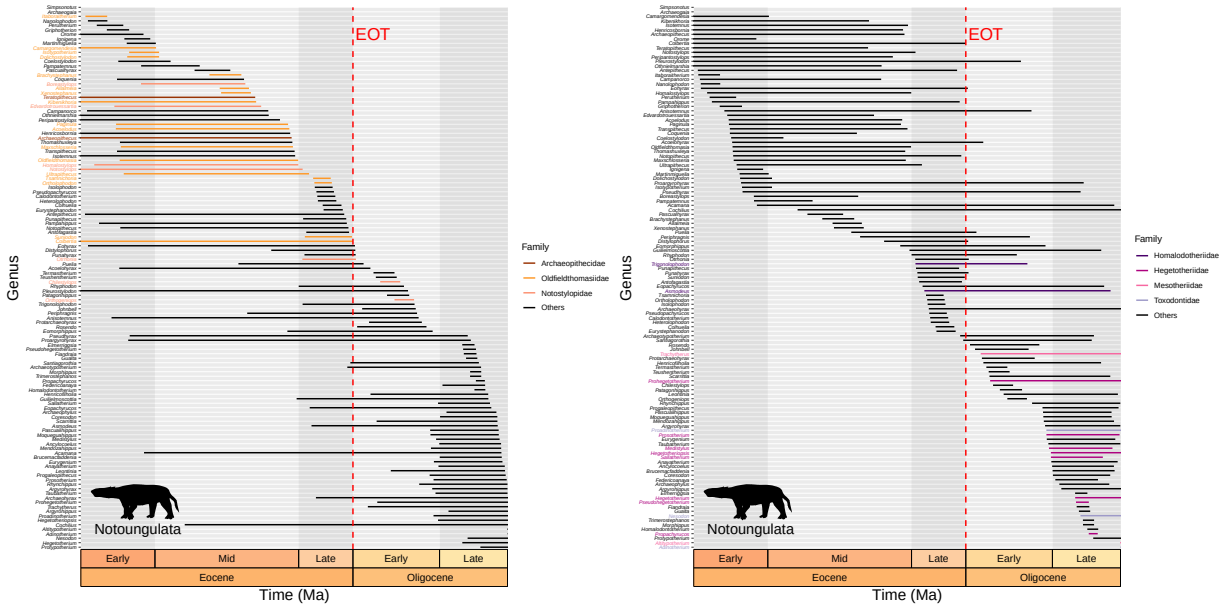

Supp. Figure 19: Notoungulate genera longevity across the Eocene-Oligocene. Both plots display the exact same information. On the left panel, genera were organised by increasing age of extinction, and we highlighted with colors members from three basal families going extinct near the EOT (Oldfieldthomasiidae, Archaeopithecidae and Notostylopidae). Conversely, on the right panel, genera were organised by increasing age of origination, and we highlighted with colors members of families originating near the EOT (Homalodotheriidae, Hegetotheriidae, Mesotheriidae, Toxodontidae).

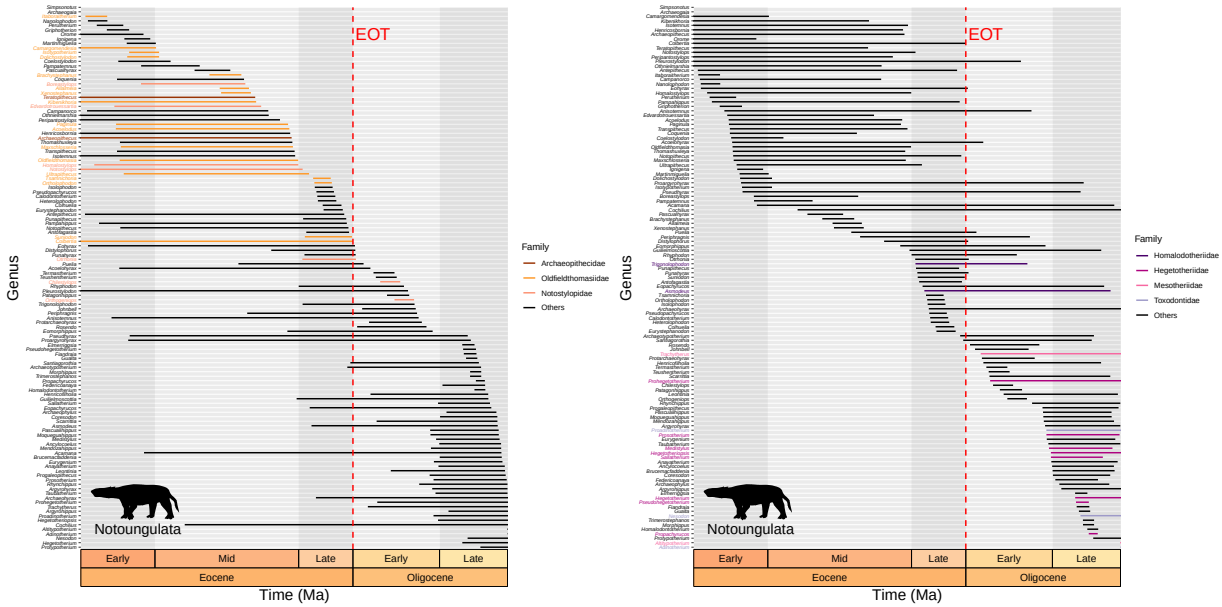

Supp. Figure 20: Notoungulate families longevity across the Eocene-Oligocene. Monophyletic families are shown in black whereas non-monophyletic families are shown in grey. Information about each family's monophyly was extracted from the phylogenetic reconstruction proposed by Billet et al. (2011).

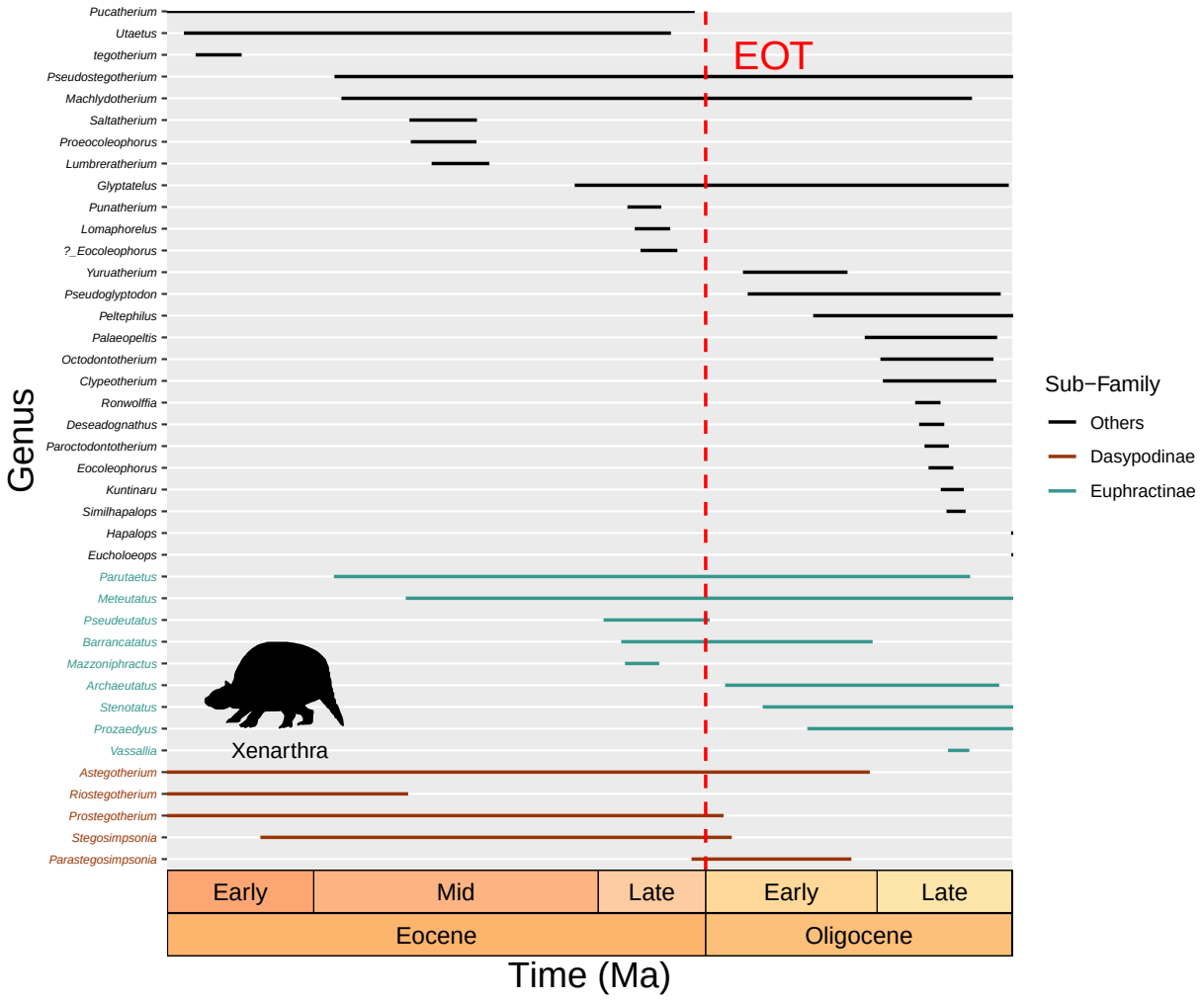

Supp. Figure 21: Xenarthran genera longevity across the Eocene-Oligocene. Genera were colored based on their affinity with two cingulate subfamilies: Dasypodinae and Euphractinae.

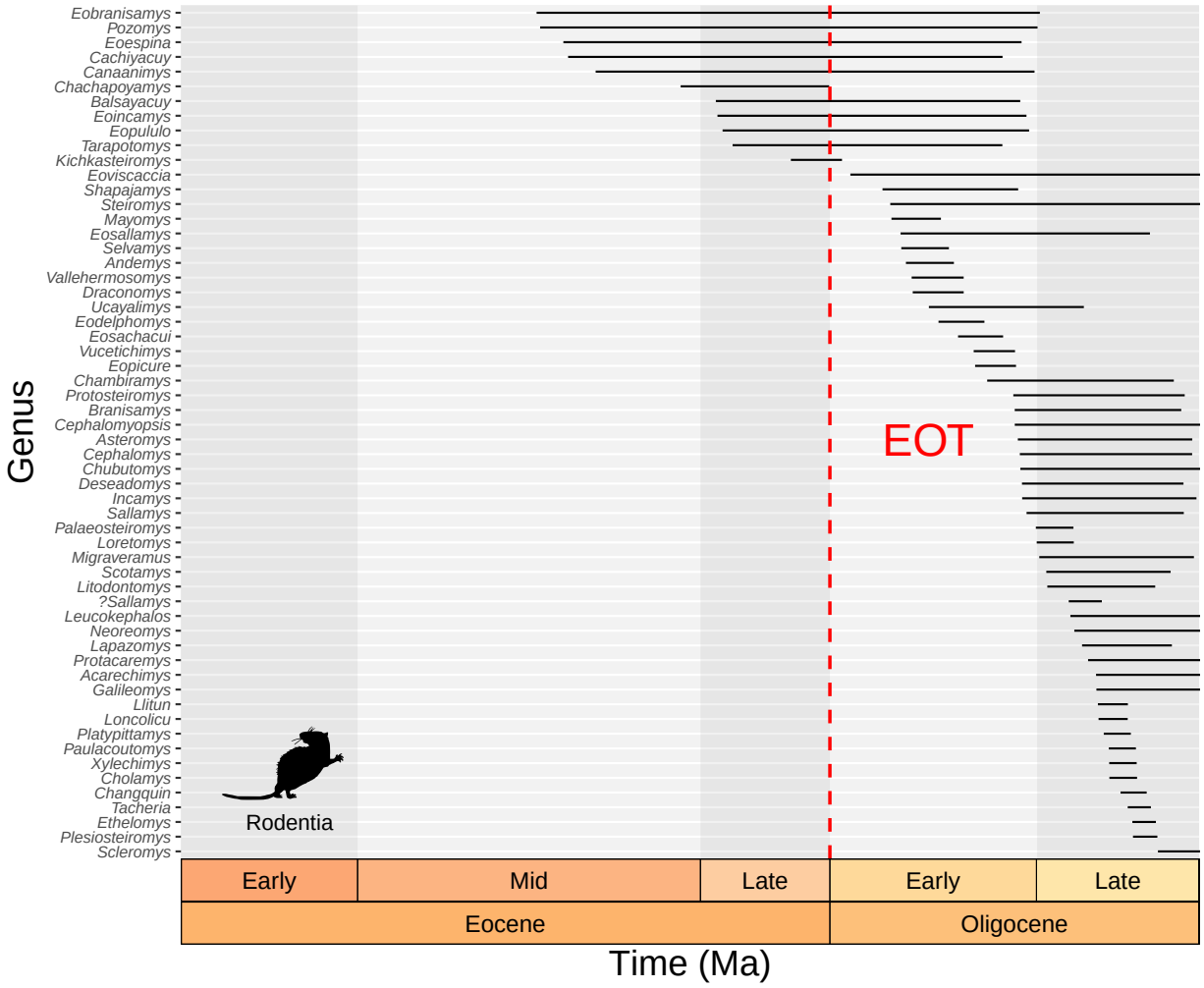

Supp. Figure 22: Rodent genera longevity across the Eocene-Oligocene interval.

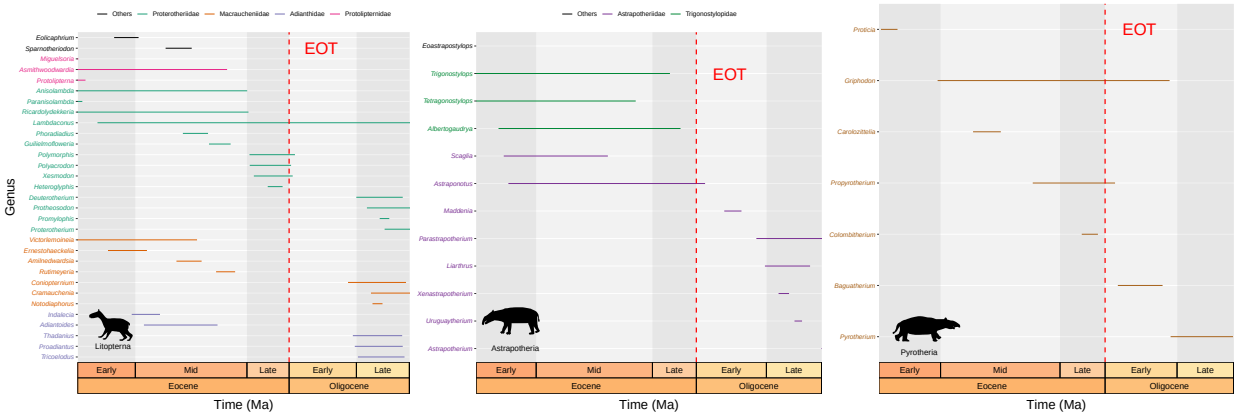

Supp. Figure 23: South American Native Ungulate genera longevity across the Eocene-Oligocene (without Notoungulata). Each panel represents a taxonomic order, within which genera are colored based on their family.

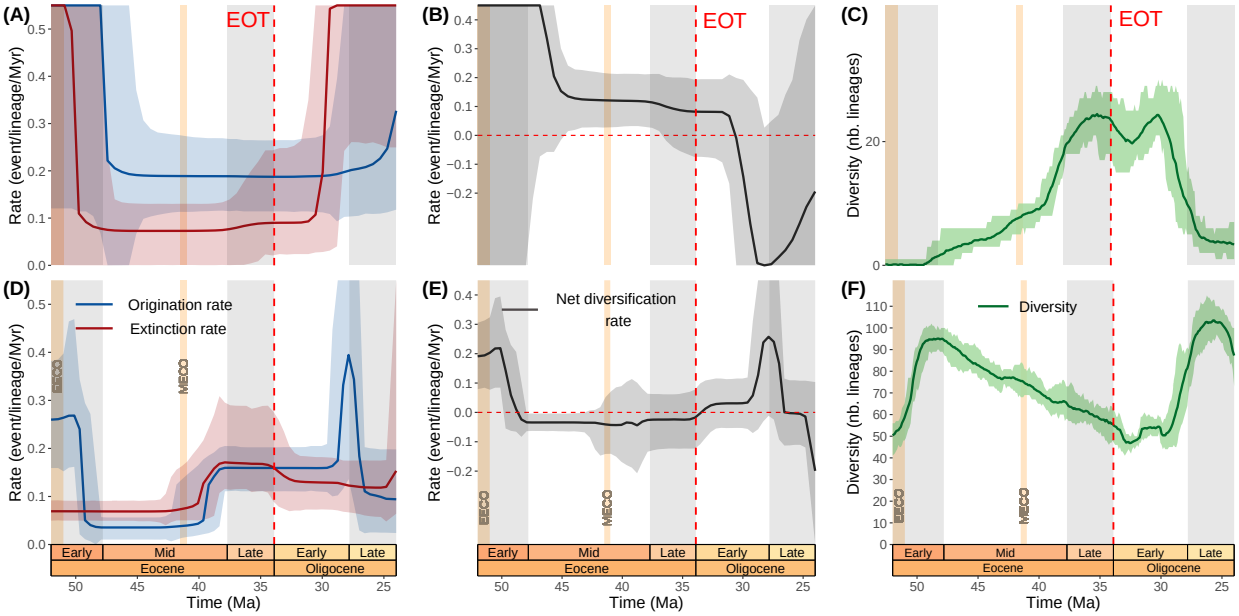

Supp. Figure 24: Diversity and diversification dynamics (inferred with RJMCMC) of South American mammal genera between the Eocene and the Oligocene arranged by latitude. Trends are assessed for the tropical (A-C) and extratropical (D-F) realms. Origination and extinction rates are respectively depicted in blue and red (A and D). Stars indicate significant rate shifts. Their net difference, being the net diversification rate, is represented in black (B and E). Diversity through time is plotted in green (C and F). The maps on the right show the localities of our extratropical (top) and tropical (bottom) occurrences. Light brown vertical bands indicate two key climate events, the early Eocene Climate Optimum (EECO, *ca.* 53–51 Ma) and the Middle Eocene Climate Optimum (MECO, *ca.* 41.5–41 Ma).

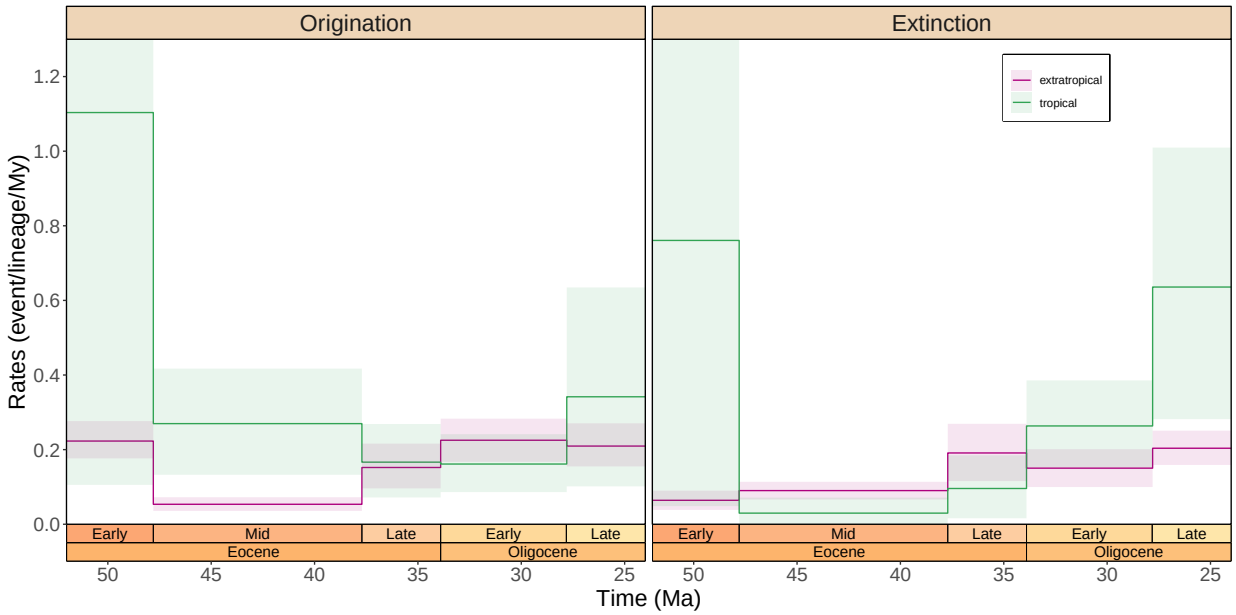

Supp. Figure 25: Tropical and extratropical origination and extinction rates inferred by the BDCS model allowing for rate shift at every geological stage (SALMA smoothed). Tropical and extratropical rates are respectively shown in green and pink, both for the origination (left) or the extinction (right) rate. SALMAs were smoothed to their corresponding sub-epoch.

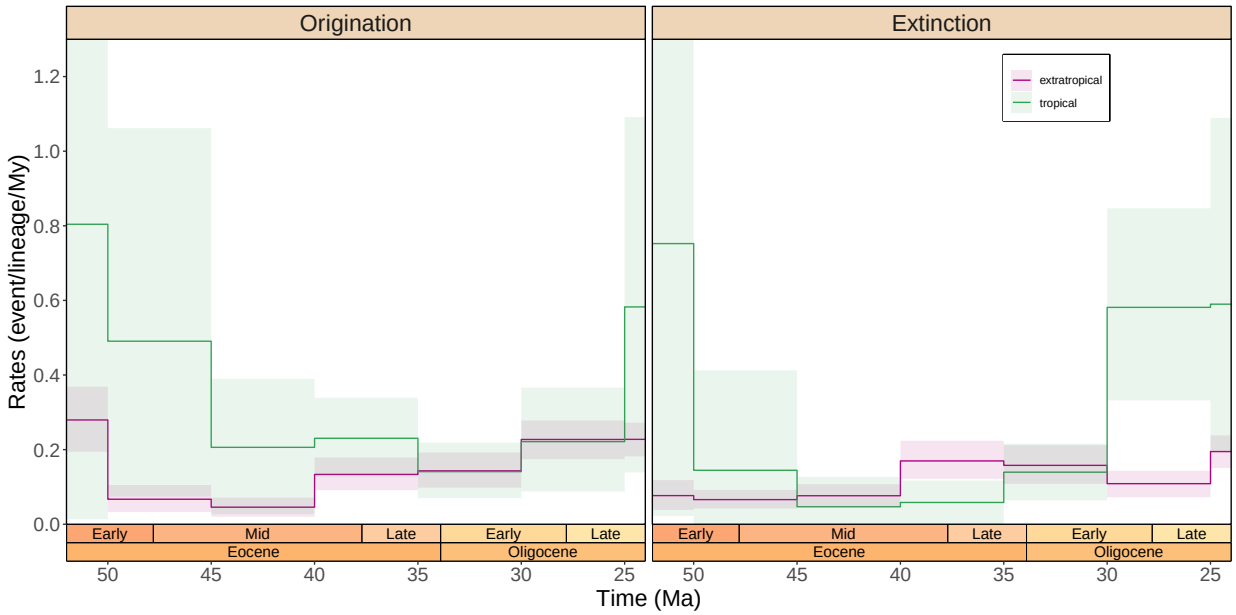

Supp. Figure 26: Tropical and extratropical origination and extinction rates inferred by the BDCS model allowing for rate shift every 5 My (SALMA smoothed). Tropical and extratropical rates are respectively shown in green and pink, both for the origination (left) or the extinction (right) rate. SALMAs were smoothed to their corresponding sub-epoch.

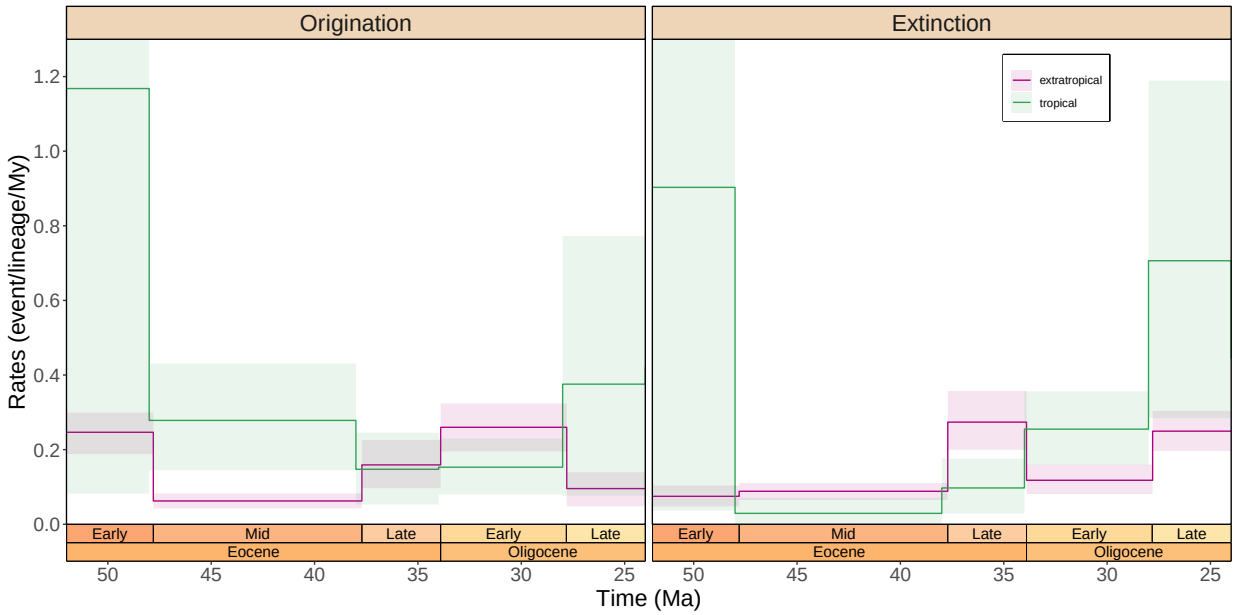

Supp. Figure 27: Tropical and extratropical origination and extinction rates inferred by the BDCS model allowing for rate shift at every geological stage (SALMA kept). Tropical and extratropical rates are respectively shown in green and pink, both for the origination (left) or the extinction (right) rate.

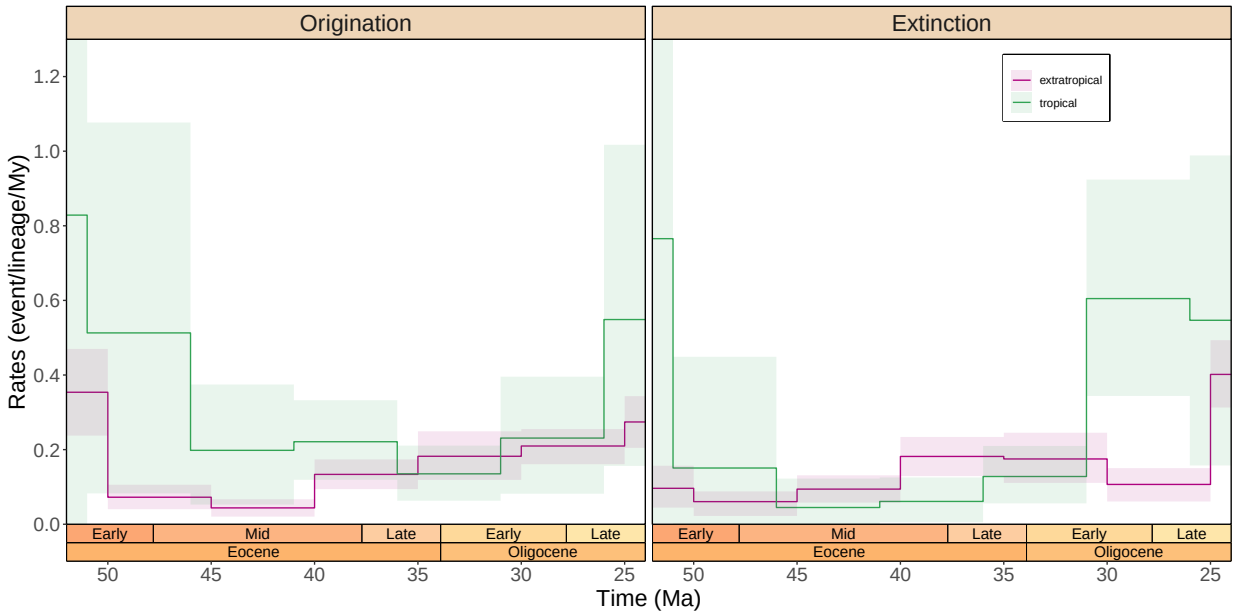

Supp. Figure 28: Tropical and extratropical origination and extinction rates inferred by the BDCS model allowing for rate shift every 5 My (SALMA kept). Tropical and extratropical rates are respectively shown in green and pink, both for the origination (left) or the extinction (right) rate.

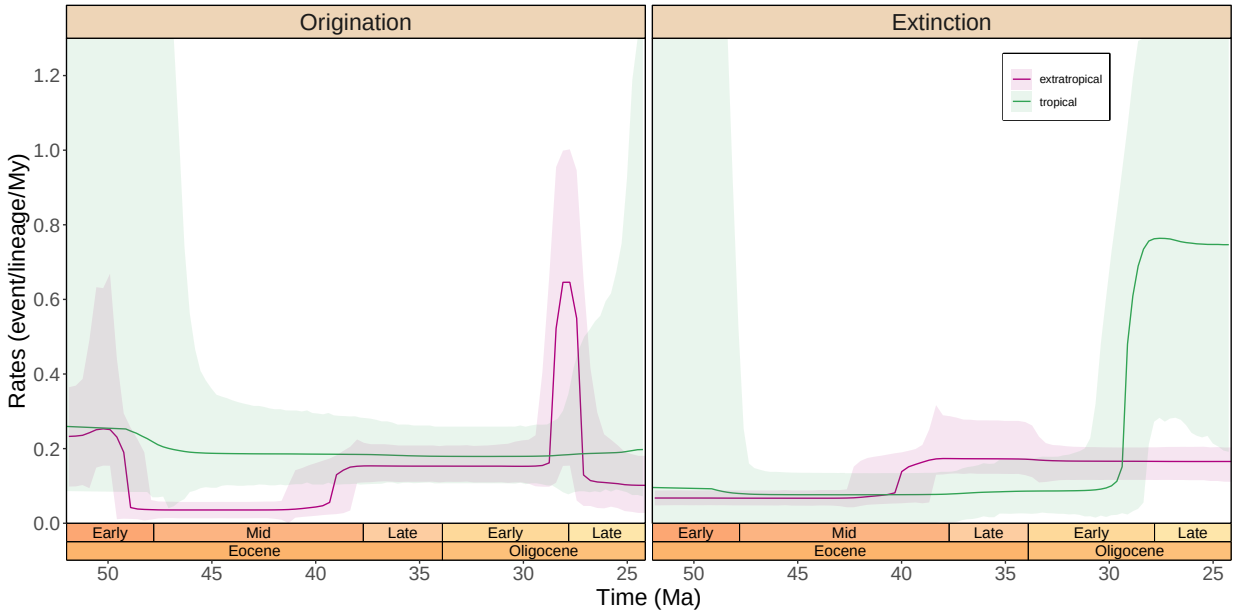

Supp. Figure 29: Tropical and extratropical origination and extinction rates inferred by the RJMCMC model allowing for rate shift every geological epoch (SALMA smoothed). Tropical and extratropical rates are respectively shown in green and pink, both for the origination (left) or the extinction (right) rate. SALMAs were smoothed to their corresponding sub-epochs.

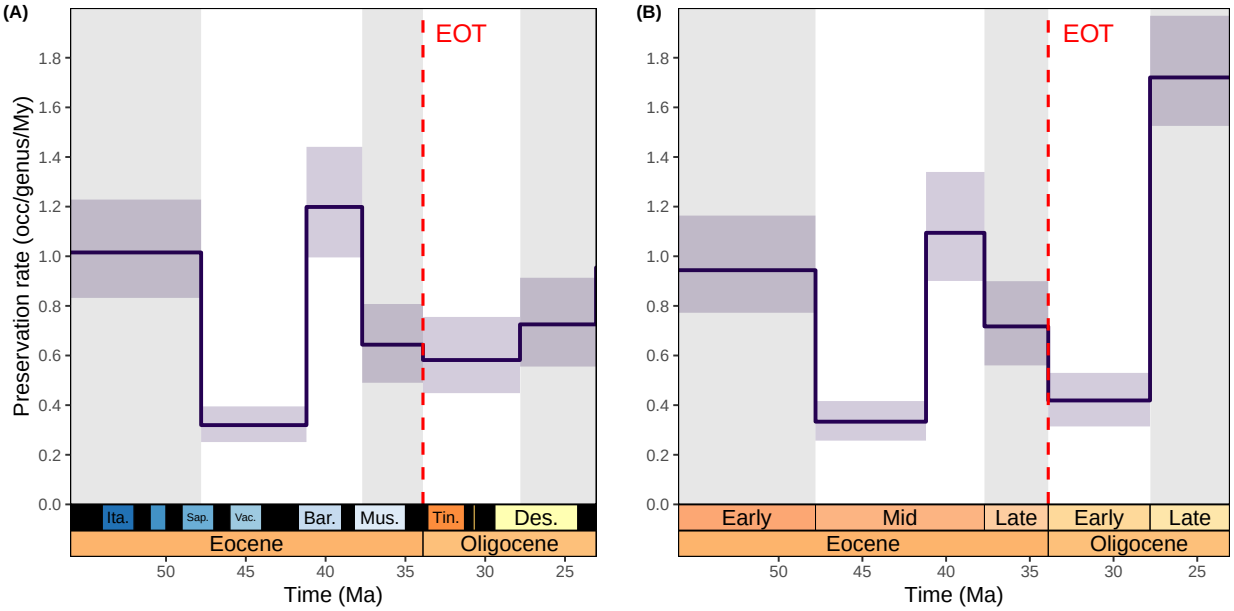

Supp. Figure 30: Estimates of the preservation rate through time in our genus-level diversification analyses. Preservation rate (*i.e.*, estimated number of preserved occurrence per genus and per million years) was estimated both in the analyses with SALMAs kept (A) and smoothed to their corresponding sub-epoch (B). Solid lines represent the mean posterior estimate, and shaded areas their 95% HPD interval. Red vertical lines show the Eocene-Oligocene Transition (EOT)

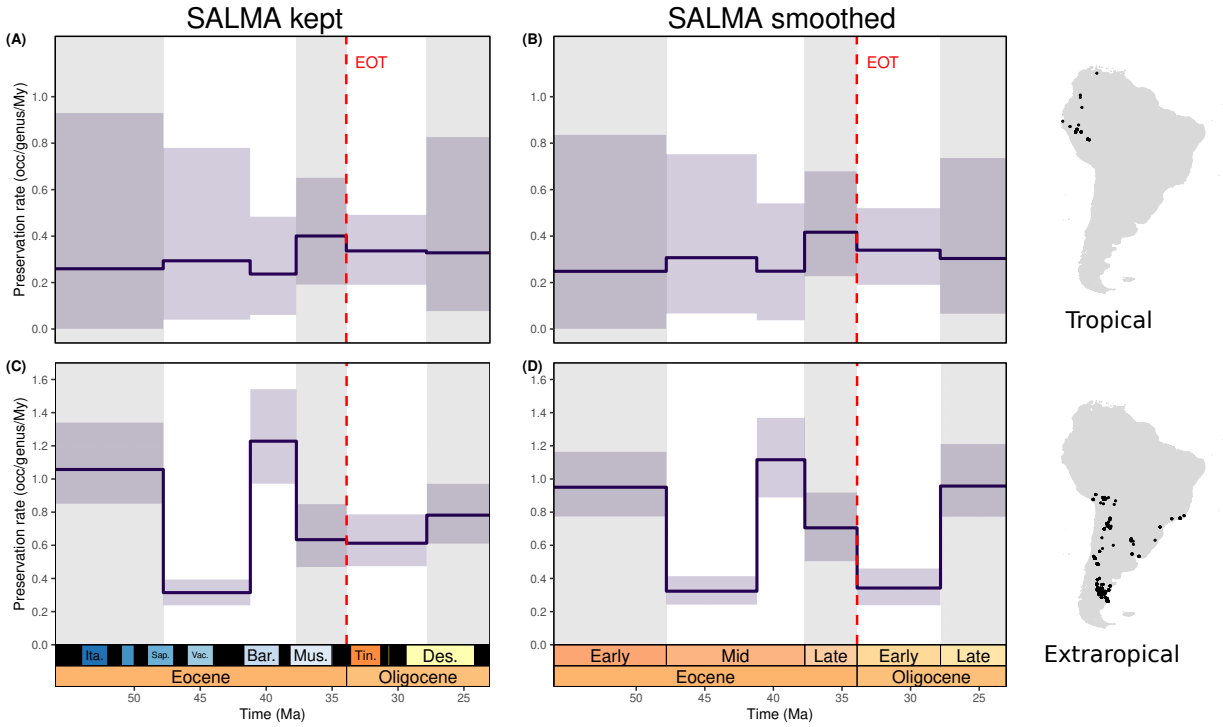

Supp. Figure 31: Estimates of the preservation rate through time and across latitude in our genus-level diversification analyses. Preservation rate (*i.e.*, estimated number of preserved occurrence per genus and per million years) was estimated for extratropical and tropical genera respectively with SALMAs kept (A and C) or smoothed to their corresponding sub-epoch (B and D). Solid lines represent the mean posterior estimate, and shaded areas their 95% HPD interval. Red vertical lines show the Eocene-Oligocene Transition (EOT).

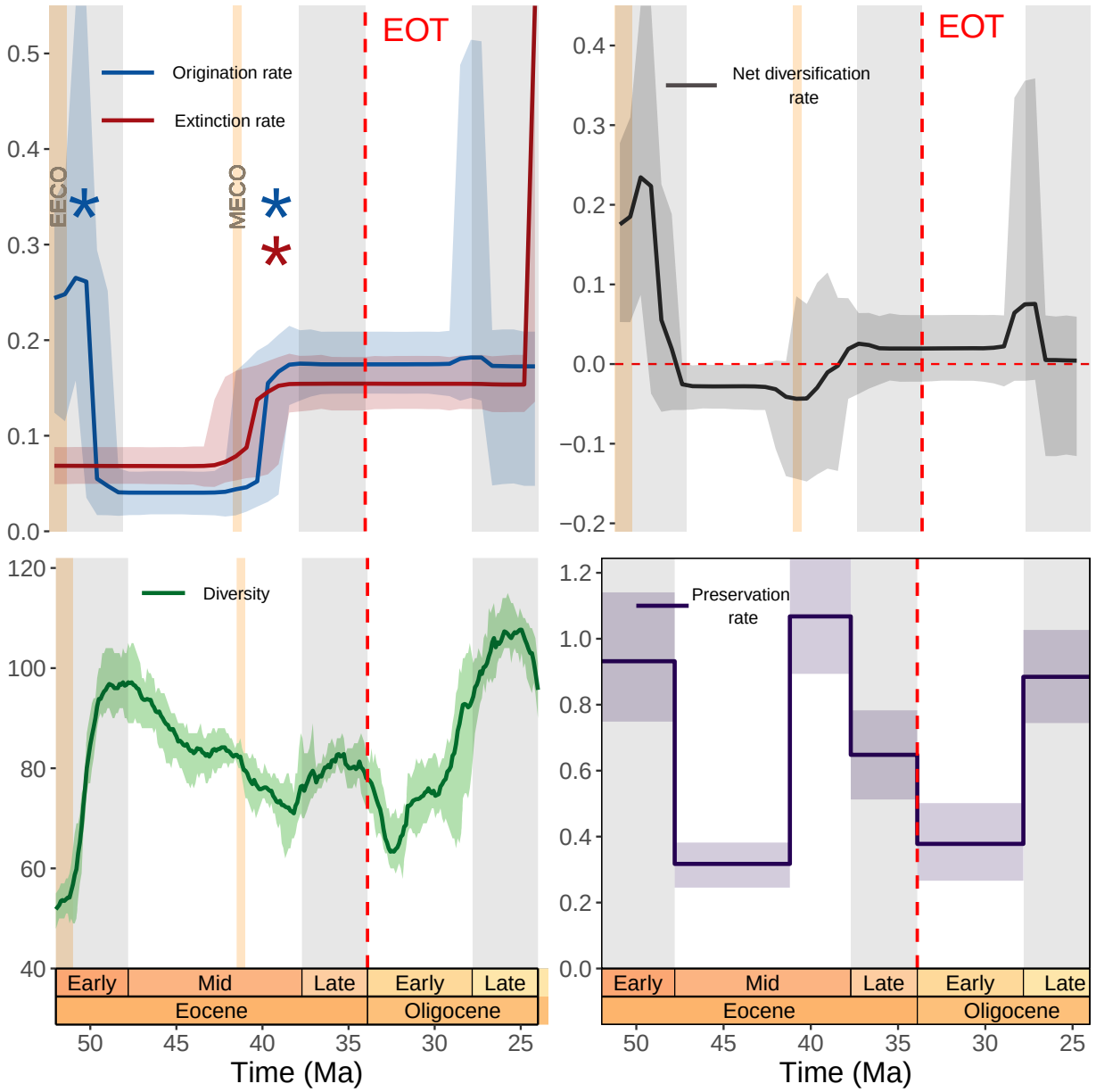

Supp. Figure 32: Diversification, diversity and preservation trends inferred from the full genus-level dataset (SALMA kept) after extending in the early Oligocene the age range western Amazonian occurrences from localities in the regions of Contamana and Tarapoto originally assigned to an Eocene age, according to Campbell et al.'s (2021) 'reverse tip-dating' inferences on concerned localities, further amalgamated as local faunas.

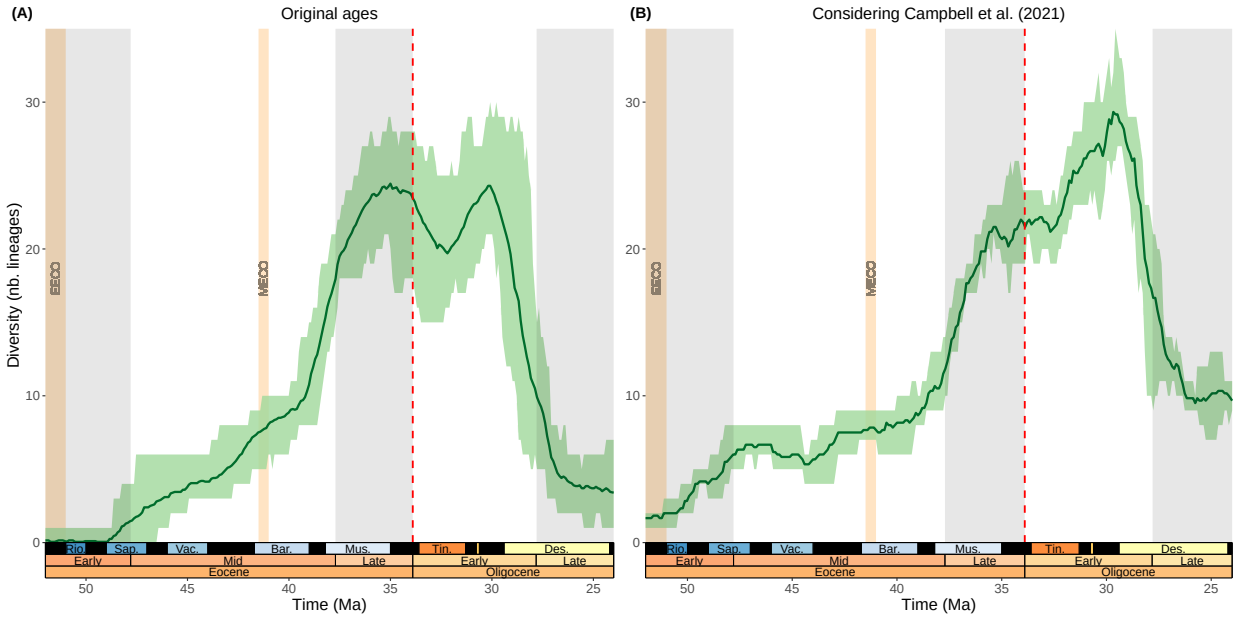

Supp. Figure 33: Diversity trends among tropical taxa obtained after extending in the early Oligocene the age range East-Amazonian occurrences from localities in the regions of Contamana and Tarapoto originally assigned to an Eocene age, according to Campbell et al.'s (2021) hypotheses (B) or not (A).

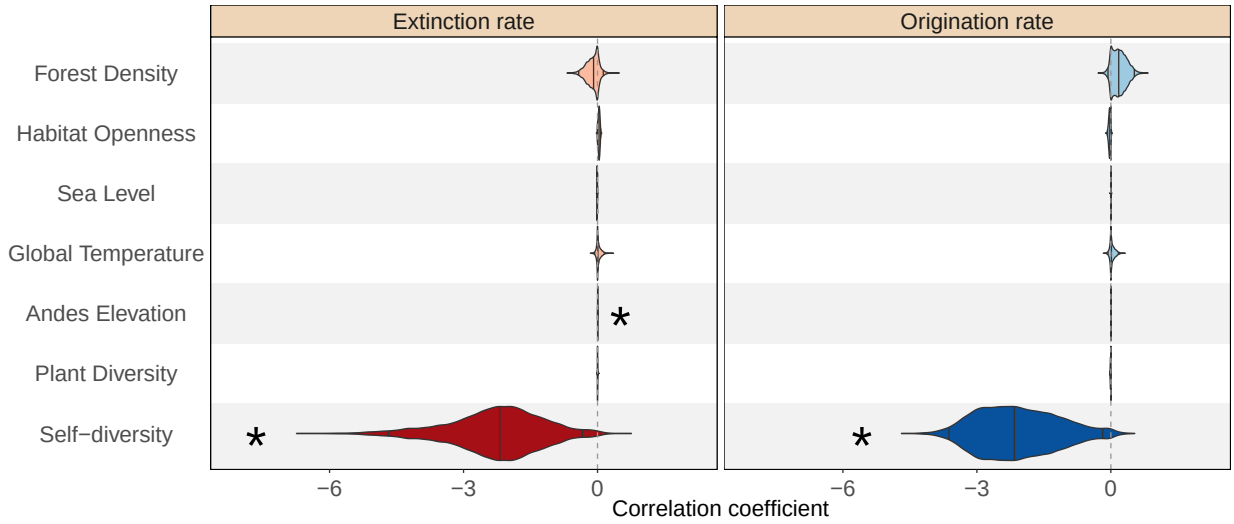

Supp. Figure 34: Bayesian estimation of correlation parameters on origination (blue) and extinction (red) rates with palaeoenvironmental covariates by considering our dataset as a whole throughout our study period. 2.5%, 50% and 97.5% quantiles are indicated in the distribution of each parameter by vertical lines, respectively from left to right. The interval between the leftmost and the rightmost vertical line of each parameter is therefore its 95% Highest Posterior Density (HPD) interval. Significant correlation coefficients, *i.e.*, having shrinkage weights > 0.5 and not including 0 in their 95% HPD are highlighted by stars and darker shades.

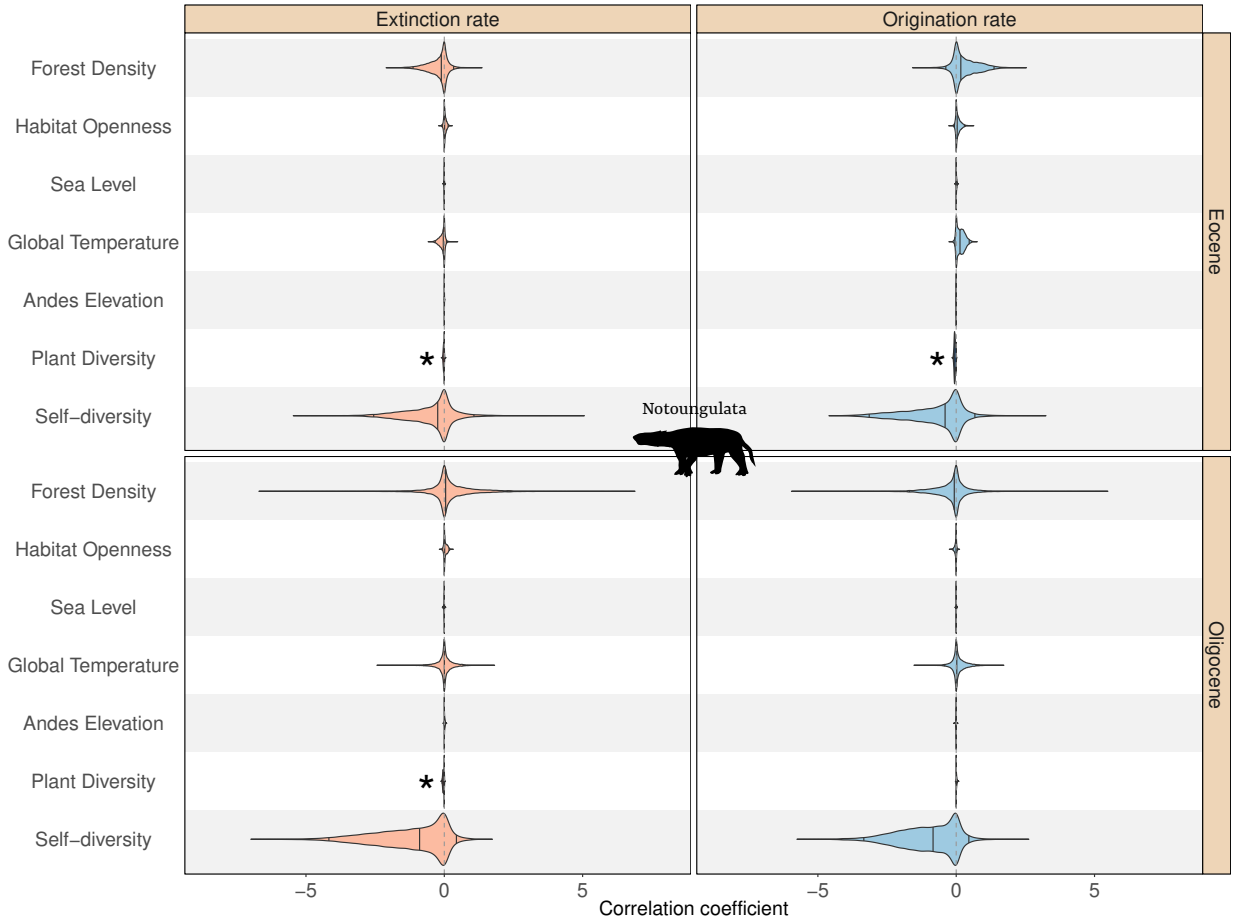

Supp. Figure 35: Bayesian estimation of correlation parameters on origination (blue) and extinction (red) rates with palaeoenvironmental covariates by constraining our analyses to notoungulate taxa. 2.5%, 50% and 97.5% quantiles are indicated in the distribution of each parameter by vertical lines, respectively from left to right. The interval between the leftmost and the rightmost vertical line of each parameter is therefore its 95% Highest Posterior Density (HPD) interval. Significant correlation coefficients, *i.e.*, having shrinkage weights > 0.5 and not including 0 in their 95% HPD are highlighted by stars and darker shades.

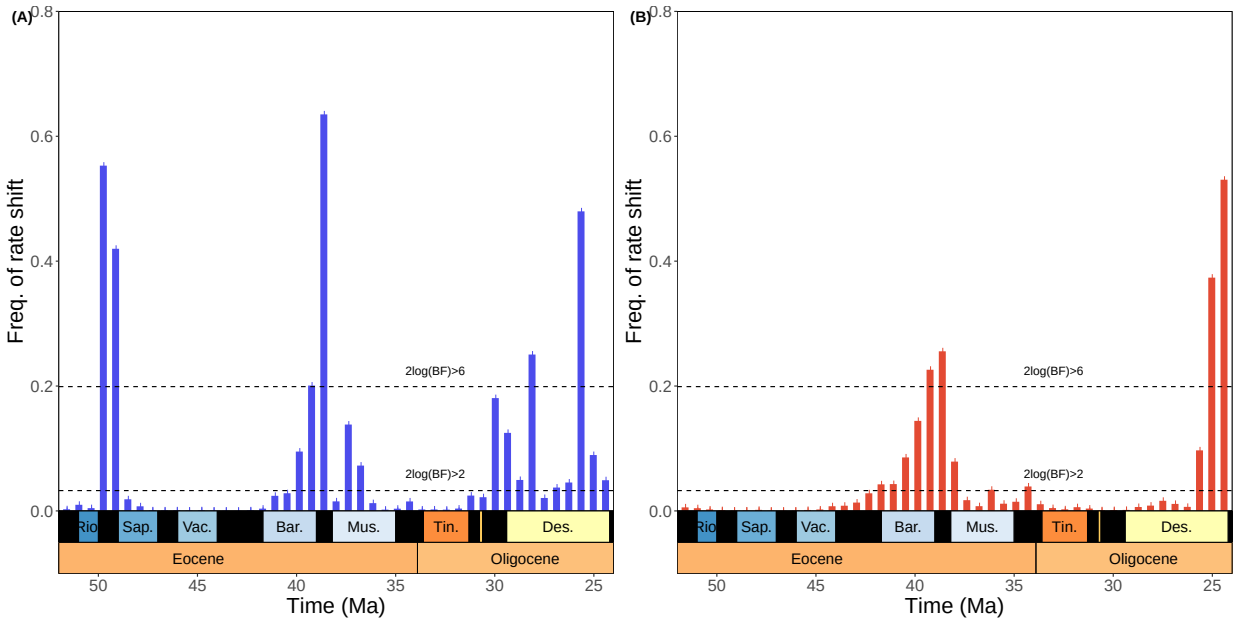

Supp. Figure 36: Frequency of extinction (A) and origination (B) rate shifts obtained from analysis of the full genus dataset with RJMCMC (SALMAs kept). Dashed horizontal lines indicate 2 * log Bayes factor of 2 and 6, respectively indicating significant and strongly-supported rate shifts

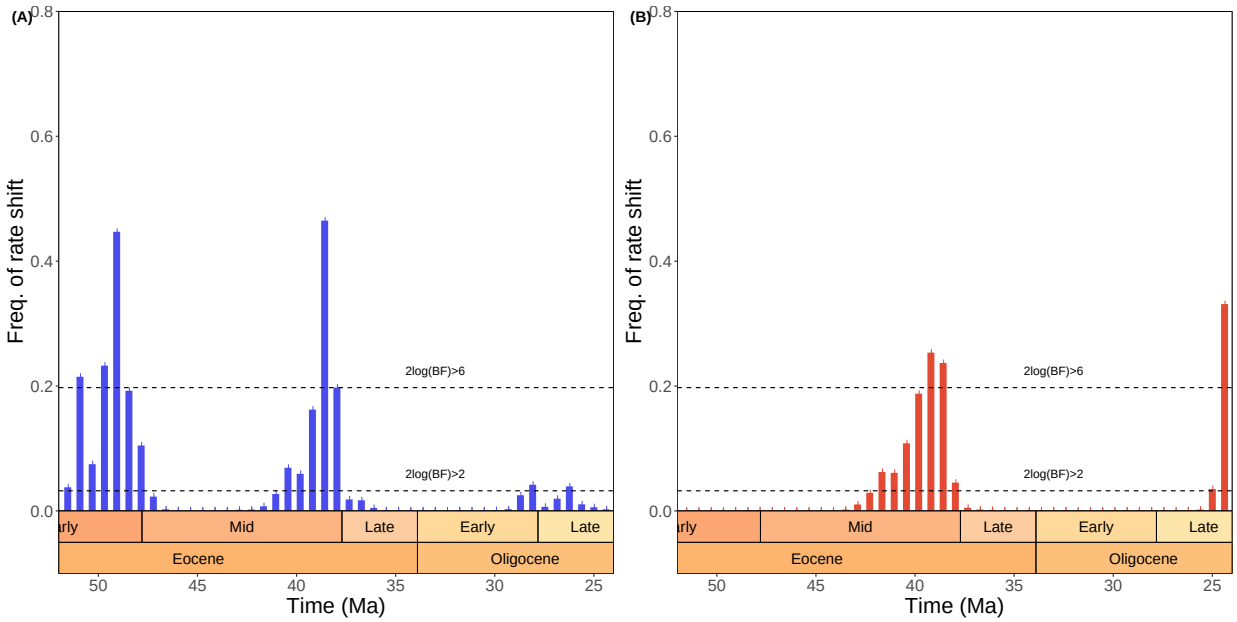

Supp. Figure 37: Frequency of extinction (A) and origination (B) rate shifts obtained from analysis of the genus dataset with RJMCMC (SALMAs smoothed). Dashed horizontal lines indicate 2 * log Bayes factor of 2 and 6, respectively indicating significant and strongly-supported rate shifts.

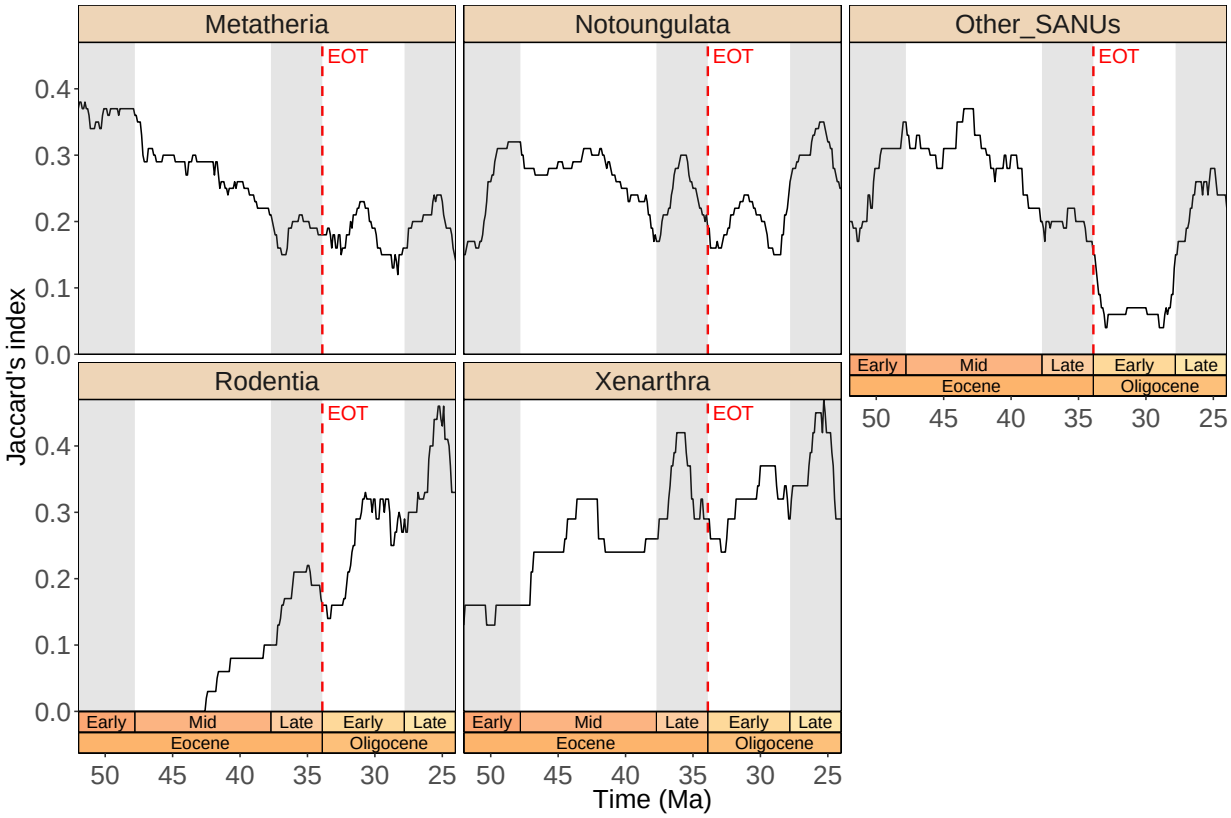

Supp. Figure 38: Taxonomic Jaccard's similarity indices through time for the five main mammal groups. Given a time t, they report how similar (in terms of shared genera) mammal assemblages were before and after t. The dashed red vertical lines indicate the EOT. Similarity values between Eocene and Oligocene faunas are always located near a local or global minimum of the similarity curve.

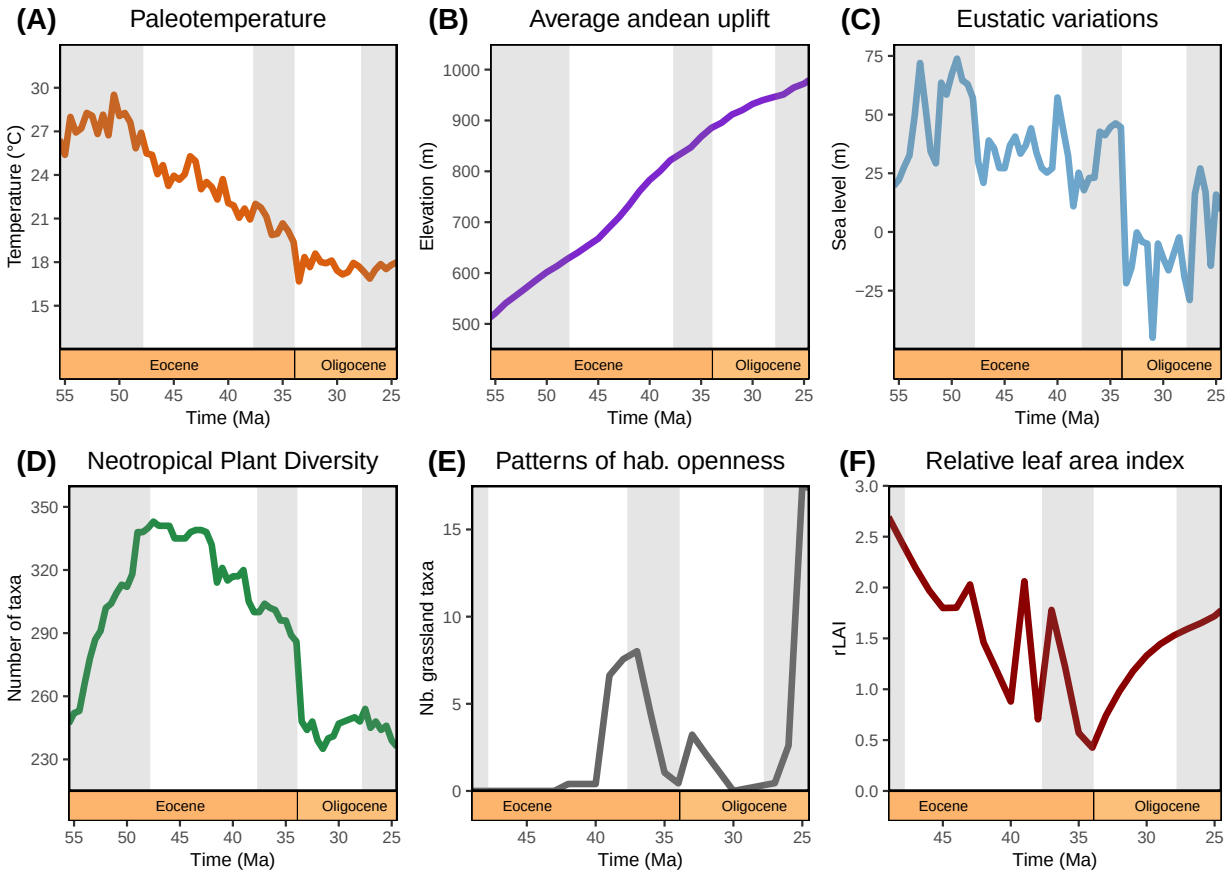

Supp. Figure 39: Environmental variables used in the Multivariate Birth-Death analyses carried out in this study. (A) Planktonic-based paleotemperature (28). (B) Andean paleoelevation (30). (C) Eustatic variations (29). (D) Neotropical plant diversity (31). (E) Temporal patterns of Patagonian open habitats (33). (F) Relative leaf area index (35). Further details on the variables are provided in **Tab. S2**.

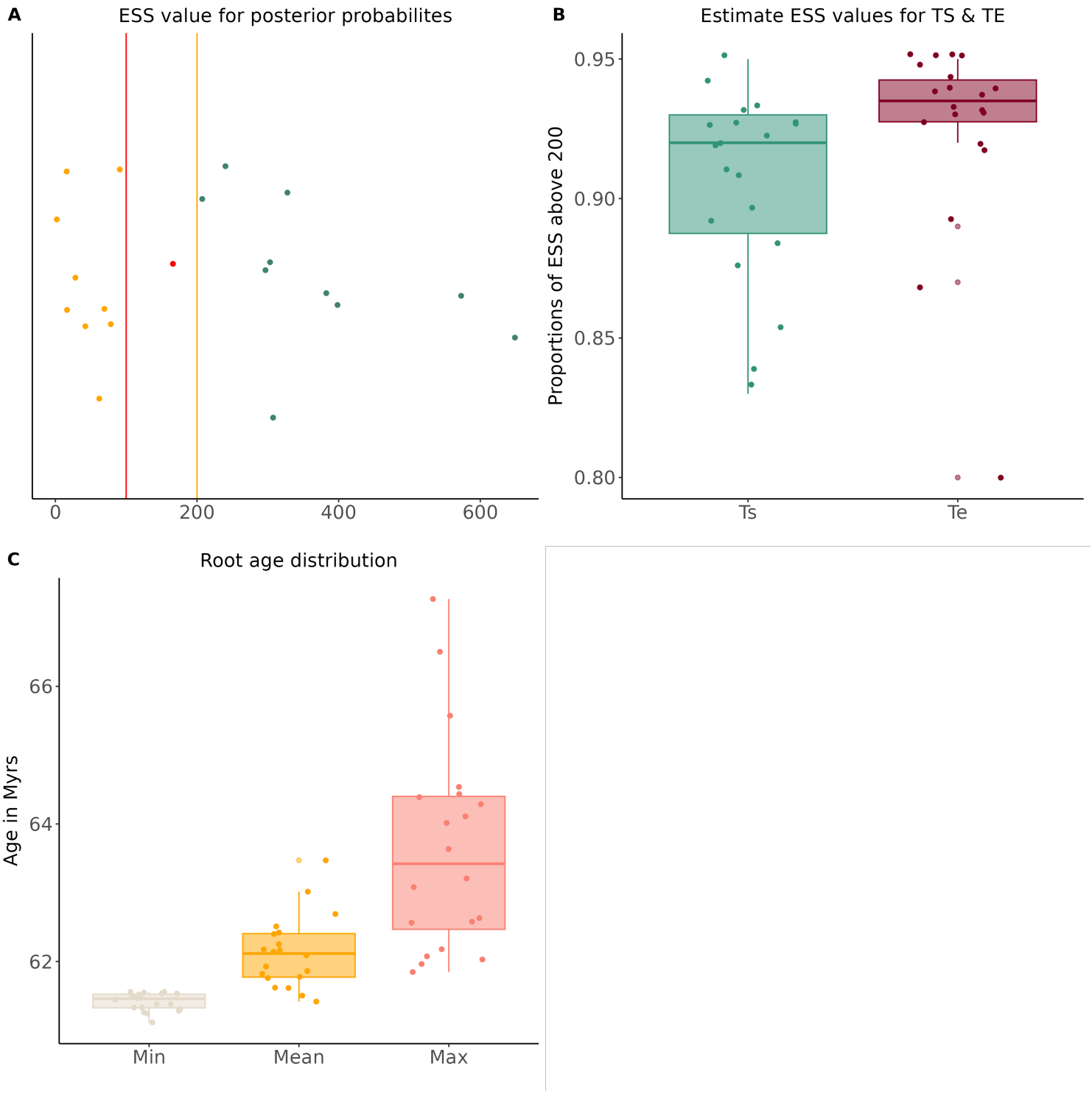

Supp. Figure 40: Convergence of our main PyRate runs.

We displayed the ESS of the model posterior probability for all the 20 replicates we ran (A). ESS greater than 200 (first-scale indicator of a run that converged, $n = 11$) are displayed in green. The proportion of origination and extinction times (resp. T_S and T_E) that converged (*i.e.*, with ESS > 200) are shown in, for each of our 20 replicates (B). The plot (C) is artefactual as it shows the posterior estimates of the mean death age of our group, together with their lower and upper boundaries of the 95% HPD interval. However, we excluded on purpose the occurrences older that 60 My.

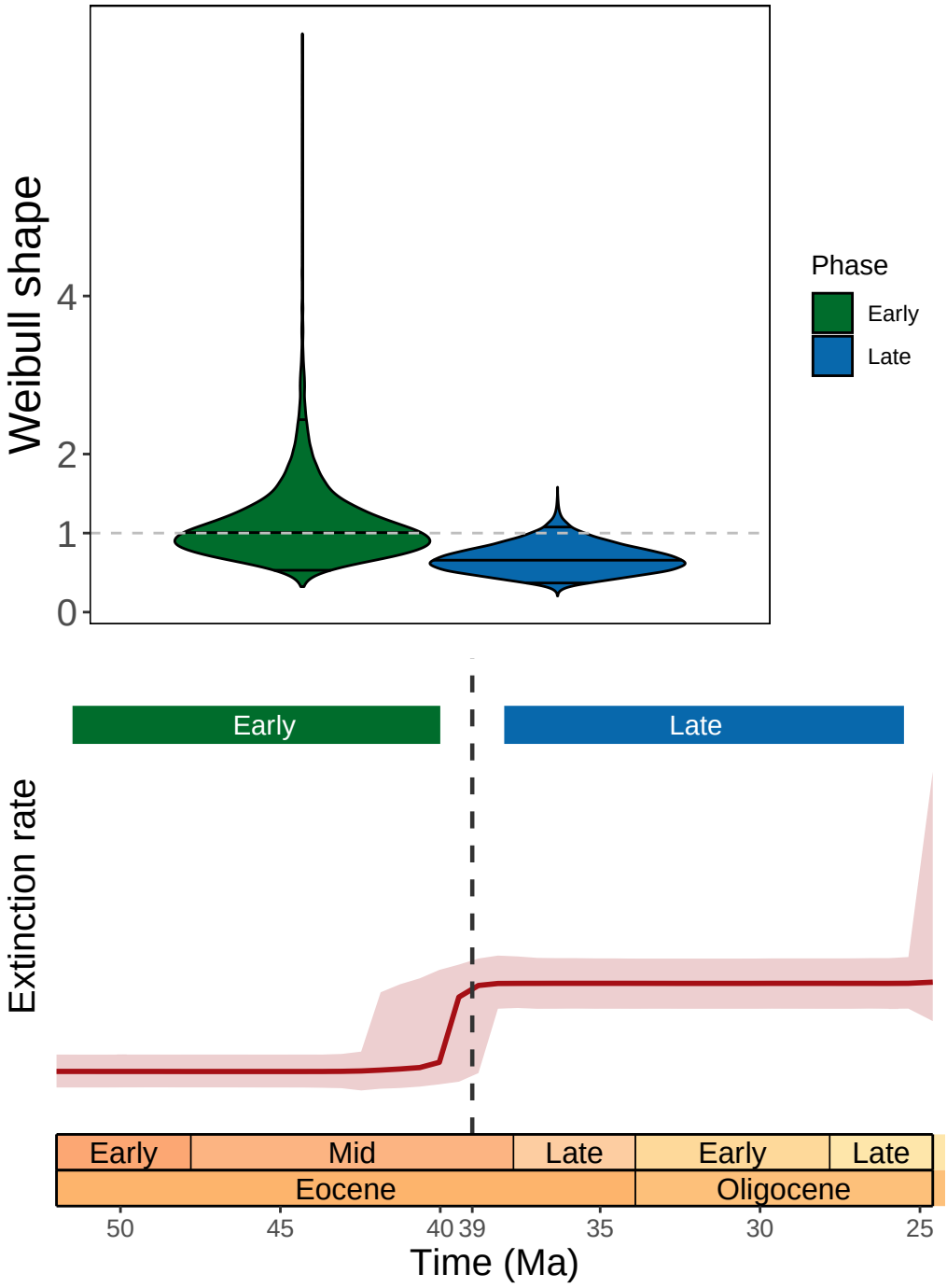

Supp. Figure 41: Posterior estimate of the shape parameter of the Weibull distribution for the ADE analyses of the 'Early' and 'Late' occurrence datasets, with constant extinction rate. 2.5%, 50% and 97.5% quantiles are indicated in the distribution of each parameter by black horizontal lines, respectively from bottom to top.

Supplementary tables

Supp. Table 1: Number of occurrences (n_occ), of genera (n_gen), of species (n_sp), of singleton (*i.e.*, genera or species only represented by a single occurrence, n_singl_gen and n_singl_sp respectively) and proportion of singletons (prop_singl_gen and prop_singl_sp) per order. The 96 occurrences (49 genera) without specified order are not displayed here, but counted in the 'Total' row.

order	n_occ	n_gen	n_singl_gen	prop_singl_gen	n_sp	n_singl_sp	prop_singl_sp
Astrapotheria	137	15	5	0.33	33	19	0.58
Stem Metatheria	46	21	9	0.43	36	28	0.78
Chiroptera	2	1	0	0	2	2	1
Cingulata	308	45	17	0.38	118	65	0.55
Dasyuromorphia	3	1	0	0	2	1	0.5
Didelphimorphia	13	5	3	0.6	7	4	0.57
Gondwanatheria	1	1	1	1	1	1	1
Groeberida	3	1	0	0	2	1	0.5
Litopterna	218	44	18	0.41	88	48	0.55
Microbiotheria	60	8	2	0.25	19	8	0.42
Notoungulata	1097	136	39	0.29	301	147	0.49
Paucituberculata	160	27	13	0.48	49	30	0.61
Pilosa	118	26	14	0.54	54	33	0.61
Polydolopimorphia	140	30	12	0.4	68	43	0.63
Primates	57	14	9	0.64	19	11	0.58
Pyrotheria	35	11	8	0.73	15	10	0.67
Rodentia	700	101	31	0.31	216	110	0.51
SANU	47	9	4	0.44	23	16	0.7
Sparassodonta	218	29	7	0.24	49	21	0.43
Xenungulata	4	2	1	0.5	4	4	1
Total	**3378**	**536**	**200**	**0.37**	**1115**	**609**	**0.55**

Supp. Table 2: Selected environmental variables chosen for the Multivariate Birth-Death analyses.

Covariate	Description	Unit	Source
Temperature	Global average temperature across the Cenozoic derived from oxygen isotopes generated using benthic Foraminifera	°C	Boshman and Condamine (2022) from Westerhold et al. (2020)
Andean uplift	Elevation data compiled from 36 geomorphological domains all across the Andes	m	Boschman (2021)
Sea level	Global eustatic variations derived from d18O and Mg/Ca records	m	Miller et al. (2020)
Neotropical plant diversity	Cenozoic (66-20 Ma) plant diversity in the Neotropics	nb. taxa	Jaramillo et al. (2006)
Habitat openness	Temporal patterns in the relative abundance of open habitats in Patagonia	nb. plant taxa	Solórzano and Nuñez (2021) from Palazzesi and Berrada (2012) and Dunn et al. (2015)
Relative Leaf Area Index (rLAI)	Quotient between leaf and ground areas, obtained via phytolith quantification on fossil leaves from Patagonia. Proxy for forest density.	m^2/m^2	Solórzano and Nuñez (2021) from Dunn et al. (2015)

Supp. Table 3: Posterior estimates of the multivariate birth-death correlation parameters with the origination rate (G_λ) for our full Eocene (52-33.9 Ma) dataset, and their associated Shrinkage weights (w_λ). Median estimates are shown along with their 95% Highest Posterior Density (HPD) interval. Significant correlations, *i.e.*, having a w_λ larger than 0.5 and of which the 95% HPD of the associated coefficients do not overlap 0 are shown in bold. In the case of temperature, the proportion of the posterior distribution of the associated G_λ below 0 is around 0.0348. Although this is larger than 0.025, we consider it small enough to claim for a significant correlation.

Covariate	G_λ	G_λ 95% HPD	$w_{G,\lambda}$	$w_{G,\lambda}$ 95% HPD
Self-diversity	**-3.24**	**[-4.749; -1.462]**	**0.892**	**[0.482; 0.996]**
Plant Diversity	-0.001	[-0.034; 0.021]	0.283	[0.001; 0.962]
Andes Elevation	0	[-0.003; 0.008]	0.251	[0; 0.962]
Global Temperature	**0.236**	**[-0.004; 0.492]**	**0.825**	**[0.025; 0.995]**
Sea Level	0.01	[-0.006; 0.041]	0.433	[0.001; 0.977]
Habitat Openness	0.087	[-0.029; 0.264]	0.429	[0.001; 0.972]
Forest Density	0.017	[-0.552; 0.69]	0.221	[0; 0.954]

Supp. Table 4: Posterior estimates of the multivariate birth-death correlation parameters with the extinction rate (G_μ) for our full Eocene (52-33.9 Ma) dataset, and their associated Shrinkage weights (w_μ). Median estimates are shown along with their 95% Highest Posterior Density (HPD) interval.

Covariate	G_μ	G_μ 95% HPD	$w_{G,\mu}$	$w_{G,\mu}$ 95% HPD
Self-diversity	-0.685	[-2.655; 0.568]	0.463	[0.002; 0.981]
Plant Diversity	-0.008	[-0.039; 0.011]	0.359	[0.001; 0.97]
Andes Elevation	0.002	[-0.001; 0.007]	0.417	[0.002; 0.974]
Global Temperature	-0.055	[-0.262; 0.059]	0.421	[0.001; 0.977]
Sea Level	-0.003	[-0.025; 0.011]	0.231	[0; 0.948]
Habitat Openness	0.001	[-0.081; 0.072]	0.109	[0; 0.924]
Forest Density	-0.024	[-0.511; 0.373]	0.186	[0; 0.947]

Supp. Table 5: Posterior estimates of the multivariate birth-death correlation parameters with the origination rate (G_λ) for our full Oligocene (33.9-23.03 Ma) dataset, and their associated Shrinkage weights (G_μ). Median estimates are shown along with their 95% Highest Posterior Density (HPD) interval.

Covariate	G_λ	G_λ 95% HPD	$w_{G,\lambda}$	$w_{G,\lambda}$ 95% HPD
Self-diversity	-0.872	[-2.399; 0.204]	0.484	[0.002; 0.973]
Plant Diversity	0.010	[-0.003; 0.036]	0.505	[0.002; 0.981]
Andes Elevation	-0.002	[-0.022; 0.008]	0.290	[0.001; 0.969]
Global Temperature	0.020	[-0.454; 0.579]	0.232	[0.001; 0.952]
Sea Level	0.000	[-0.012; 0.008]	0.149	[0; 0.929]
Habitat Openness	-0.011	[-0.101; 0.024]	0.203	[0.001; 0.95]
Forest Density	-0.007	[-1.024; 1.179]	0.208	[0; 0.959]

Supp. Table 6: Posterior estimates of the multivariate birth-death correlation parameters with the extinction rate (G_μ) for our full Oligocene (33.9-23.03 Ma) dataset, and their associated Shrinkage weights (w_μ). Median estimates are shown along with their 95% Highest Posterior Density (HPD) interval. Significant correlations, *i.e.*, having a w_μ larger than 0.5 and of which the 95% HPD of the associated coefficients do not overlap 0 are shown in bold. In the case of Andean elevation, the proportion of the posterior distribution of the associated G_μ below 0 is around 0.045. Although this is larger than 0.025, we consider it small enough to claim for a significant correlation.

Covariate	G_μ	G_μ 95% HPD	$w_{G,\mu}$	$w_{G,\mu}$ 95% HPD
Self-diversity	**-2.434**	**[-3.936; -0.811]**	**0.833**	**[0.311; 0.994]**
Plant Diversity	-0.002	[-0.047; 0.012]	0.344	[0.001; 0.981]
Andes Elevation	**0.025**	**[-0.001; 0.056]**	**0.875**	**[0.025; 0.996]**
Global Temperature	-0.009	[-0.762; 0.464]	0.2	[0; 0.959]
Sea Level	0	[-0.013; 0.016]	0.17	[0; 0.945]
Habitat Openness	-0.005	[-0.103; 0.05]	0.235	[0; 0.96]
Forest Density	0.058	[-1.328; 2.632]	0.326	[0; 0.983]

Supp. Table 7: Posterior estimates of the multivariate birth-death correlation parameters with the origination rate (G_λ) for our full dataset (56-23.03 Ma), and their associated Shrinkage weights (w_λ). Median estimates are shown along with their 95% Highest Posterior Density (HPD) interval. Significant correlations, *i.e.*, having a G_λ larger than 0.5 and of which the 95% HPD of the associated coefficients do not overlap 0 are shown in bold.

Covariate	G_μ	G_μ 95% HPD	$w_{G,\mu}$	$w_{G,\mu}$ 95% HPD
Self-diversity	**-2.434**	**[-3.936; -0.811]**	**0.833**	**[0.311; 0.994]**
Plant Diversity	-0.002	[-0.047; 0.012]	0.344	[0.001; 0.981]
Andes Elevation	**0.025**	**[-0.001; 0.056]**	**0.875**	**[0.025; 0.996]**
Global Temperature	-0.009	[-0.762; 0.464]	0.2	[0; 0.959]
Sea Level	0	[-0.013; 0.016]	0.17	[0; 0.945]
Habitat Openness	-0.005	[-0.103; 0.05]	0.235	[0; 0.96]
Forest Density	0.058	[-1.328; 2.632]	0.326	[0; 0.983]

Supp. Table 8: Posterior estimates of the multivariate birth-death correlation parameters with the origination rate (G_μ) for our full dataset (56-23.03 Ma), and their associated Shrinkage weights (w_μ). Median estimates are shown along with their 95% Highest Posterior Density (HPD) interval. Significant correlations, *i.e.*, having a G_μ larger than 0.5 and of which the 95% HPD of the associated coefficients do not overlap 0 are shown in bold.

Covariate	G_μ	G_μ 95% HPD	$w_{G,\mu}$	$w_{G,\mu}$ 95% HPD
Self-diversity	**-2.182**	**[-4.666; -0.339]**	**0.811**	**[0.155; 0.994]**
Plant Diversity	0.001	[-0.006; 0.017]	0.272	[0.001; 0.968]
Andes Elevation	0.003	[0; 0.007]	0.703	[0.059; 0.987]
Global Temperature	0.009	[-0.063; 0.155]	0.246	[0; 0.957]
Sea Level	-0.007	[-0.015; 0.001]	0.455	[0.004; 0.974]
Habitat Openness	0.035	[-0.001; 0.07]	0.382	[0.007; 0.961]
Forest Density	-0.086	[-0.42; 0.13]	0.178	[0; 0.928]

Supp. Table 9: Median estimates and associated 90 and 95% Highest Posterior Density (HPD) intervals of the Weibull shape parameters for the Age-Dependent Extinction analysis of the “early” and “late” datasets (cf. Fig. S41). We can see that one is included in the 95% HPD of both parameters. However, in the case of the “late” dataset, the upper boundary of the 95% HPD is almost equal to one, and one is not included in the 90% HPD of the parameter, meaning that at least 90% of the distribution differs from one, which we judge large enough to claim for a significant effect of genus age on its extinction probability.

Phase	Median estimate	95% HPD	90% HPD
Early	1.01049	[0.554; 2.4363]	[0.61321; 2.04203]
Late	0.65766	[0.37816; 1.07411]	[0.40979; 0.99998]

Supp. Table 10: Size of the different climate zones (‘Tropical Affinity’) and Dental Ecomorphotypes (‘Diet’) categories, expressed in number of occurrences, genera and species.

	Tropical	**Affinity**			**Diet**	
	Tropical	Extratropical	Carnivorous	Herbivorous	Omnivorous	Insectivorous
Nb. occurrences	158	3226	220	2301	573	290
Nb. genera	78	470	31	324	116	57
Nb. species	116	1005	51	698	232	127

SI References

1. J. P. Scholl, J. J. Wiens, Diversification rates and species richness across the tree of life. *Proceedings of the Royal Society B: Biological Sciences* **283**, 20161334 (2016).

2. S. D. Tarquini, S. Ladevèze, F. J. Prevosti, The multicausal twilight of south american native mammalian predators (metatheria, sparassodonta). *Sci Rep* **12**, 1224 (2022).

3. R. E. Dunn, *et al.*, A new chronology for middle eocene–early miocene south american land mammal ages. *GSA Bulletin* **125**, 539–555 (2013).

4. M. Kouvari, "Palaeoenvironmental constraints on the diversity of eutherian terrestrial mammals through the cenozoic of south america, and the emergence of the modern-day latitudinal biodiversity gradient on the continent," University College of London. (2023).

5. H. Wickham, *et al.*, Welcome to the tidyverse. *Journal of Open Source Software* **4**, 1686 (2019).

6. L. A. Jones, *et al.*, Palaeoverse: A community-driven r package to support palaeobiological analysis. *Methods in Ecology and Evolution* **14**, 2205–2215 (2023).

7. W. Gearty, Deeptime: Plotting tools for anyone working in deep time. R package version 1.0.1. (2023).

8. C. Jouault, A. Nel, F. Legendre, F. L. Condamine, Estimating the drivers of diversification of stoneflies through time and the limits of their fossil record. *Insect Systematics and Diversity* **6**, 4 (2022).

9. F. L. Condamine, J. Romieu, G. Guinot, Climate cooling and clade competition likely drove the decline of lamniform sharks. *Proceedings of the National Academy of Sciences* **116**, 20584–20590 (2019).

10. G. Guinot, F. L. Condamine, Global impact and selectivity of the cretaceous-paleogene mass extinction among sharks, skates, and rays. *Science* **379**, 802–806 (2023).

11. P. C. Fitzgerald, S. J. Carlson, Examining the latitudinal diversity gradient in paleozoic terebratulide brachiopods: Should singleton data be removed? *Paleobiology* **32**, 367–386 (2006).

12. M. Foote, Origination and extinction components of taxonomic diversity: General problems. *Paleobiology* **26**, 74–102 (2000).

13. D. Silvestro, N. Salamin, A. Antonelli, X. Meyer, Improved estimation of macroevolutionary rates from fossil data using a bayesian framework. *Paleobiology* **45**, 546–570 (2019).

14. I. Quintero, M. J. Landis, W. Jetz, H. Morlon, The build-up of the present-day tropical diversity of tetrapods. *Proceedings of the National Academy of Sciences* **120**, e2220672120 (2023).

15. A. S. Meseguer, F. L. Condamine, Ancient tropical extinctions at high latitudes contributed to the latitudinal diversity gradient. *Evolution* **74**, 1966–1987 (2020).

16. C. Scotese, N. M. Wright, PALEOMAP paleodigital elevation models (PaleoDEMs) for the phanerozoic PALEOMAP project (2018).

17. C. R. Scotese, H. Song, B. J. W. Mills, D. G. van der Meer, Phanerozoic paleotemperatures: The earth's changing climate during the last 540 million years. *Earth-Science Reviews* **215**, 103503 (2021).

18. D. Silvestro, J. Schnitzler, L. H. Liow, A. Antonelli, N. Salamin, Bayesian estimation of speciation and extinction from incomplete fossil occurrence data. *Systematic Biology* **63**, 349–367 (2014).

19. D. Silvestro, N. Salamin, J. Schnitzler, PyRate: A new program to estimate speciation and extinction rates from incomplete fossil data. *Methods in Ecology and Evolution* **5**, 1126–1131 (2014).

20. D. Silvestro, B. Cascales-Miñana, C. D. Bacon, A. Antonelli, Revisiting the origin and diversification of vascular plants through a comprehensive bayesian analysis of the fossil record. *New Phytologist* **207**, 425–436 (2015).

21. T. Wiecki, *et al.*, Pymc-devs/pymc: v5.9.2 (2023) https:/doi.org/10.5281/zenodo.4603970 (November 15, 2023).

22. O. Tange, GNU parallel 20231222 ('sundhnúkagígur') (2023).

23. R Core Team, *R: A language and environment for statistical computing* (R Foundation for Statistical Computing, 2024).

24. O. Hagen, T. Andermann, T. B. Quental, A. Antonelli, D. Silvestro, Estimating age-dependent extinction: Contrasting evidence from fossils and phylogenies. *Systematic Biology* **67**, 458–474.

25. S. Lehtonen, *et al.*, Environmentally driven extinction and opportunistic origination explain fern diversification patterns. *Sci. Rep.* **7**, 4831 (2017).

26. F. L. Condamine, J. Rolland, H. Morlon, Assessing the causes of diversification slowdowns: Temperature-dependent and diversity-dependent models receive equivalent support. *Ecology Letters* **22**, 1900–1912 (2019).

27. L. M. Boschman, F. L. Condamine, Mountain radiations are not only rapid and recent: Ancient diversification of south american frog and lizard families related to paleogene andean orogeny and cenozoic climate variations. *Global and Planetary Change* **208**, 103704 (2022).

28. T. Westerhold, *et al.*, An astronomically dated record of earth's climate and its predictability over the last 66 million years. *Science* **369**, 1383–1387 (2020).

29. K. G. Miller, *et al.*, Cenozoic sea-level and cryospheric evolution from deep-sea geochemical and continental margin records. *Science Advances* **6**, eaaz1346 (2020).

30. L. M. Boschman, Andean mountain building since the late cretaceous: A paleoelevation reconstruction. *Earth-Science Reviews* **220**, 103640 (2021).

31. C. Jaramillo, M. J. Rueda, G. Mora, Cenozoic plant diversity in the neotropics. *Science* **311**, 1893–1896 (2006).

32. A. Solorzano, A. Others, Evolutionary trends of body size and hypsodonty in notoungulates and their probable drivers. *Palaeogeography, Palaeoclimatology, Palaeoecology* **568**, 123–456 (2021).

33. C. A. E. Strömberg, R. E. Dunn, R. H. Madden, M. J. Kohn, A. A. Carlini, Decoupling the spread of grasslands from the evolution of grazer-type herbivores in south america. *Nat Commun* **4**, 1478 (2013).

34. L. Palazzesi, V. Barreda, Fossil pollen records reveal a late rise of open-habitat ecosystems in patagonia. *Nat Commun* **3**, 1294 (2012).

35. R. E. Dunn, C. A. E. Strömberg, R. H. Madden, M. J. Kohn, A. A. Carlini, Linked canopy, climate, and faunal change in the cenozoic of patagonia. *Science* **347**, 258–261 (2015).

36. F. Moharrek, *et al.*, Diversification dynamics of cheilostome bryozoans based on a bayesian analysis of the fossil record. *Palaeontology* **65**, e12586 (2022).

37. M. F. Tejedor, *et al.*, New early eocene mammalian fauna from western patagonia, argentina. *American Museum Novitates* **2009**, 1–43 (2009).

38. G. G. Simpson, The beginning of the age of mammals in south america. Part 2, systematics: Notoungulata, concluded (typotheria, hegetotheria, toxodonta, notoungulata incertae sedis), astrapotheria, trigonostylopoidea, pyrotheria, xenungulata, mammalia incertae sedis. Bulletin of the AMNH; v. 137 (1967).

39. S. Roth, Noticias preliminares sobre nuevos mamíferos fósiles del cretáceo superior y terciario inferior de la patagonia. *Revista del Museo de la Plata* **11**, 135–158 (1904).

40. C. D. Frailey, Late miocene and holocene mammals, exclusive of the notoungulata, of the rio acre region, western amazonia (1986).

41. A. M. Ribeiro, Mamíferos fósiles y biocronología en el suroeste de la amazonia, brasil. *Publicación Electrónica de la Asociación Paleontológica Argentina* **14** (2013).

42. C. Goillot, P.-O. Antoine, J. Tejada, F. Pujos, R. S. Gismondi, Middle miocene uruguaytheriinae (mammalia, astrapotheria) from peruvian amazonia and a review of the astrapotheriid fossil record in northern south america. *Geodiversitas* **33**, 331–345 (2011).

43. A. Tournouër, *Note sur la géologie et la paléontologie de la patagonie* (1903).

44. F. J. Goin, A. M. Candela, New paleogene marsupials from the amazon basin of eastern peru. *The Paleogene Mammalian Fauna of Santa Rosa, Amazonian Peru. Natural History Museum of Los Angeles County, Science Series* **40**, 15–60 (2004).

45. A. M. Candela, *et al.*, The late miocene mammals from the humahuaca basin (northwestern argentina) provide new evidence on the initial stages of the great american biotic interchange. *Papers in Palaeontology* **9**, e1527 (2023).

46. P. Teta, U. F. Pardiñas, G. D'Elía, Rediscovery of chacodelphys: A south american marsupial genus previously known from a single specimen. *Mammalian Biology* **71**, 309–314 (2006).

47. N. S. Stutz, *et al.*, Late middle miocene metatheria (mammalia: Didelphimorphia and paucituberculata) from juan guerra, san martín department, peruvian amazonia. *Journal of South American Earth Sciences* **118**, 103902 (2022).

48. L. Marivaux, *et al.*, New record of neosaimiri (cebidae, platyrrhini) from the late middle miocene of peruvian amazonia. *Journal of human evolution* **146**, 102835 (2020).

49. M. A. Reguero, A. M. Candela, Late cenozoic mammals from the northwest of argentina. *Cenozoic geology of the Central Andes of Argentina* **458**, 411–426 (2011).

50. F. J. Goin, U. F. J. Pardiñas, Revisión de las especies del género hyperdidelphys ameghino, 1904 (mammalia, marsupialia, didelphidae). *Estudios geológicos* **52** (1996).

51. J. N. Gelfo, Los didolodontidae (mammalia: Ungulatomorpha) del terciario sudamericano. Sistemática, origen y evolución. *Mastozoología Neotropical* **13**, 275–277 (2006).

52. P.-O. Antoine, *et al.*, Biotic community and landscape changes around the eocene–oligocene transition at shapaja, peruvian amazonia: Regional or global drivers? *Global and Planetary Change* **202**, 103512 (2021).

53. G. Simpson, The beginning of the age of mammals in south america. Part i introduction. Edentata, condrylarthra, liptoterna, and notioprotogonia. *Bulletin of the American Museum of Natural History* **91**, 1–232 (1948).

54. F. J. Goin, M. A. Abello, Los metatheria sudamericanos de comienzos del neógeno (mioceno temprano, edad mamífero colhuehuapense): Microbiotheria y polydolopimorphia. *Ameghiniana* **50**, 51–78 (2013).

55. D. A. Croft, A. Mariano joint author Depto. Científico de Paleontología de Vertebrados Bond (Museo de La Plata La Plata, J. John, Large archaeohyracids (typotheria, notoungulata) from central chile and patagonia: Including a revision of archaeotypotherium (2003).

56. B. J. Shockey, J. J. Flynn, Morphological diversity in the postcranial skeleton of casamayoran (? Middle to late eocene) notoungulata and foot posture in notoungulates. *American Museum Novitates* **2007**, 1–26 (2007).

57. M. A. Abello, "Sistemática y bioestratigrafía de los paucituberculata (mammalia: Marsupialia) del cenozoico de américa del sur," Universidad Nacional de La Plata. (2007).

58. B. Sigé, T. Sempere, R. F. Butler, L. G. Marshall, J.-Y. Crochet, Age and stratigraphic reassessment of the fossil-bearing laguna umayo red mudstone unit, SE peru, from regional stratigraphy, fossil record, and paleomagnetism. *Geobios* **37**, 771–794 (2004).

59. G. G. Simpson, J. L. Minoprio, B. Patterson, *The mammalian fauna of the divisadero largo formation, mendoza, argentina* (Museum of Comparative Zoology at Harvard College, 1962).

60. L. Chornogubsky, Interrelationships of polydolopidae (mammalia: Marsupialia) from south america and antarctica. *Zoological Journal of the Linnean Society* **192**, 1195–1236 (2021).

61. F. Ameghino, *Notices préliminaires sur des mammifères nouveaux des terrains crétacés de patagonie* (Impr. Coni Fréres, 1902).

62. L. G. Marshall, Systematics of the extinct south american marsupial family polydolopidae (1982).

63. L. Marivaux, *et al.*, Neotropics provide insights into the emergence of new world monkeys: New dental evidence from the late oligocene of peruvian amazonia. *Journal of Human Evolution* **97**, 159–175 (2016).

64. P.-O. Antoine, *et al.*, A 60-million-year cenozoic history of western amazonian ecosystems in contamana, eastern peru. *Gondwana Research* **31**, 30–59 (2016).

65. P.-O. Antoine, *et al.*, Middle eocene rodents from peruvian amazonia reveal the pattern and timing of caviomorph origins and biogeography. *Proceedings of the Royal Society B: Biological Sciences* **279**, 1319–1326 (2012).

66. M. Boivin, *et al.*, Late middle miocene caviomorph rodents from tarapoto, peruvian amazonia. *PLoS One* **16**, e0258455 (2021).

67. M. Arnal, M. E. Pérez, L. M. Tejada Medina, K. E. Campbell Jr, The high taxonomic diversity of the palaeogene hystricognath rodents (caviomorpha) from santa rosa (peru, south america) framed within a new geochronological context. *Historical Biology* **34**, 2350–2373 (2022).

68. M. Reguero, A. Candela, R. Alonso, Biochronology and biostratigraphy of the uquía formation (pliocene–early pleistocene, NW argentina) and its significance in the great american biotic interchange. *Journal of South American Earth Sciences* **23**, 1–16 (2007).

69. M. Boivin, *et al.*, Early oligocene caviomorph rodents from shapaja, peruvian amazonia. *Palaeontographica A* **311**, 87–156 (2018).

70. M. Arnal, A. G. Kramarz, M. G. Vucetich, C. D. Frailey, K. E. Campbell Jr, New palaeogene caviomorphs (rodentia, hystricognathi) from santa rosa, peru: Systematics, biochronology, biogeography and early evolutionary trends. *Papers in Palaeontology* **6**, 193–216 (2020).

71. A. Assemat, *et al.*, Restes inédits de rongeurs caviomorphes du paléogène de la région de juanjui (amazonie péruvienne): Systématique, implications macro-évolutives et biostratigraphiques. *Geodiversitas* **41**, 699–730 (2019).

72. M. Boivin, *et al.*, Late oligocene caviomorph rodents from contamana, peruvian amazonia. *Papers in Palaeontology* **3**, 69–109 (2017).

73. C. D. Frailey, K. E. Campbell, Paleogene rodents from amazonian peru: The santa rosa local fauna. *The Paleogene Mammalian Fauna of Santa Rosa, Amazonian Peru* **40**, 71–130 (2004).

74. R. Lavocat, RONGEURS CAVIOMORPHES DE l'OLIGOCENE DE BOLIVIE. II. RONGEURS DU BASSIN DESEADIEN DE SALLA-LURIBAY.(COLLECTION HOFFSTETTER). (1976).

75. B. Patterson, A. E. Wood, *Rodents from the deseadan oligocene of bolivia and the relationships of the caviomorpha* (Museum of Comparative Zoology, Harvard University, 1982).

76. J. Hartenberger, Nouvelles découvertes de rongeurs dans le déseadien (oligocène inférieur) de salla luribay (bolivie). (1975).

77. L. Kerber, Imigrantes em um continente perdido: O registro fossilífero de roedores caviomorpha (mammalia: Rodentia: Ctenohystrica) do cenozoico do brasil. *Terrae Didática* **13**, 185–211 (2017).

78. M. Lacerda, P. S. Romano, K. L. Bandeira, L. G. SOUZA, Georeferencing fossiliferous localities from solimões and acre basins (brazil)-what we know so far about solimões formation and future perspectives. *Anais da Academia Brasileira de Ciências* **93** (2021).

79. M. E. Pérez, *et al.*, New caviomorph rodents from the late oligocene of salla, bolivia: Taxonomic, chronological, and biogeographic implications for the deseadan faunas of south america. *Journal of Systematic Palaeontology* **17**, 821–847 (2019).

80. L. G. Marshall, *Evolution of the borhyaenidae, extinct south american predaceous marsupials* (Univ of California Press, 1978).

81. F. J. Prevosti, A. M. Forasiepi, *Evolution of south american mammalian predators during the cenozoic: Paleobiogeographic and paleoenvironmental contingencies* (Springer, 2018).